

# Functional Silicon Nanoparticles

Loes Ruizendaal

### **Thesis committee**

#### **Thesis supervisors**

Prof. dr. J.T. Zuilhof  
Professor of Organic Chemistry  
Wageningen University

Prof. dr. E.J.R. Sudhölter  
Professor of Nano-organic Chemistry  
Delft University of Technology

#### **Thesis co-supervisor**

dr. J.M.J. Paulusse  
Associate professor, Laboratory of Organic Chemistry  
Wageningen University

#### **Other members**

dr. ir. M.A. Jongsma, Plant Research International, Wageningen UR  
Prof. dr. T. Gregorkiewicz, University of Amsterdam  
Prof. dr. J.J.L.M. Cornelissen, University of Twente, Enschede  
Prof. dr. ir. I.M.C.M. Rietjens, Wageningen University

This research was conducted under the auspices of the graduate school VLAG.

# Functional Silicon Nanoparticles

Loes Ruizendaal

## **Thesis**

submitted in fulfilment of the requirements for the degree of doctor  
at Wageningen University  
by the authority of the Rector Magnificus  
Prof. dr. M.J. Kropff,  
in the presence of the  
Thesis Committee appointed by the Academic Board  
to be defended in public  
on Tuesday October 18, 2011  
at 4 p.m. in the Aula.

**Loes Ruizendaal**

Functional Silicon Nanoparticles

122 pages

Thesis, Wageningen University, Wageningen, NL (2011)

With references, with summaries in Dutch and English

ISBN: 978-94-6173-021-3



# Table of Contents

Chapter 1	Introduction	7
Chapter 2	Detailed Characterization and Size Separation of Butyl-Terminated Silicon Nanoparticles	27
Chapter 3	Functional Silicon Nanoparticles <i>via</i> a Thiol-ene Click-Chemistry Approach	45
Chapter 4	DNA Functionalized Silicon Nanoparticles	65
Chapter 5	Synthesis and Cytotoxicity of Silicon Nanoparticles with Covalently Attached Organic Monolayers	83
Chapter 6	General Discussion	99
Summary		105
Samenvatting		109
Curriculum Vitae		113
List of Publications		115
Overview of Completed Training Activities		117
Dankwoord		119



# Chapter 1

## Introduction

### **Abstract**

In recent years, widely used organic fluorescent dyes are more and more being replaced by semiconductor-based (II-VI and III-V) quantum dots. The reasons for this development are the superior photostability of quantum dots and the relatively easy tuning of the fluorescence emission wavelength. However, issues about toxicity and specific functionalization still remain, especially in their application in biological systems. Silicon nanoparticles smaller than ~5 nm can be considered as quantum dots as well, they are fluorescent, and can be covalently coated with functional groups via a Si-C bond.

## **1.1 Introduction**

Material properties change dramatically when the size of a particle is reduced down to the nanometer scale. There are mainly two types of effects that play a role on such small scales: surface effects and quantum confinement effects.<sup>1</sup> As the particle becomes smaller, the fraction of atoms on the surface increases. Surface effects are responsible for the changes in melting temperature of nanoclusters as compared to bulk materials. For example the melting temperature of gold nanoparticles drops from 1250 K to 500 K when particle size decreases from 16 to 1.6 nm.<sup>2</sup> Quantum confinement effects induce magnetism in small clusters, such as Pt nanoparticles consisting of up to 13 atoms, whereas bulk Pt is not magnetic.<sup>3</sup> Exciting catalytic behavior is also observed for nanomaterials; while bulk gold is intrinsically inert, on the nanoscale it becomes an excellent catalyst for oxidation and hydrogenation reactions.<sup>4</sup> Another most interesting property that arises from quantum confinement effects is fluorescence.<sup>5</sup>

## **1.2 Quantum Confinement Effects and Fluorescence**

When a semiconductor material is irradiated with a photon, an electron-hole pair may form. Initially this electron-hole pair (exciton) is bound by Coulomb interactions. The electrons and holes can move freely in bulk semiconductors, however, when the distance between the electron and hole becomes larger than the nanometer-scale Bohr exciton radius, the interaction is lost. When the size of a semiconductor material is decreased to approximately the Bohr exciton radius, the movement of electrons and holes will also be restricted to this scale, which implies that their interaction starts to depend on the overall size of the particle.<sup>5</sup> Due to this quantum confinement effect, the energy gap between the valence and conduction band becomes dependent on the particle size,<sup>6-8</sup> thereby influencing both the optical absorbance and fluorescence properties, and both of these in regard of the corresponding energies as well as their intensities.

## **1.3 II-VI and III-V Quantum Dots**

The first quantum dots (QDs) were discovered in the early 1980's<sup>9-11</sup> and are nanoclusters, in general consisting of group II and VI elements (e.g. CdS<sup>9-11</sup> or CdTe<sup>12</sup>), or group III and V elements (e.g. InP<sup>13,14</sup> or GaAs<sup>14</sup>). The first chemically stable and

monodisperse QDs were synthesized via a novel “hot injection” method developed by the group of Bawendi in 1993.<sup>15</sup> The introduction of core-shell type QDs further resolved the problem of chemical stability. Interactions of the exciton with the surface were minimized in this way, resulting in higher quantum yields (QYs) up to 90%.<sup>16</sup>

Current QDs mostly consist of a core-shell composition. Herein, two core-shell combinations may be distinguished.<sup>17</sup> Type I core-shell type QDs have a shell with a higher bandgap than the core. The use of a shell with a higher bandgap limits the excited state (exciton) to the core of the QD, since the energy of the exciton is not high enough to enter the shell material. This prevents interactions with the surface of the QD, and therefore limits the negative effects of surface states.<sup>18,19</sup> Examples are CdSe/ZnS<sup>20,21</sup> or CdSe/CdS<sup>21,22</sup> core-shell QDs. In type II QDs, the core is coated with a material of which the band levels are shifted as compared to the core material.<sup>23,24</sup> These types of QDs may give rise to selective carrier confinement.<sup>23</sup> Examples are CdTe/CdSe core-shell QDs,<sup>23,25</sup> in which the excited electron is mainly located in the shell, and the hole in the core. Since the recombination energy is now related to the differences in the core and shell energy levels, photoluminescence is often more red-shifted and the material is characterized by a larger Stokes shift. A schematic representation of a core-shell QD and corresponding schematic energy diagrams for type I and type II QDs are shown in Figure 1.

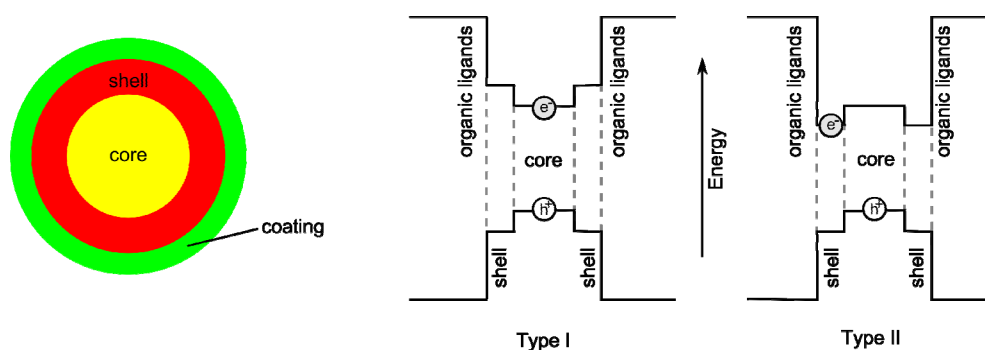


Figure 1. Left: General structure of a QD, covered by an organic or inorganic coating for stabilization and/or functionalization. Right: Schematic energy diagram of type I and type II QDs.

### 1.3.1 Applications of II-VI and III-V Quantum Dots

Applications of QDs are mainly focused towards biological systems, and have attracted considerable attention.<sup>26-30</sup> The advantages of using QDs in such systems, instead of organic dyes, are the size-tunable emission wavelength and the lack of photobleaching.<sup>31</sup> An example of the photostability of QDs as compared to an organic dye is shown in Figure 2. For biological applications, QDs should be biocompatible, for example by making them water soluble and less toxic, which may for example be achieved through the attachment of polyethylene glycol.<sup>32</sup> To be able to label specific parts of cells or certain cell types (e.g. tumor cells), the coupling of targeting groups on the QDs is needed. Specific targeting can be achieved by the attachment of antibodies onto the QD surface.<sup>33-36</sup> An alternative approach makes use of the enhanced permeability and retention effect (EPR effect). Since tumor cells grow relatively quickly, the blood vessels towards the tumor grow fast and thereby form leaky vessels. Therefore, materials of a certain size, such as liposomes, macromolecular drugs and QDs, tend to accumulate in the tissue around these vessels. Tumor targeting *in vivo* may therefore also be a passive process.<sup>26</sup> The group of Gao was the first to specifically target tumor tissues in live animals.<sup>37</sup> Human prostate cancer cells in live mice were specifically labeled with QDs, (Figure 2) with significantly better accumulation in the tumor tissue than the unlabeled material.

Another application of QDs is found in light-emitting diodes (LEDs).<sup>38</sup> These have been fabricated using a sandwich design on glass. Electrons and holes are injected from the two sides and recombine in the QD monolayer, resulting in light emission.<sup>39,40</sup> By combining multiple sizes of QDs, white light emitting LEDs were made.<sup>41</sup> By making use of the same electroluminescent effect, altering the device in such a way that synchronized photons are produced, laser sources were assembled.<sup>38,42</sup> Furthermore, QDs can be used in photovoltaic cells as sensitizers, converting UV light to the, for solar cells, more efficient visible region.<sup>43-46</sup> A photovoltaic device was assembled, consisting of thin films of QDs, in which light is converted into electricity. The main issue to address is to bring the QDs close enough to each other to provide long range transport of holes and electrons, while maintaining the quantum confinement.<sup>47</sup>

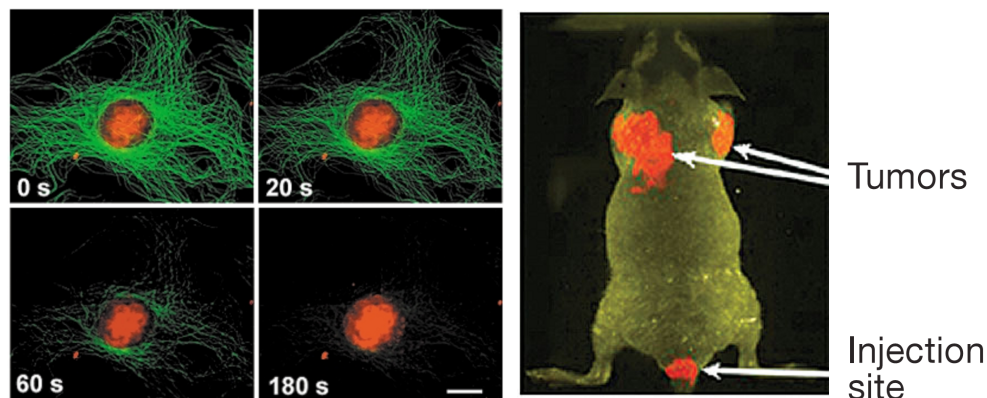


Figure 2. Left: Photostability comparison between QDs and Alexa 488, an organic dye. Nuclear antigens were incubated with QDs (red) and microtubules were labeled with Alexa 488 (green). The specimen was illuminated continuously with light from a 100W mercury lamp. The Alexa 488 dye is fully photobleached after 180 sec, whereas the QDs remain fluorescent.<sup>31</sup> Right: 0.4 nmol of QD probes modified with PEG-PMSA antibody conjugates were injected in a mouse and incubated for 2 h after which a fluorescence image was recorded. The tumors are specifically labeled due to the antibody-conjugated QDs.<sup>37</sup>

#### 1.4 Group IV Nanomaterials

Group IV semiconductor nanoparticles (based on silicon and germanium) with dimensions smaller than the Bohr exciton radius (nm scale) display fluorescent properties, similar to II-VI and III-V semiconductor quantum dots. Again, quantum confinement effects are the reason for this luminescent behaviour.<sup>48-50</sup> However, in contrast to the II-VI and III-V QDs, bulk silicon and germanium are indirect bandgap semiconductors. Therefore, the assistance of a phonon is required to promote an electron from the valence band into the conduction band. However, when the crystal size is reduced down to nanometer size, the electronic transitions are more characteristic of a direct bandgap,<sup>51</sup> which is observed from the relatively short fluorescence lifetimes (ns scale), instead of microsecond scale as generally observed for indirect bandgap materials.<sup>52,53</sup>

Since the quantum confined energy states are dependent on the crystal size, silicon nanoparticles (Si NPs) and germanium nanoparticles (Ge NPs) display size-dependent

fluorescent behavior.<sup>54</sup> As the nanoparticle size distribution becomes broader, the fluorescence emission wavelength broadens accordingly. The ability to tune Si NP size and hence fluorescence emission wavelength is of particular interest to device applications, which require QDs with distinct emission wavelengths.

### 1.4.1 Carbon Nanoparticles

Diamond nanocrystals do not display photoluminescence due to the very wide bandgap. Therefore, the observed luminescence in the visible light can only stem from defects.<sup>55</sup> The best known color source in diamond is the nitrogen-vacancy (N-V) complex,<sup>56</sup> but also nickel sources in synthetic diamonds appear to cause defects responsible for luminescence.<sup>57</sup> Nearly all of the naturally occurring diamond contains some nitrogen impurities, and electron, proton or ion irradiation followed by annealing at 700 - 900°C creates nitrogen-vacancy defects that result in luminescent properties.<sup>56</sup>

In general, two methods are employed for the synthesis of carbon nanocrystals. The first method consists of the detonation of 1,3,5-trinitro-1,3,5-triazacyclohexane or trinitrotoluene, and yields non-fluorescent carbon nanocrystals.<sup>58,59</sup> These are typically used in cutting tools and abrasives. The second method involves the formation of micrometer-sized crystals, which are reduced in size by high energy ball milling.<sup>60</sup> By using N-V rich microcrystals, fluorescent nanocrystals are obtained.<sup>60-62</sup>

Another type of carbon nanomaterials are the so-called carbon nanodots (C-dots). These contain, in contrast to the nanocrystals, a larger fraction of carbon atoms with  $sp^2$ -character, and may therefore be considered rather as graphene quantum dots.<sup>63</sup> They also contain more oxygen than the aforementioned carbon nanocrystals. However, although the origin is poorly understood, C-dots possess luminescent properties. The C-dots may be synthesized by different methods, such as the top-down method of arc discharge, from which the C-dots were discovered as a by-product in the production of single-walled carbon nanotubes.<sup>64</sup> Other methods are laser ablation of graphite powder,<sup>65-67</sup> electrochemical synthesis from multi-walled carbon nanotubes<sup>68</sup> or graphite,<sup>69,70</sup> from soot of candles or natural gas,<sup>71-73</sup> and synthesis on solid supports such as silica<sup>74</sup> or zeolites.<sup>75,76</sup> In general, these C-dots are carboxylic acid terminated, owing to a typically applied synthetic step involving refluxing in  $HNO_3$ . This facilitates functionalization of the C-dots, making them suitable for use in bioimaging.<sup>65,66,74</sup>



### 1.4.2 Germanium Nanoparticles

As mentioned above, germanium nanoparticles (Ge NPs) smaller than the Bohr exciton radius ( $\sim 11$  nm)<sup>77</sup> display photoluminescent properties. When compared to silicon nanoparticles (Si NPs), similarly sized Ge NPs will display fluorescence emission at a longer wavelength than Si NPs.<sup>78</sup> This is accounted for by the lower intrinsic bandgap energy.

Ge NPs have been prepared via synthesis in reversed micelles using Ge halides as precursors,<sup>77</sup> yielding Ge NPs of 1 - 10 nm in diameter. The synthesis from Zintl salts, such as  $\text{Mg}_2\text{Ge}$ , yielded Ge NPs with an average diameter of  $4 \pm 2$  nm, which were capped with a tetrahydropyranyl (THP)-protected alcohol group. After deprotection and subsequent attachment of an initiator for radical polymerization, polystyrene and poly(methyl methacrylate) were grown from the Ge NPs.<sup>79</sup> Another method is the thermolysis of  $\text{Ge}[\text{N}(\text{SiMe}_3)_2]_2$ . The resulting Ge NPs have a relatively broad size distribution with diameters of  $7 \pm 4$  nm.<sup>80</sup> By encapsulating these Ge NPs with PEG phospholipids, they are rendered water soluble and bio-compatible.<sup>81</sup> Heating diphenylgermane or tetraethylgermane in supercritical hexane and octanol resulted in Ge NPs with an octanol coating in tunable sizes between 2 - 70 nm.<sup>82</sup> The obtained Ge NPs with sizes of 3 - 4 nm were further investigated and display fluorescence. Chemical laser deposition was also employed in the preparation of Ge NPs, yielding NPs with an organic covering layer, but with a rather broad size distribution of 2 - 50 nm.<sup>83</sup> Finally, the reduction of  $\text{GeCl}_4$  with sodium naphthalide allowed for the development of Ge NPs with different shapes and sizes, depending on the reaction time. With a reaction time of 10 min, spherical Ge NPs of 3 - 7 nm were produced, while a reaction time of 45 min yielded tetrahedral Ge NPs of 30 - 49 nm as observed in TEM. Optical properties of both type of Ge NPs were not studied.<sup>84</sup>

Reports on applications of Ge NPs are still limited. Bioimaging studies with PEG-encapsulated Ge NPs displayed only very weak fluorescence in bioimaging explorations,<sup>81</sup> while amine-terminated Ge-NPs are slightly cytotoxic.<sup>55</sup> This lack of literature reports is likely due to the early stage of development of the synthesis of Ge NPs and the relative high costs of the Ge precursors, as compared to e.g. Si precursors.

## 1.5 Synthetic Routes Towards Silicon Nanoparticles

Since the first bottom-up synthesis to prepare Si NPs via the reduction of  $\text{SiCl}_4$  and  $\text{RSiCl}_3$  with sodium in 1992,<sup>85</sup> various different methods have been developed. These can be divided into two approaches: top-down, i.e. the reduction of bulk materials to nanometer-sized objects, and bottom-up, i.e. the annealing or assembly of Si atoms up to the size of nanometers. Several reviews about the synthesis and optoelectronic properties of Si NPs have been published.<sup>86,87</sup> The main synthetic methods, including their advantages and disadvantages – in terms of reaction yield, dispersity of particle size distribution, particle stability and optical properties – are described below in more detail.

In general, the produced Si nanocrystals are hydrogen- or halogen-terminated, but require a second surface passivation step to prevent the particle from oxidation and subsequent degradation. The oxidation has a large influence on the optical properties, since the initial luminescence originates from quantum confinements effects in non-oxidized Si NPs, which shifts to luminescence effects originating from surface-state effects in oxidized particles.<sup>55,88,89</sup>

### 1.5.1 Top-Down Synthetic Methods

#### 1.5.1.1 Electrochemical Etching and Ultrasonication of Silicon Wafers

Heinrich and co-workers have electrochemically etched n-type or p-type silicon wafers to form porous silicon by applying an electric potential on a wafer upon soaking in a 50% HF ethanol solution. After etching, the material was ultrasonically dispersed to form suspensions of Si NPs, however, no surface passivation was applied. The material formed is polydisperse (nm to  $\mu\text{m}$  sizes) and irregularly shaped.<sup>90</sup> Carboxylic acid-terminated and methyl-ester terminated Si NPs were prepared via  $\text{HF}/\text{H}_2\text{O}_2$  anodization of crystalline Si wafers. The resulting H-terminated Si NPs were functionalized by performing a hydrosilylation reaction under thermal conditions.<sup>91</sup> The obtained Si NPs were 1 - 1.5 nm in diameter. Horrocks and coworkers<sup>92,93</sup> have synthesized Si NPs by galvanostatic anodization of Si(100) wafers in the presence of aqueous HF and ethanol. The resulting particles were capped with undecene, yielding 100  $\mu\text{g}$  of Si NPs per batch. Addition of THF or DMSO allowed for suspending of the particles in water. The group of Amato has anodically etched Si wafers to form a porosified p-type layer. The layer was etched with aqueous HF in ethanol. These etched layers were treated with ultrasound in

either THF or toluene, and yielded 2 - 5 nm sized Si NPs. Afterwards the particles were stabilized by adding undecene, undecylenic acid or paraffin, followed by further ultrasonication (Figure 3, top left). The addition of paraffin resulted in a blue-shift of the fluorescence emission from 670 nm to 620 nm.<sup>94,95</sup>

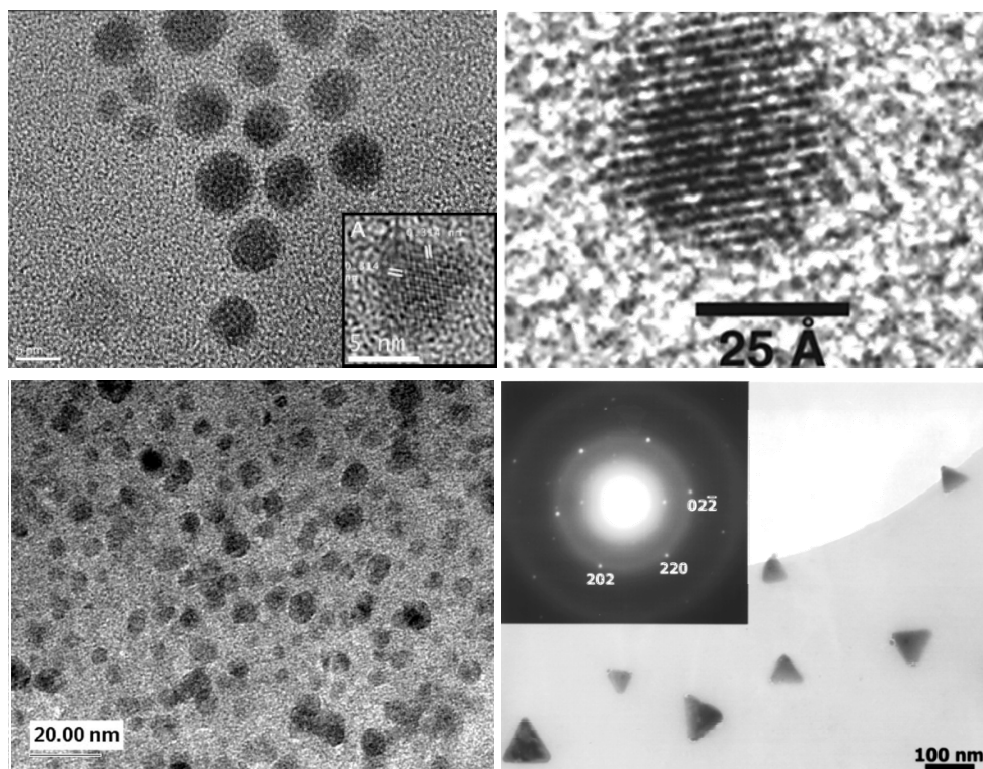


Figure 3. TEM pictures of Si NPs made with various methods. Top left: Si NPs prepared by ultrasonication of porous silicon. Scale bar indicates 5 nm. Inset shows a single particle with crystalline fringes.<sup>94</sup> Top right: Si NP synthesized from diphenylsilane in supercritical fluids. The lattice spacing of 3.1 Å is consistent with the (111) separation in the Si diamond-like lattice.<sup>52</sup> Bottom left: n-octanol-capped Si NPs, produced by the reduction of  $\text{SiCl}_4$  by sodium naphthalide<sup>101</sup> Bottom right: Silicon nanocrystals produced by the reduction of  $\text{SiCl}_4$  by sodium naphthalide and the subsequent capping with excess n-BuLi. The inset shows the SAED spot pattern for the particles, consistent with diamond crystalline silicon.<sup>102</sup>

### 1.5.1.2 Laser ablation

Niu and co-workers synthesized Si NPs with a diameter of ca. 4 nm and at a rate of 400 - 500 mg/h by pulsed laser ablation of a Si (100) wafer in inert gas.<sup>96</sup> Similarly, Umezu and co-workers prepared Si NPs by laser ablation in He/H gas by pulsing a laser on a Si single crystal. By varying the H partial pressure it was found that higher H pressures result in higher particle crystallinity.<sup>97</sup> The laser ablation method was rendered into a one-pot synthesis by Shiharata and co-workers, who performed the ablation of a Si wafer in the presence of 1-octene, which effectively capped the NPs resulting in octyl-terminated Si NPs. The diameter of the Si NPs ranges from 1 to 10 nm and the highest fluorescence emission is found around 375 nm.<sup>98</sup>

### 1.5.1.3 High energy ball milling

High energy ball milling (HEBM) was successfully applied to produce Si NPs. Heintz and co-workers have synthesized alkyl-capped Si NPs by milling silicon pieces in the presence of 1-octene or 1-octyne. The resulting particles were 5 - 10 nm in diameter and show fluorescence emission with a maximum around 450 nm.<sup>99</sup> Recently, they have expanded the capping groups to acids, aldehydes, and alcohols.<sup>100</sup> However, this resulted in attachment of the capping groups *via* the oxygen atoms of the functional groups, which renders them unavailable for further use and affects both their optical properties and long-term stability.

## 1.5.2 Bottom-up Synthetic Methods

### 1.5.2.1 Laser-Driven Pyrolysis

Significant quantities of Si NPs were obtained by employing laser pyrolysis. A CO<sub>2</sub> laser beam was used to pyrolyze SiH<sub>4</sub>, yielding Si NPs of 5 nm in diameter at a rate of 20 - 200 mg/h. These particles required further etching with HF and HNO<sub>3</sub> to reduce the size and to remove the surface oxidation layer. By controlling etching time and conditions, particle photoluminescence was tuned. However, the photophysical properties did not remain constant.<sup>103</sup> When the Si NPs were further etched with HF and subsequently thermally hydrosilylated with a series of alkenes, the surface and thereby the optical properties could be stabilized.<sup>104,105</sup>

### 1.5.2.2 Plasma synthesis

Si NPs with a native oxide layer were produced using a non-thermal low pressure plasma, with a gas mixture of argon and  $\text{SiH}_4$ . Changing the flow rate of the gases allowed for tuning of the particle size.<sup>106</sup> The Si NPs form a native oxide layer on the surface upon exposure to air, which is observed by the appearance of intense photoluminescence during the reaction. The reaction yields Si NPs at a rate of 50 mg/h with a high degree of crystallinity. This method resulted in Si NPs with high quantum yields of up to 60%.<sup>107</sup>

### 1.5.2.3 Synthesis in Supercritical Fluids

The first NPs synthesized in supercritical fluids were platinum NPs generated in a polymer substrate, which was immersed in supercritical  $\text{CO}_2$ .<sup>108</sup> After this, Korgel *et al.* further developed this concept to produce Si NPs. In general, to produce Si NPs in supercritical fluids (SCFs), relatively high temperatures are required to achieve core crystallinity.<sup>109</sup> Similarly, thermal degradation of diphenylsilane in the presence of octanol at 500 °C and 345 bar in supercritical hexane resulted in alkoxide-stabilized Si NPs with a diameter of 1.5 - 4 nm (Figure 3, top right). The fluorescence emission maxima lie around 400 - 500 nm, depending on the size of the nanocrystals.<sup>52</sup> Further studies revealed “blinking” behavior as well as size-dependent photoluminescence.<sup>110</sup> Unfortunately, no other surface capping groups were investigated, which limits the functionalization of these Si NPs, and hence their further application.

### 1.5.2.4 Oxidation and Reduction in Solution

The solution-phase oxidation-reduction reactions are mainly based a few different types of reactions, as shown in Figure 4. Nearly all of these Si NPs are initially halogen-terminated or hydrogen-terminated, but may be capped with organic molecules to stabilize the NPs.

The reaction of  $\text{SiCl}_4$  with sodium naphthalide in a mixture of THF and 1,2-dimethoxyethane yielded Si NPs with sizes of 3.4 - 7.1 nm.<sup>101,116</sup> The Si NPs are alkoxy-terminated, stable against degradation and display fluorescence emission maxima around 400 nm. Tetrahedrally shaped, non-fluorescent Si NPs of 40 - 80 nm were produced by performing the reaction in 1,2-dimethoxyethane and subsequent capping with *n*-BuLi, in a smaller excess (2.3 eq to  $\text{SiCl}_4$ ) than in the case of the alkoxy-capping (5.2 eq to  $\text{SiCl}_4$ ).<sup>102</sup> This shows that the solvent and exact reagent ratios in this reaction is of great importance and determines the final Si NP size and shape. Since it is

suggested that the Si NP formation is complete before addition of the capping group, the solvent polarity and with that the solubility of the reagents and products is responsible for the shape of the formed Si NPs. TEM pictures of both the 3.4 - 7.1 nm Si NPs as well as the tetrahedrally shaped Si NPs are shown in Figure 3 (bottom).

The oxidation of  $\text{Mg}_2\text{Si}$  with  $\text{Br}_2$  yields Br-capped Si NPs, which may be capped with either  $n\text{-BuLi}$ <sup>111</sup> or a Grignard reagent. The resulting Si NPs are 2 - 3 nm in diameter and show fluorescence emission maxima around 340 - 500 nm, depending on the silicon core size.

The reduction of  $\text{SiCl}_4$  and  $n\text{-octyltrichlorosilane}$  by sodium at elevated pressure and temperature yields Si NPs of  $5.5 \pm 2.5$  nm. Variation of the ratio between  $\text{SiCl}_4$  and  $\text{RSiCl}_3$  allowed for altering of the surface-to-volume ratio.<sup>85</sup> Unfortunately, no other capping moieties than alkyl groups were investigated, limiting the application potential of these Si NPs.

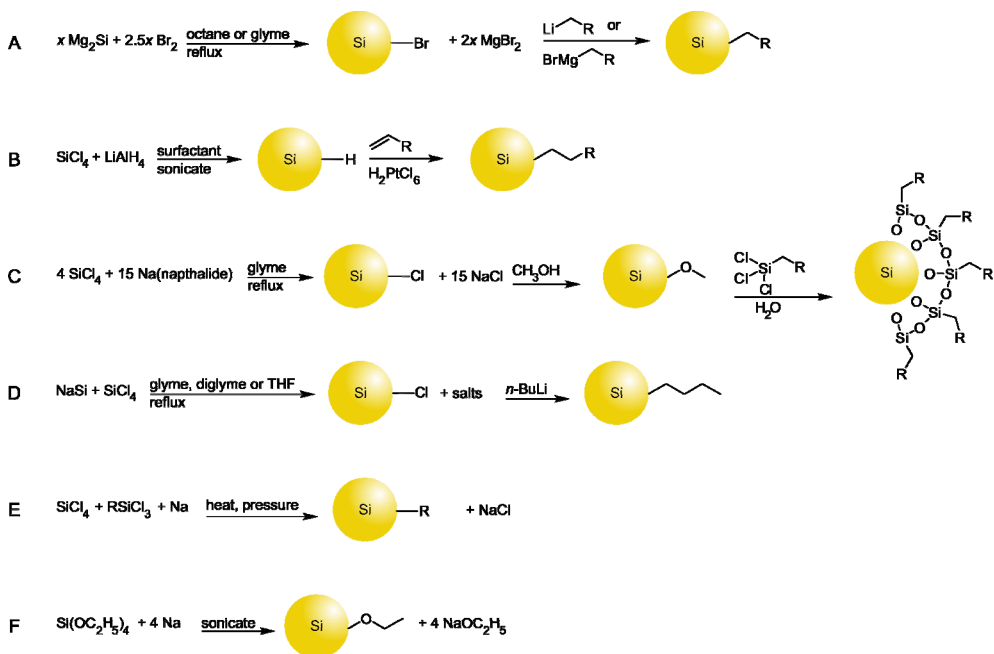


Figure 4. Various methods to synthesize Si NPs by oxidation and reduction in solution. A: oxidation of  $\text{Mg}_2\text{Si}$  with  $\text{Br}_2$ <sup>111</sup> B: reduction of  $\text{SiCl}_4$  with  $\text{LiAlH}_4$ <sup>53,112,113</sup> C: reduction of  $\text{SiCl}_4$  with sodium naphthalide,<sup>101,102,114-116</sup> D: reduction of  $\text{SiCl}_4$  with  $\text{NaSi}$ ,<sup>117</sup> E: reduction of  $\text{SiCl}_4$  and  $\text{RSiCl}_3$  with  $\text{Na}$ ,<sup>85</sup> F: reduction of  $\text{Si(OC}_2\text{H}_5)_4$  with  $\text{Na}$ .<sup>118</sup>

In order to gain more control over the size of the Si NPs and their size distribution, a synthesis in reversed micelles was developed by the group of Wilcoxon.<sup>112</sup> Performing the reaction in nanoreactors limits the size of the resulting Si NPs, and a narrower size distribution is achieved. The reduction of  $\text{SiCl}_4$  with  $\text{LiAlH}_4$  in such nanoreactors, was carried out by Wilcoxon and coworkers,<sup>112</sup> and resulted in Si NPs with a broad size distribution of 2 - 10 nm. The group of Tilley attached allylamine onto the H-terminated Si NPs and used tetraoctylammonium bromide as a surfactant.<sup>113</sup> This yielded Si NPs with a relatively monodisperse Si core diameter of  $1.8 \pm 0.2$  nm. The synthesis was further developed by attaching terminal alkenes,<sup>53</sup> PEG<sup>119</sup> and amides,<sup>120</sup> resulting in gram-scale quantities. This allowed for more detailed characterization and opened new ways to attach carboxylic acid-terminated groups, as evidenced by energy transfer between the Si NP and an attached fluorophore.<sup>121</sup>

## 1.6 Applications of Silicon Nanoparticles

Si NPs have the same advantages over organic dyes as conventional QDs: their lack of photobleaching and the size-tunable emission wavelength. Moreover, their core consists of non-toxic silicon, which has been further studied for Si NPs in particular,<sup>122,123</sup> whereas the conventional group II-VI or III-V QDs often consist of the inherently toxic Cd, Zn or Se.<sup>124,125</sup> In general, II-VI or III-V QDs are typically stabilized by attachment of non-covalently bound organic molecules such as oleic acid, thiols or phosphine oxide derivatives.<sup>126</sup> This leaves them intolerant to many solvents, since the stability of such a layer is highly dependent on the chemical environment, and these non-covalently attached molecules can thus dissociate from the QDs and thereby cause them to precipitate. Furthermore, a lot of effort has been invested in preventing leakage of the toxic Cd, Zn and Se ions from the core of the II-VI or III-V QDs by applying organic polymeric coatings, since the small capping molecules are not sufficient.<sup>32,127</sup> Next to the non-toxicity of the Si core, the covalently attached organic monolayer tolerates a wide range of solvents. So far, less applications with Si NPs have been developed than with II-VI or III-V QDs, which is most likely caused by the lack of a method to prepare well-defined, functional Si NPs in large amounts with relatively easy methods. Furthermore, in contrast to II-VI or III-V QDs, the Si NPs have an indirect bandgap, which is characterized by a relatively low luminescence efficiency.

### 1.6.1 Bioimaging

In order to employ Si NPs in biological applications, the particles have to be water soluble, are non-toxic and should have the ability to be labeled with targeting agents to direct the particles to for example specific tissues or areas inside cells. The water solubility may be achieved by either a hydrophilic layer,<sup>81,119,128</sup> or by dispersion in micelles or suspensions.<sup>93</sup> The toxicity of Si NPs has been studied by exposing HeLa cells to solutions of alkyl-terminated Si NPs in diethyl ether, and no evidence for cytotoxicity was found.<sup>129</sup> Other studies show that the toxicity of Si NPs seems mostly dependent on surface charge, and toxic effects do not appear to originate from the Si core.<sup>122,123</sup>

Several groups have synthesized water-soluble or water-dispersible Si NPs and demonstrated their use in the imaging of cells. An example is the visualization of amine-terminated Si NPs in HeLa cells<sup>113</sup> and BV2 cells, which keep multiplying upon uptake of the particles.<sup>120</sup> Clusters of acid-coated Si NPs were added to HEK2-293T cells, showing no decrease in cell viability after 24 h.<sup>130</sup> PEGylated micelles containing hydrophobic Si NPs were taken up by pancreas cancer cells and also showed no observable cytotoxicity.<sup>131</sup> In an alternative approach, hybrid micelles, containing both iron(III) oxide and alkyl-terminated Si NPs, were taken up by macrophage RAW cells, and injected in mice tumors. The fluorescence intensity remained constant for 24 h.<sup>132</sup> The above results are all examples of non-specific uptake of Si NPs by cells. Uptake may be significantly improved by appropriate modification of the Si NP surface. The possibility to label cells with Si NPs, without notable toxic effects, strongly supports the use of Si NPs in bioimaging.

### 1.6.2 Other Applications

Si NPs can also act as a drug delivery system, by making use of porous silicon. This was shown by Foraker *et al.* who investigated the delivery of insulin into Caco-2 cells, which was approximately 10 times faster when Si NPs were used instead of without a carrier. The porous silicon was loaded with a permeation enhancer and insulin, thereby creating a local high concentration of the molecules, which was responsible for the faster uptake.<sup>133</sup> Another interesting application makes use of the electroluminescent properties of QDs. Cheng and co-workers developed an infrared-LED made of Si NPs spun-cast between a hole-transporting layer of poly[2-methoxy-5-(2-ethylhexyl-oxy)1,4-phenylene-vinylene] (MEH-PV) and an electron-transporting layer of bathocuproine



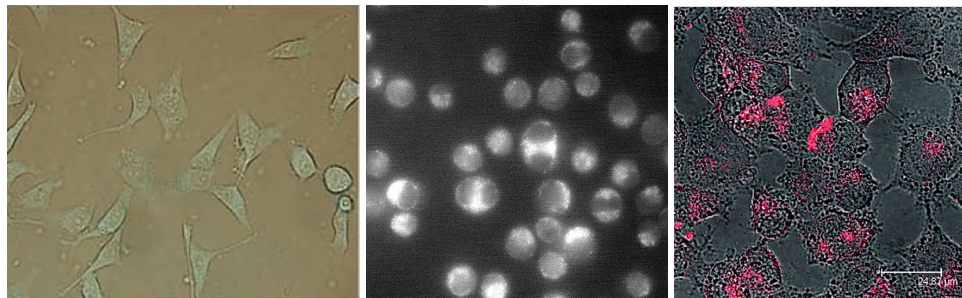


Figure 5. Left: HeLa cells with allylamine-capped Si NPs incorporated in the cytosol, illuminated with a UV lamp.<sup>113</sup> Center: Epifluorescence image of Si NP stained BV2 cells showing mitosis, illuminated with blue light.<sup>120</sup> Right: Transferrin functionalized micelle encapsulations of Si NPs in pancreas cancer cells. The overlay of the transmission and luminescence images is shown.<sup>131</sup>

(BCP).<sup>134</sup> The resulting LED has an electroluminescence wavelength of 868 nm and a high-peak external quantum efficiency of only 0.6%, which may be further improved by variations in the capping ligand of the SiNPs.

## 1.7 Concluding Remarks

Since the discovery of the fluorescent properties of semiconductor nanomaterials, major steps have been made in the synthesis and surface modification of these materials. Stability issues have been appropriately treated, and the synthesis of QDs and Si NPs has been significantly optimized. Nowadays, a broad range of functional groups can be attached onto the NPs, making them suitable for various applications such as in bioimaging or photovoltaic devices, which all require specific properties regarding solubility, hydrophilicity, fluorescence emission wavelength, as well as suitable surface groups.

## 1.8 Thesis Outline

Si NPs are fluorescent nanomaterials with unique photophysical properties. In this thesis, the development of a reproducible synthetic approach towards biocompatible and biofunctional Si NPs is described, as well as the investigations into their toxicity.

In **Chapter 2** the synthesis of *n*-butyl-terminated Si NPs via the oxidation of magnesium silicide is described. The purified Si NPs were studied in detail by IR, NMR, UV-Vis absorption spectroscopy and steady-state and time-resolved fluorescence. The silicon core size was determined via TEM measurements. The Si NPs were fractionated on size, after which the optical properties were investigated, revealing the size dependent photophysical properties of Si NPs.

**Chapter 3** describes the synthesis of butylene-terminated Si NPs, making use of a functional Grignard reagent. Thiol-ene coupling chemistry allowed for the facile and versatile functionalization of these Si NPs. This resulted in a series of functional Si NPs, of which the optical properties remained unaltered. The versatility of the thiol-ene coupling is shown to be promising for further functionalization with biomolecules, as described in the next chapter.

**Chapter 4** describes the attachment of  $\alpha$ -mercapto,  $\omega$ -carboxy-functional molecules onto the Si NPs via thiol-ene chemistry. Three differently sized spacers were employed, after which DNA was coupled via the carboxylic acid end groups. The attachment of ss-DNA and subsequent hybridization to a complementary DNA strand was confirmed by a combination of UV-Vis absorption, fluorescence and gel electrophoresis experiments.

**Chapter 5** treats the toxicology of Si NPs. Si NPs were prepared via the reduction of silicon tetrachloride, followed by the coupling of functional alkenes via hydrosilylation. Si NPs with three different end groups were tested on human Caco-2 cells, namely:  $\text{-NH}_2$  (positively charged),  $\text{-N}_3$  (neutral) and  $\text{-COOH}$  (negatively charged) end groups. Surface charge on the Si NPs is likely the main factor causing toxic effects of Si NPs, since the  $\text{NH}_2$ -terminated Si NPs display cytotoxic effects, the  $\text{N}_3$ -terminated Si NPs only moderate cytotoxic effects, while the  $\text{COOH}$ -terminated Si NPs showed no significant cytotoxicity.

In **Chapter 6** the achievements and remaining issues are discussed, as well as recommendations for further research, which places this work into context.

## 1.9 References

- (1) Roduner, E. *Chem. Soc. Rev.* **2006**, 35, 583.
- (2) Shim, J.-H.; Lee, B.-J.; Cho, Y. W. *Surf. Sci.* **2002**, 512, 262.
- (3) Yamamoto, Y.; Miura, T.; Nakae, Y.; Teranishi, T.; Miyake, M.; Hori, H. *Physica B* **2003**, 329-333, 1183.
- (4) Haruta, M. *Catal. Today* **1997**, 36, 153.
- (5) Brus, L. E. *J. Chem. Phys.* **1984**, 80, 4403.
- (6) Nirmal, M.; Brus, L. *Acc. Chem. Res.* **1998**, 32, 407.
- (7) Krishna, M. V. R.; Friesner, R. A. *J. Chem. Phys.* **1991**, 95, 8309.
- (8) Zorman, B.; Ramakrishna, M. V.; Friesner, R. A. *J. Phys. Chem.* **1995**, 99, 7649.
- (9) Rossetti, R.; Nakahara, S.; Brus, L. E. *J. Chem. Phys.* **1983**, 79, 1086.
- (10) Kuczynski, J. P.; Milosavljevic, B. H.; Thomas, J. K. *J. Phys. Chem.* **1983**, 87, 3368.
- (11) Ramsden, J. J.; Gratzel, M. *J. Chem. Soc., Faraday Trans.* **1984**, 80, 919.
- (12) Rajh, T.; Micic, O. I.; Nozik, A. J. *J. Phys. Chem.* **1993**, 97, 11999.
- (13) Micic, O. I.; Sprague, J.; Lu, Z.; Nozik, A. J. *Appl. Phys. Lett.* **1996**, 68, 3150.
- (14) Micic, O. I.; Nozik, A. J. *J. Lumin.* **1996**, 70, 95.
- (15) Murray, C. B.; Norris, D. J.; Bawendi, M. G. *J. Am. Chem. Soc.* **1993**, 115, 8706.
- (16) Michalet, X.; Pinaud, F. F.; Bentolila, L. A.; Tsay, J. M.; Doose, S.; Li, J. J.; Sundaresan, G.; Wu, A. M.; Gambhir, S. S.; Weiss, S. *Science* **2005**, 307, 538.
- (17) Chin, P. T. K. *PhD thesis Eindhoven University of Technology* **2008**.
- (18) Lakowicz, J. R. *Principles of Fluorescence Spectroscopy*; third ed.; Springer: Singapore, 2006.
- (19) Hines, M. A.; Guyot-Sionnest, P. *J. Phys. Chem.* **1996**, 100, 468.
- (20) Dabbousi, B. O.; Rodriguez-Viejo, J.; Mikulec, F. V.; Heine, J. R.; Mattoussi, H.; Ober, R.; Jensen, K. F.; Bawendi, M. G. *J. Phys. Chem. B* **1997**, 101, 9463.
- (21) Talapin, D. V.; Mekis, I.; Gotzinger, S.; Kornowski, A.; Benson, O.; Weller, H. *J. Phys. Chem. B* **2004**, 108, 18826.
- (22) Peng, X.; Schlamp, M. C.; Kadavanich, A. V.; Alivisatos, A. P. *J. Am. Chem. Soc.* **1997**, 119, 7019.
- (23) Kim, S.; Fisher, B.; Eisler, H.-J.; Bawendi, M. *J. Am. Chem. Soc.* **2003**, 125, 11466.
- (24) Balet, L. P.; Ivanov, S. A.; Piryatinski, A.; Achermann, M.; Klimov, V. I. *Nano Lett.* **2004**, 4, 1485.
- (25) Yu, K.; Zaman, B.; Romanova, S.; Wang, D.-s.; Ripmeester, J. A. *Small* **2005**, 1, 332.
- (26) Zrazhevskiy, P.; Sena, M.; Gao, X. *Chem. Soc. Rev.* **2010**, 39, 4326.
- (27) Sharma, P.; Brown, S.; Walter, G.; Santra, S.; Moudgil, B. *Adv. Colloid Interface Sci.* **2006**, 123-126, 471.
- (28) Biju, V.; Itoh, T.; Anas, A.; Sujith, A.; Ishikawa, M. *Anal. Bioanal. Chem.* **2008**, 391, 2469.
- (29) Biju, V.; Itoh, T.; Ishikawa, M. *Chem. Soc. Rev.* **2010**, 39, 3031.
- (30) Wang, Y.; Tang, Z.; Kotov, N. A. *Mater. Today* **2005**, 8, 20.
- (31) Wu, X.; Liu, H.; Liu, J.; Haley, K. N.; Treadway, J. A.; Larson, J. P.; Ge, N.; Peale, F.; Bruchez, M. P. *Nat. Biotechnol.* **2003**, 21, 41.
- (32) Wang, L.; Nagesha, D. K.; Selvarasah, S.; Dokmeci, M. R.; Carrier, R. L. *J. Nanobiotechnology* **2008**, 6.
- (33) Winter, J. O.; Liu, T. Y.; Korgel, B. A.; Schmidt, C. E. *Adv. Mater.* **2001**, 13, 1673.
- (34) Dahan, M.; Levi, S.; Luccardini, C.; Rostaing, P.; Riveau, B.; Triller, A. *Science* **2003**, 302, 442.
- (35) Lidke, D. S.; Nagy, P.; Heintzmann, R.; Arndt-Jovin, D. J.; Post, J. N.; Grecco, H. E.; Jares-Erijman, E. A.; Jovin, T. M. *Nat. Biotechnol.* **2004**, 22, 198.
- (36) Howarth, M.; Liu, W.; Puthenveetil, S.; Zheng, Y.; Marshall, L. F.; Schmidt, M. M.; Wittrup, K. D.; Bawendi, M. G.; Ting, A. Y. *Nat. Methods* **2008**, 5, 397.
- (37) Gao, X.; Cui, Y.; Levenson, R. M.; Chung, L. W. K.; Nie, S. *Nat. Biotechnol.* **2004**, 22, 969.
- (38) Shields, A. J. *Nat. Photonics* **2007**, 1, 215.
- (39) Coe, S.; Woo, W. K.; Bawendi, M.; Bulovic, V. *Nature* **2002**, 420, 800.
- (40) Coe-Sullivan, S.; Woo, W. K.; Steckel, J. S.; Bawendi, M.; Bulovic, V. *Org. Electron.* **2003**, 4, 123.
- (41) Anikeeva, P. O.; Halpert, J. E.; Bawendi, M. G.; Bulovic, V. *Nano Lett.* **2007**, 7, 2196.

- (42) Rafailov, E. U.; Cataluna, M. A.; Sibbett, W. *Nat. Photonics* **2007**, *1*, 395.
- (43) Gratzel, M. *Inorg. Chem.* **2005**, *44*, 6841.
- (44) Ruhle, S.; Shalom, M.; Zaban, A. *ChemPhysChem* **2010**, *11*, 2290.
- (45) Tsakalakos, L. *Mater. Sci. Eng., R* **2008**, *62*, 175.
- (46) Yu, K.; Chen, J. *Nanoscale Res. Lett.* **2009**, *4*, 1.
- (47) Hillhouse, H. W.; Beard, M. C. *Curr. Opin. Colloid Interface Sci.* **2009**, *14*, 245.
- (48) Calcott, P. D. J.; Nash, K. J.; Canham, L. T.; Kane, M. J.; Brumhead, D. *J. Lumin.* **1993**, *57*, 257.
- (49) Dinh, L. N.; Chase, L. L.; Balooch, M.; Siekhaus, W. J.; Wooten, F. *Phys. Rev. B: Condens. Matter* **1996**, *54*, 5029.
- (50) Koch, F.; Petrova-Koch, V.; Muschik, T. *J. Lumin.* **1993**, *57*, 271.
- (51) van Buuren, T.; Dinh, L. N.; Chase, L. L.; Siekhaus, W. J.; Terminello, L. J. *Phys. Rev. Lett.* **1998**, *80*, 3803.
- (52) Holmes, J. D.; Ziegler, K. J.; Doty, R. C.; Pell, L. E.; Johnston, K. P.; Korgel, B. A. *J. Am. Chem. Soc.* **2001**, *123*, 3743.
- (53) Rosso-Vasic, M.; Spruijt, E.; van Lagen, B.; De Cola, L.; Zuilhof, H. *Small* **2008**, *4*, 1835.
- (54) Huisken, F.; Ledoux, G.; Guillois, O.; Reynaud, C. *Adv. Mater.* **2002**, *14*, 1861.
- (55) Fan, J.; Chu, P. K. *Small* **2010**, *6*, 2080.
- (56) Kartsiefer, C.; Mayer, S.; Zarda, P.; Weinfurter, H. *Phys. Rev. Lett.* **2000**, *85*, 290.
- (57) Lindblom, J.; Holsa, J.; Papunen, H.; Hakkanen, H. *Am. Mineral.* **2005**, *90*, 428.
- (58) Krüger, A.; Kataoka, F.; Ozawa, M.; Fujino, T.; Suzuki, Y.; Aleksenskii, A. E.; Vul, A. Y.; Osawa, E. *Carbon* **2005**, *43*, 1722.
- (59) Ozawa, M.; Inaguma, M.; Takahashi, M.; Kataoka, F.; Krüger, A.; Osawa, E. *Adv. Mater.* **2007**, *19*, 1201.
- (60) Boudou, J. P.; Curmi, P. A.; Jelezko, F.; Wrachtrup, J.; Aubert, P.; Sennour, M.; Balasubramanian, G.; Reuter, R.; Thorel, A.; Gaffet, E. *Nanotechnology* **2009**, *20*.
- (61) Smith, B. R.; Inglis, D. W.; Sandnes, B.; Rabeau, J. R.; Zvyagin, A. V.; Gruber, D.; Noble, C. J.; Vogel, R.; Osawa, E.; Plakhotnik, T. *Small* **2009**, *5*, 1649.
- (62) Tisler, J.; Balasubramanian, G.; Naydenov, B.; Kolesov, R.; Grotz, B.; Reuter, R.; Boudou, J.-P.; Curmi, P. A.; Sennour, M.; Thorel, A.; Borsch, M.; Aulenbacher, K.; Erdmann, R.; Hemmer, P. R.; Jelezko, F.; Wrachtrup, J. *ACS Nano* **2009**, *3*, 1959.
- (63) Baker, S. N.; Baker, G. A. *Angew. Chem., Int. Ed.* **2010**, *49*, 6726.
- (64) Xu, X.; Ray, R.; Gu, Y.; Ploehn, H. J.; Gearheart, L.; Raker, K.; Scrivens, W. A. *J. Am. Chem. Soc.* **2004**, *126*, 12736.
- (65) Sun, Y.-P.; Zhou, B.; Lin, Y.; Wang, W.; Fernando, K. A. S.; Pathak, P.; Meziani, M. J.; Harruff, B. A.; Wang, X.; Wang, H.; Luo, P. G.; Yang, H.; Kose, M. E.; Chen, B.; Veca, L. M.; Xie, S.-Y. *J. Am. Chem. Soc.* **2006**, *128*, 7756.
- (66) Yang, S.-T.; Wang, X.; Wang, H.; Lu, F.; Luo, P. G.; Cao, L.; Meziani, M. J.; Liu, J.-H.; Liu, Y.; Chen, M.; Huang, Y.; Sun, Y.-P. *J. Phys. Chem. C* **2009**, *113*, 18110.
- (67) Hu, S.-L.; Niu, K.-Y.; Sun, J.; Yang, J.; Zhao, N.-Q.; Du, X.-W. *J. Mater. Chem.* **2009**, *19*, 484.
- (68) Zhou, J.; Booker, C.; Li, R.; Zhou, X.; Sham, T.-K.; Sun, X.; Ding, Z. *J. Am. Chem. Soc.* **2007**, *129*, 744.
- (69) Zhao, Q.-L.; Zhang, Z.-L.; Huang, B.-H.; Peng, J.; Zhang, M.; Pang, D.-W. *Chem. Commun.* **2008**, 5116.
- (70) Zheng, L.; Chi, Y.; Dong, Y.; Lin, J.; Wang, B. *J. Am. Chem. Soc.* **2009**, *131*, 4564.
- (71) Tian, L.; Ghosh, D.; Chen, W.; Pradhan, S.; Chang, X.; Chen, S. *Chem. Mater.* **2009**, *21*, 2803.
- (72) Liu, H.; Ye, T.; Mao, C. *Angew. Chem., Int. Ed.* **2007**, *46*, 6473.
- (73) Ray, S. C.; Saha, A.; Jana, N. R.; Sarkar, R. *J. Phys. Chem. C* **2009**, *113*, 18546.
- (74) Liu, R.; Wu, D.; Liu, S.; Koynov, K.; Knoll, W.; Li, Q. *Angew. Chem., Int. Ed.* **2009**, *48*, 4598.
- (75) Bourlinos, A. B.; Stassinopoulos, A.; Anglos, D.; Zboril, R.; Georgakilas, V.; Giannelis, E. *P. Chem. Mater.* **2008**, *20*, 4539.
- (76) Zhu, H.; Wang, X.; Li, Y.; Wang, Z.; Yang, F.; Yang, X. *Chem. Commun.* **2009**, 5118.
- (77) Wilcoxon, J. P.; Provencio, P. P.; Samara, G. A. *Phys. Rev. B: Condens. Matter* **2001**, *64*, 03.
- (78) Garoufalis, C. *J. Math. Chem.* **2009**, *46*, 934.

- (79) Tanke, R. S.; Kauzlarich, S. M.; Patten, T. E.; Pettigrew, K. A.; Murphy, D. L.; Thompson, M. E.; Lee, H. W. H. *Chem. Mater.* **2003**, *15*, 1682.
- (80) Gerung, H.; Bunge, S. D.; Boyle, T. J.; Brinker, C. J.; Han, S. M. *Chem. Commun.* **2005**, 1914.
- (81) Lambert, T. N.; Andrews, N. L.; Gerung, H.; Boyle, T. J.; Oliver, J. M.; Wilson, B. S.; Han, S. M. *Small* **2007**, *3*, 691.
- (82) Lu, X.; Ziegler, K. J.; Ghezelbash, A.; Johnston, K. P.; Korgel, B. A. *Nano Lett.* **2004**, *4*, 969.
- (83) Segura, R. A.; Reyes-Gasga, J.; Cardenas-Trivino, G. *Colloid Polym. Sci.* **2005**, *283*, 854.
- (84) Hope-Weeks, L. J. *Chem. Commun.* **2003**, *9*, 2980.
- (85) Heath, J. R. *Science* **1992**, *258*, 1131.
- (86) Shirahata, N. *Phys. Chem. Chem. Phys.* **2011**, *in print*.
- (87) Veinot, J. G. C. *Chem. Commun.* **2006**, 4160.
- (88) Wolkin, M. V.; Jorne, J.; Fauchet, P. M.; Allan, G.; Delerue, C. *Phys. Rev. Lett.* **1999**, *82*, 197.
- (89) Zhou, Z.; Brus, L.; Friesner, R. *Nano Lett.* **2003**, *3*, 163.
- (90) Heinrich, J. L.; Curtis, C. L.; Credo, G. M.; Kavanagh, K. L.; Sailor, M. J. *Science* **1992**, *255*, 66.
- (91) Rogozhina, E. V.; Eckhoff, D. A.; Gratton, E.; Braun, P. V. *J. Mater. Chem.* **2006**, *16*, 1421.
- (92) Lie, L. H.; Duerdin, M.; Tuite, E. M.; Houlton, A.; Horrocks, B. R. *J. Electroanal. Chem.* **2002**, *538-539*, 183.
- (93) Dickinson, F. M.; Alsop, T. A.; Al-Sharif, N.; Berger, C. E. M.; Datta, H. K.; Siller, L.; Chao, Y.; Tuite, E. M.; Houlton, A.; Horrocks, B. R. *Analyst* **2008**, *133*, 1573.
- (94) Troia, A.; Giovannozzi, A.; Amato, G. *Ultrason. Sonochem.* **2009**, *16*, 448.
- (95) Giovannozzi, A. M.; Rocchia, M.; Troia, A.; Bertinetti, L.; Amato, G. *Phys. Status Solidi C* **2009**, *6*, 1601.
- (96) Niu, H.; Zhang, L.; Zhu, J.; Zhang, M.; Bai, X. D. *Optoelectronics Lett.* **2010**, *6*, 81.
- (97) Umez, I.; Kondo, I.; Sugimura, A. *Appl. Phys. A: Mater. Sci. Process.* **2008**, *93*, 717.
- (98) Shirahata, N.; Linford, M. R.; Furumi, S.; Pei, L.; Sakka, Y.; Gates, R. J.; Asplund, M. C. *Chem. Commun.* **2009**, 4684.
- (99) Heintz, A. S.; Fink, M. J.; Mitchell, B. S. *Adv. Mater.* **2007**, *19*, 3984.
- (100) Heintz, A. S.; Fink, M. J.; Mitchell, B. S. *Appl. Organomet. Chem.* **2010**, *24*, 236.
- (101) Baldwin, R. K.; Pettigrew, K. A.; Ratai, E.; Augustine, M. P.; Kauzlarich, S. M. *Chem. Commun.* **2002**, *8*, 1822.
- (102) Baldwin, R. K.; Pettigrew, K. A.; Garino, J. C.; Power, P. P.; Liu, G.-Y.; Kauzlarich, S. M. *J. Am. Chem. Soc.* **2002**, *124*, 1150.
- (103) Li, X.; He, Y.; Talukdar, S. S.; Swihart, M. T. *Langmuir* **2003**, *19*, 8490.
- (104) Hua, F.; Swihart, M. T.; Ruckenstein, E. *Langmuir* **2005**, *21*, 6054.
- (105) Li, X.; He, Y.; Swihart, M. T. *Langmuir* **2004**, *20*, 4720.
- (106) Mangolini, L.; Thimsen, E.; Kortshagen, U. *Nano Lett.* **2005**, *5*, 655.
- (107) Jurbergs, D.; Rogojina, E.; Mangolini, L.; Kortshagen, U. *Appl. Phys. Lett.* **2006**, *88*.
- (108) Watkins, J. J.; McCarthy, T. J. *Chem. Mater.* **1995**, *7*, 1991.
- (109) Shah, P. S.; Hanrath, T.; Johnston, K. P.; Korgel, B. A. *J. Phys. Chem. B* **2004**, *108*, 9574.
- (110) English, D. S.; Pell, L. E.; Yu, Z.; Barbara, P. F.; Korgel, B. A. *Nano Lett.* **2002**, *2*, 681.
- (111) Pettigrew, K. A.; Liu, Q.; Power, P. P.; Kauzlarich, S. M. *Chem. Mater.* **2003**, *15*, 4005.
- (112) Wilcoxon, J. P.; Samara, G. A. *Appl. Phys. Lett.* **1999**, *74*, 3164.
- (113) Warner, J. H.; Hoshino, A.; Yamamoto, K.; Tilley, R. D. *Angew. Chem., Int. Ed.* **2005**, *44*, 4550.
- (114) Zou, J.; Sanelle, P.; Pettigrew, K. A.; Kauzlarich, S. M. *J. Cluster Sci.* **2006**, *17*, 565.
- (115) Baldwin, R. K.; Pettigrew, K. A.; Garino, J. C.; Power, P. P.; Liu, G. Y.; Kauzlarich, S. M. *J. Am. Chem. Soc.* **2002**, *124*, 1150.
- (116) Zou, J.; Baldwin, R. K.; Pettigrew, K. A.; Kauzlarich, S. M. *Nano Lett.* **2004**, *4*, 1181.
- (117) Mayeri, D.; Phillips, B. L.; Augustine, M. P.; Kauzlarich, S. M. *Chem. Mater.* **2001**, *13*, 765.
- (118) Dhas, N. A.; Raj, C. P.; Gedanken, A. *Chem. Mater.* **1998**, *10*, 3278.
- (119) Sudeep, P. K.; Page, Z.; Emrick, T. *Chem. Commun.* **2008**, 6126.

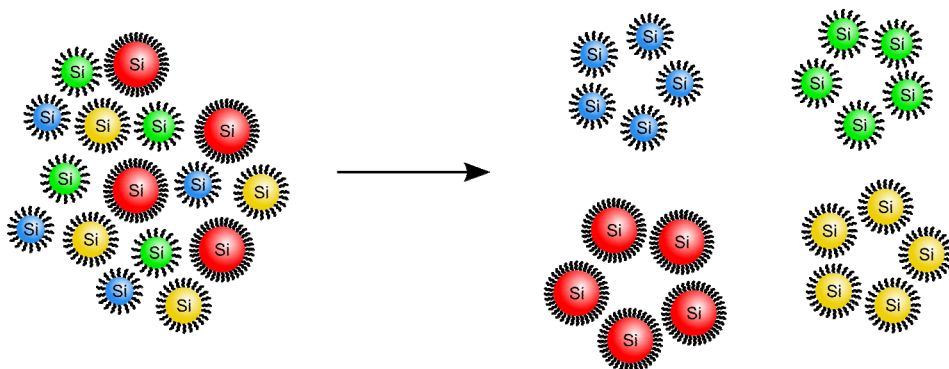
- (120) Rosso-Vasic, M.; Spruijt, E.; Popovic, Z.; Overgaag, K.; van Lagen, B.; Grandidier, B.; Vanmaekelbergh, D.; Dominguez-Gutierrez, D.; De Cola, L.; Zuilhof, H. *J. Mater. Chem.* **2009**, *19*, 5926.
- (121) Rosso-Vasic, M.; De Cola, L.; Zuilhof, H. *J. Phys. Chem. C* **2009**, *113*, 2235.
- (122) Ruizendaal, L.; Bhattacharjee, S.; Pournazari, K.; Rosso-Vasic, M.; De Haan, L. H. J.; Alink, G. M.; Marcelis, A. T. M.; Zuilhof, H. *Nanotoxicology* **2009**, *3*, 339.
- (123) Bhattacharjee, S.; de Haan, L.; Evers, N.; Jiang, X.; Marcelis, A.; Zuilhof, H.; Rietjens, I.; Alink, G. *Part. Fibre Toxicol.* **2010**, *7*, 25.
- (124) Derfus, A. M.; Chan, W. C. W.; Bhatia, S. N. *Nano Lett.* **2004**, *4*, 11.
- (125) Lewinski, N.; Colvin, V.; Drezeck, R. *Small* **2008**, *4*, 26.
- (126) Chan, W. C. W.; Nie, S. *Science* **1998**, *281*, 2016.
- (127) Selvan, S. T.; Tan, T. T.; Ying, J. Y. *Adv. Mater.* **2005**, *17*, 1620.
- (128) Hessel, C. M.; Rasch, M. R.; Hueso, J. L.; Goodfellow, B. W.; Akhavan, V. A.; Puvanakrishnan, P.; Tunnel, J. W.; Korgel, B. A. *Small* **2010**, *6*, 2026.
- (129) Alsharif, N. H.; Berger, C. E. M.; Varanasi, S. S.; Chao, Y.; Horrocks, B. R.; Datta, H. K. *Small* **2009**, *5*, 221.
- (130) He, Y.; Kang, Z. H.; Li, Q. S.; Tsang, C. H. A.; Fan, C. H.; Lee, S. T. *Angew. Chem., Int. Ed.* **2009**, *48*, 128.
- (131) Erogbogbo, F.; Yong, K.-T.; Roy, I.; Xu, G.; Prasad, P. N.; Swihart, M. T. *ACS Nano* **2008**, *2*, 873.
- (132) Erogbogbo, F.; Yong, K. T.; Hu, R.; Law, W. C.; Ding, H.; Chang, C. W.; Prasad, P. N.; Swihart, M. T. *ACS Nano* **2010**, *4*, 5131.
- (133) Foraker, A. B.; Walczak, R. J.; Cohen, M. H.; Boiarski, T. A.; Grove, C. F.; Swaan, P. W. *Pharm. Res.* **2003**, *20*, 110.
- (134) Cheng, K.-Y.; Anthony, R.; Kortshagen, U. R.; Holmes, R. J. *Nano Lett.* **2010**, *10*, 1154.

# Chapter 2

## Detailed Characterization and Size Separation of Butyl-Terminated Silicon Nanoparticles

### Abstract

Butyl-terminated silicon nanoparticles (Si NPs;  $2.6 \pm 0.7$  nm according to TEM measurements) were synthesized by the oxidation of  $\text{Mg}_2\text{Si}$  with bromine. NMR spectroscopy confirmed the structure of the Si NPs, whereas IR revealed only minor oxidation. A fluorescence emission maximum was observed at 414 nm when exciting the Si NPs at 340 nm. Size fractionation of these Si NPs by size exclusion chromatography yielded four differently sized fractions of Si NPs of narrowed size distribution. The corresponding UV-absorption spectra show in general a gradual increase of absorption towards shorter wavelengths, without an absorption maximum but a gradual increase in absorption upon shorter wavelengths. The spectra for the fractionated Si NP differ in slope; the smallest Si NPs display a blue-shift throughout the spectrum, while the larger Si NPs display a red-shift throughout the spectrum with respect to the non-fractionated Si NPs. The fluorescence emission maximum shifts from 383 nm to 445 nm from the smallest to the largest Si NPs. Fluorescence anisotropy revealed hydrodynamic radii between 1.32 and 2.34 nm for the smallest and largest particles, respectively, which is in line with the NP size as measured by TEM. The fluorescence quantum yield was measured and has values from 1.8% up to 5.2% for the largest Si NPs.



## 2.1 Introduction

Fluorescent quantum dots (QDs) are semiconductor nanomaterials that display unique optical properties due to quantum confinement effects. The size-dependent band-gap energy is responsible for the size-dependent fluorescence emission wavelength.<sup>1,2</sup> Furthermore, QDs generally have high quantum yields, narrow fluorescence emissions and they are resistant to photobleaching and chemical degradation.<sup>3</sup> Due to their size-tunable photophysical properties, many promising applications are foreseen for QDs, for example in bioimaging,<sup>4-6</sup> and solar cells.<sup>7</sup> Particularly bioanalysis<sup>3,4</sup> requires the ability to tune the desired fluorescence emission wavelength, since it allows for multiplex analysis<sup>8,9</sup> and even the individual labeling of multiple cell parts.<sup>10</sup> The more monodisperse the QDs, the more narrow their corresponding emission wavelength will be, significantly adding to their application potential.

Silicon nanoparticles (Si NPs) were shown to have similar properties as conventional group III-V QDs, as they show fluorescent behavior, which is attributed to quantum confinement effects.<sup>11-13</sup> Depending on the particle size, fluorescence emissions throughout the visible spectrum have been demonstrated, consistent with quantum confinement effects.<sup>14,15</sup> A variety of methods has been developed to prepare fluorescent Si NPs of sizes below 10 nm, such as ultrasonication of silicon wafers,<sup>16,17</sup> electrochemical dispersion of crystalline silicon,<sup>18</sup> laser-driven pyrolysis of silane<sup>15,19</sup> and synthesis in supercritical fluids by the thermal degradation of diphenylsilane.<sup>20,21</sup> Also wet-chemical methods were developed, such as the reverse micelle synthesis using organosilanes as a silicon source<sup>22-27</sup> or via the oxidation of Zintl salts.<sup>28-30</sup> These wet-chemical methods result in either hydrogen-terminated or halogen-terminated Si NPs, which are highly prone to oxidation. Since this dramatically affects the photophysical properties of the NPs,<sup>31</sup> passivation of the Si NPs using terminal alkenes<sup>22</sup> or alkyl-lithium reagents<sup>28</sup> is essential. The resulting Si-C bonds provide a robust organic shell. The advantages of Si NPs over conventional, heavy metal-containing QDs center around their non-toxicity, as has been shown in an extensive toxicological study for a set of Si NPs with organic coatings of various charges.<sup>32</sup> Furthermore, like conventional QDs, Si NPs are highly stable against photobleaching.<sup>22,23,27</sup> These characteristics open up a broad range of applications for Si NPs, particularly in bioimaging.<sup>5,6,33-35</sup> For application, it is important to minimize the width of the emission band, to allow the simultaneous use of multiple, non-overlapping fluorophores. To this aim, we envisaged the use of size fractionation of disperse Si NPs to obtain a more narrow size distribution. Furthermore, it is generally observed that quantum-confined Si NPs show a size dependence of the fluorescence lifetime, where the decrease in excitation wavelength leads to a decrease



in fluorescence lifetime.<sup>36-38</sup> These properties are important in for example fluorescence lifetime imaging (FLIM) in biological samples.

There are several ways in which NPs (<10 nm) may be fractionated on size and collected for further analysis. Field-flow fractionation (FFF) was successfully employed in the analysis of gold NPs<sup>39</sup> and fluorescent silica NPs.<sup>40</sup> However, these examples still deal with relative broad size distributions (5-100 nm). Size exclusion chromatography (SEC) fractionation has been demonstrated for the separation of polydimethylsiloxane (PDMA)-coated QDs from free polymer.<sup>41</sup> However, in this case the PDMA-coated QDs and the free polymer differ significantly in size, which gave a baseline separation on the column and makes fractionation easy. In this chapter, we demonstrate the size fractionation of a polydisperse mixture of Si NPs by preparative SEC. Furthermore, the fractionated Si NPs are characterized in detail in terms of fluorescence emission, fluorescence lifetime and fluorescence anisotropy, and the results are evaluated with respect to their sizes.

## 2.2 Results & Discussion

### 2.2.1 Synthesis and Characterization of Butyl-Terminated Si NPs

Si NPs were prepared via a wet-chemical method adapted from Kauzlarich and co-workers.<sup>28</sup> Magnesium silicide ( $\text{Mg}_2\text{Si}$ ) was oxidized with bromine in refluxing *n*-octane during 72 hours. The resulting bromine-terminated Si NPs were passivated using *n*-butyl lithium, resulting in butyl-terminated Si NPs. The main side-product, bromo-octane, and other impurities were removed using silica column chromatography, yielding approximately 50 mg of a brown / orange, waxy material.

The Si NPs were characterized by FTIR spectroscopy (Figure 1). Strong signals corresponding to C-H stretching vibrations were observed, with the symmetric  $\text{CH}_2$  stretch located at  $2873\text{ cm}^{-1}$ , the antisymmetric  $\text{CH}_2$  stretch at  $2931\text{ cm}^{-1}$  and the

antisymmetric  $\text{CH}_3$  stretch at  $2960\text{ cm}^{-1}$ . The Si-C scissoring and stretching vibrations are visible at  $1459\text{ cm}^{-1}$  and  $1260\text{ cm}^{-1}$ , respectively, in agreement with the covalent attachment of the alkyl tails to the Si NPs. The signal at  $1070\text{ cm}^{-1}$  corresponds to Si-O vibrations. The low intensity of this peak indicates that only minimal oxidation of the silicon core has taken place, as this is typically a strong signal due to the polarity of the Si-O bond.

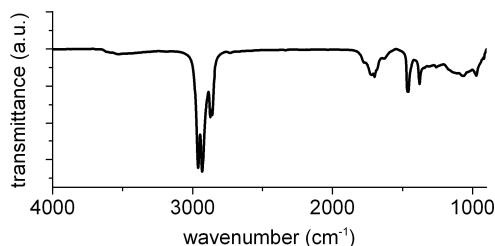


Figure 1. FT-IR spectrum of butyl-terminated Si NPs.

The butyl-terminated Si NPs were characterized in detail with NMR spectroscopy. The <sup>1</sup>H NMR spectrum (Figure 2, left) shows two broad peaks, which are attributed to the CH<sub>2</sub> (a) and CH<sub>3</sub> (b) groups of the butyl chain on the Si NPs. The broadness of the peaks indicates that the chains that are connected to the Si NPs are all slightly different, due to differences in the silicon atoms to which they are connected. The small, broad signals in the areas between 3.5 - 4.5 and 5.0 - 6.0 ppm indicate that the coating of the Si NPs does not merely consist of butyl chains. The formation of (multiply) brominated octanes under the reaction conditions used was confirmed by GC-MS and <sup>1</sup>H NMR spectroscopy on the reaction mixture, and while mono-brominated octanes are readily removed by evaporation, this is not possible for multiple brominated octanes. Upon capping of the bromine-terminated Si NPs, side reactions of *n*-butyl lithium with these brominated octanes are likely to occur, resulting in attachment of octyl bromides and elimination products thereof, and hence additional signals in the <sup>1</sup>H NMR spectrum. Diffusion-ordered spectroscopy (DOSY) NMR studies reveal that these signals belong to objects with the same diffusion coefficients as the alkyl signals of the Si NPs (Figure 2, right). This confirms that these altered moieties are indeed attached to the Si NPs.

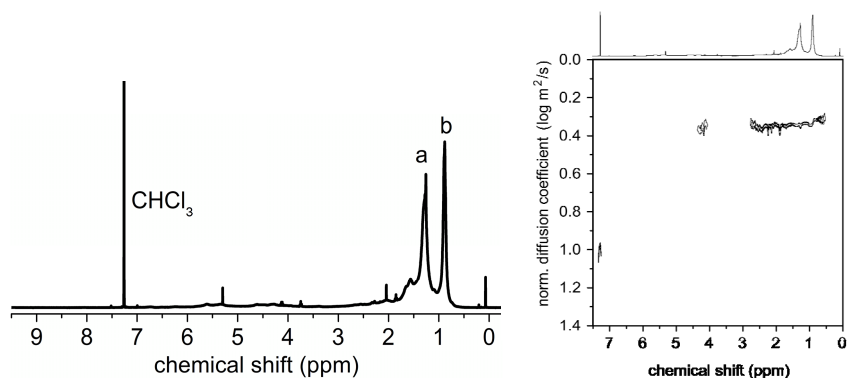


Figure 2. Left: <sup>1</sup>H NMR spectrum of butyl-terminated Si NPs; Right: DOSY NMR spectrum of butyl-terminated Si NPs.

The  $^{13}\text{C}$  NMR spectrum of the Si NPs (depicted in Figure 3, left) reveals 4 broad signals, which are assigned to  $\text{Si}-\text{CH}_2$  (b),  $\text{Si}-\text{CH}_2\text{CH}_2$  (a),  $\text{SiCH}_2\text{CH}_2\text{CH}_2$  (c) and  $\text{CH}_3$  (d) moieties. No other signals than of the solvent ( $\text{CDCl}_3$ ,  $\delta = 77.36$  ppm) were observed, confirming that the alkyl attachment onto Si is primarily as butyl chains, with only a small fraction of octyl chains. This assignment was corroborated by  $^{13}\text{C}$ -DEPT-135 and  $^1\text{H}$ - $^{13}\text{C}$ -coupled NMR spectra. In the  $^{13}\text{C}$ -DEPT-135 the signal at 14 ppm (d) gives a positive signal, and the other three negative signals, respectively corresponding to mono- and di-substituted carbon atoms. The  $^1\text{H}$ - $^{13}\text{C}$ -coupled NMR spectrum is shown in Figure 3, right. The signal resulting from (b) in the  $^1\text{H}$  NMR spectrum is coupled with signal (d) in the  $^{13}\text{C}$  NMR spectrum, hence the signals for the terminal  $\text{CH}_3$  group.

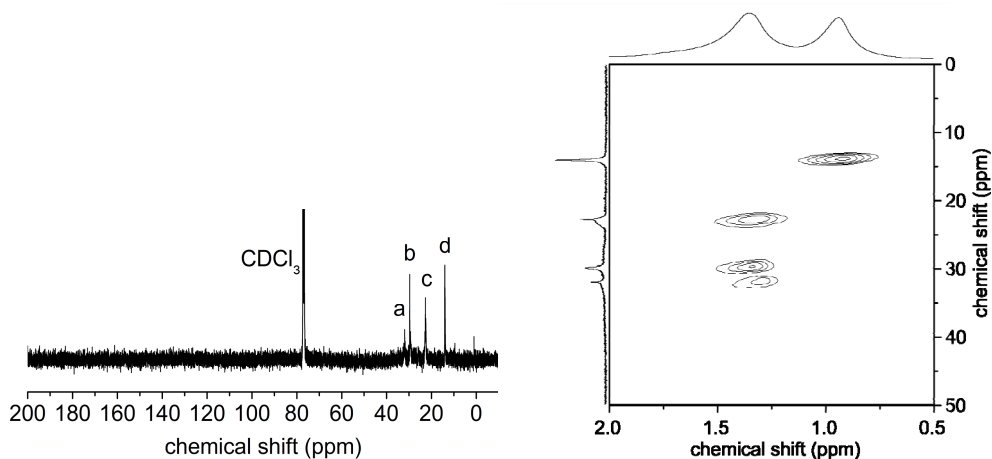


Figure 3. Left:  $^{13}\text{C}$  NMR spectrum of butyl-terminated Si NPs; Right:  $^1\text{H}$ - $^{13}\text{C}$ -coupled NMR spectrum of butyl-terminated Si NPs.

The size of the Si NPs was determined with transmission electron microscopy (TEM), where the Si core of the NPs was measured without further staining. By measuring the size of a representative number of Si NPs (141) in multiple images a reliable size-distribution was determined. No Si NPs were excluded in this measurement. The synthesized butyl-capped Si NPs have a core diameter of  $2.6 \pm 0.7$  nm (Figure 4, left) and the radius-based PDI is 1.30 (see appendix for formula). This measured size is significantly smaller than reported earlier for Si NPs synthesized using the same method ( $4.9 \pm 2.3$  nm);<sup>28</sup> moreover, the size-distribution is narrower, even without the exclusion of Si NPs above or under a certain size. These differences are likely due to the use of a different (commercially available) source of magnesium silicide.

The UV-Vis absorption spectrum of the Si NPs shows an onset of absorption around 450 nm, and a gradual monotonous increase with decreasing wavelengths (Figure 4, right). The emission spectrum is shown for an excitation wavelength of 340 nm, and displays a maximum emission at 414 nm with a full width at half maximum (FWHM) of 132 nm. The Stokes shift in this sample is thereby larger than measured before for similar Si NPs, where the  $\lambda_{\text{max, em}} = 390$  nm when excited at 340 nm.<sup>28</sup>

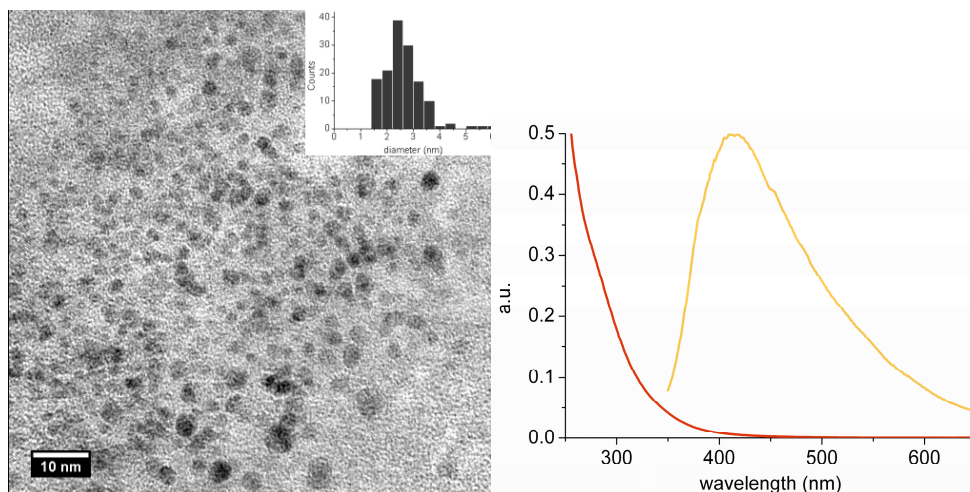


Figure 4. Left: TEM image of butyl-terminated Si NPs with size distribution histogram; Right: UV absorption and fluorescence emission of these Si NPs measured in 1,2-dichloroethane ( $\lambda_{\text{exc}} = 340$  nm).

### 2.2.2 Size Separation of Butyl-Capped Si NPs

Although the observed size distribution ( $2.6 \pm 0.7$  nm) is relatively narrow, the need for further fractionation on size becomes apparent in the fluorescence emission spectrum, since a more narrow size-distribution of the Si NPs is expected to lead to a more narrow fluorescence emission wavelength. This has important implications, since there will be less overlap between different fluorophores, allowing for more precise labeling and detection. The Si NPs were analyzed with size exclusion chromatography (SEC) as shown in Figure 5, left. The trace shows that the Si NPs elute over a large part of the exclusion area of the column (PLgel 5  $\mu\text{m}$  500 Å), with the peak maximum located at a mass of  $5 \times 10^2$  (based on calibration with polystyrene standards); this value is not quantitatively

accurate, but gains significance when compared with the corresponding data obtained from the fractionated samples (*vide infra*). From multiple injections, four fractions were collected and the SEC traces are depicted in Figure 5, right. The fractionation indeed yielded material of different sizes, as demonstrated (Figure 5, left). The separate fractions still have relatively broad size distributions, and although the high molecular weight areas are distinctly different, all fractions still contain a significant amount of low molecular-weight material. The peak maxima for fraction 1 to 4 are located at masses of  $1.0 \times 10^3$ ,  $8.0 \times 10^2$ ,  $5.0 \times 10^2$  and  $3.0 \times 10^2$ , respectively (based on polystyrene reference compounds).

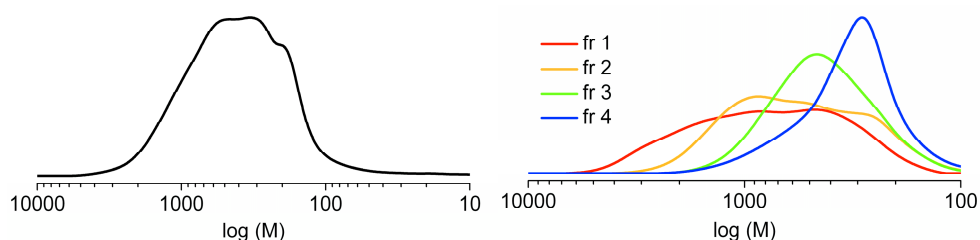


Figure 5. Left: GPC trace of Si NPs before fractionation. Right: GPC traces of Si NPs after fractionation. (Normalized area)

### 2.2.3 Size-Dependent Photophysical Analysis

In Figure 6, the UV-Vis absorption spectra of the different fractions are shown. In line with the resulting size distributions the samples do not display a distinct absorption maximum, however, a clear absorption red shift with increasing particle size is

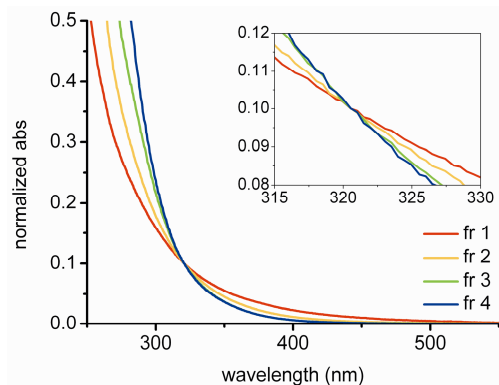


Figure 6. Normalized UV-Vis absorption of size-fractionated Si NPs in n-hexane.

observed. The inset in the graph shows the absorption around 320 nm (at which wavelength the spectra are normalized to  $\text{abs} = 0.1$ ), from which it becomes apparent that the fractions of the Si NPs all have different slopes. The largest NPs (red line) display the highest absorption at longer wavelengths, and the lowest at smaller wavelengths. For the smallest NPs the opposite trend is observed. This is in line with the earlier observations for QDs of increasing size where larger QDs display an absorption red-shift.<sup>15</sup>

Steady-state fluorescence measurements on the Si NPs revealed a red-shift for the larger Si NPs ( $\Delta = 62$  nm). In Figure 7 the normalized fluorescence emission spectra are depicted at an excitation wavelength of 340 nm. A significant red-shift of the fluorescence emission maxima from 383 nm to 445 nm was observed between fractions 4 and 1. The emission maxima and FWHM values are summarized in Table 1. The red-shift in the fluorescence emission maxima is in line with the expectations that smaller Si NPs (fraction 4) emit at shorter wavelengths than larger Si NPs (fraction 1).<sup>15</sup> The FWHM values (in eV) are decreased in the fractionated samples, as compared to the original mixture. This is due to the more narrow size distribution of the Si NPs, which results in a smaller FWHM value.

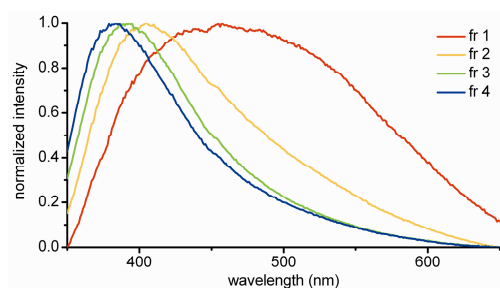


Figure 7. Normalized fluorescence emission of Si NPs in n-hexane,  $\lambda_{\text{exc}} = 340$  nm.

Table 1. Fluorescence emission properties of the Si NPs before and after fractionation, when excited at 340 nm in n-hexane.

	$\lambda_{\text{em, max}}$ [nm]	FWHM [nm]	FWHM [eV]
before fractionation	414	132	0.94
fraction 1	445	199	0.67
fraction 2	405	123	0.86
fraction 3	391	92	0.70
fraction 4	383	87	0.70

Fluorescence lifetimes and fluorescence anisotropy rotation correlation times of fractionated Si NPs were recorded at  $\lambda_{\text{exc}} = 372$  nm in 1,2-dichloroethane. The Si NPs intrinsically have a non-uniform fluorescence lifetime, due to small differences in structure and size between individual Si NPs. In general, indirect band-gap semiconductor QDs display intrinsic inhomogeneous fluorescence lifetimes.<sup>37</sup> Therefore, the fluorescence lifetime is shown as an amplitude-weighted average. The fluorescence lifetime decay was fitted with a 3-exponential fit, from which the amplitude-weighted average was calculated according to Equation 1, where  $\tau_{av}$  is the amplitude weighted average,  $a_i$  the amplitude of decay  $i$ , and  $\tau_i$  the fluorescence lifetime time constant of decay  $i$ .

$$\tau_{av} = \frac{\sum_{i=1}^n a_i \tau_i^2}{\sum_{i=1}^n a_i \tau_i} \quad (1)$$

For semiconductor QDs, an increase in fluorescence lifetime is generally observed with increasing NP size.<sup>37,38</sup> This trend is not evident from our data. This is likely due to the relatively narrow size distribution before fractionation, which results in only minor differences in the resulting fractions in fluorescence lifetime.

Table 2. Fluorescence lifetimes of fractionated Si NPs.

fraction	$\tau_{av}$ [ns], $\lambda_{exc} = 372$ nm
1	2.93
2	3.18
3	3.84
4	3.56

The fluorescence rotation correlation time ( $\tau_r$ ) was recorded at an excitation wavelength of 372 nm, at 25 °C. 1-Octanol was chosen as a solvent, because of its considerable viscosity at this temperature. The data was fit with a single component tail fit. This is only possible when the measured material is ideally spherical.<sup>42</sup> From the measured data, the hydrodynamic diameter of the Si NPs was calculated according to the Debye-Stokes-Einstein relation<sup>43</sup> (Equation 2), where  $\tau_r$  is the rotation correlation time constant  $\eta$  the viscosity of the solvent (1-octanol: 7.288 mPa s at 25 °C),<sup>44</sup>  $V$  is the hydrodynamic volume of the NP ( $V = 4/3 \cdot \pi \cdot r^3$  [m<sup>3</sup>]),  $N_A$  the Avogadro number,  $R$  the gas constant and  $T$  the temperature (K).

$$\tau_r = \frac{\eta \cdot V \cdot N_A}{R \cdot T} \quad (2)$$

The results are depicted in Table 3 and show a clear trend, in line with fraction 1 containing the largest Si NPs. The length of a stretched butyl chain attached to a silicon atom is 0.64 nm, therefore the butyl tails on the Si NPs contribute to an additional 1.3 nm on top of the diameter of the silicon core as measured by TEM ( $2.6 \pm 0.7$  nm). From the rotation correlation time the largest Si NPs have a diameter of 1.43 nm. This is smaller than expected from the TEM results, but these differences may be due to light scattering.<sup>42</sup> This plays a particularly important role in dilute solutions where the intensity is low, which is the case for the samples of the Si NPs. Although the absolute values for the Si NP diameter do not translate directly to the TEM results, the trend in the fractionation of the Si NPs is clearly visible.



Table 3. Fluorescence anisotropy data measured in 1-octanol.

fraction	$\tau_f$ [ps] $\lambda_{exc} = 372$ nm, 25 °C	hydrodynamic diameter [nm]
1	2724	1.43
2	2512	1.39
3	1667	1.21
4	1313	1.12

The quantum yields (QYs) of the different fractions of Si NPs were measured at three different wavelengths: 350 nm, 366 nm and 496 nm. As depicted in Table 4, the QY rises from about 1.8 to 5.2% when exciting the largest Si NPs at a longer wavelength. This phenomenon has been observed before for Si NPs with an emission wavelength of 693 nm, having a QY of 1.8%.<sup>45</sup> In the same study, the Si NPs at an emission maximum of 765 nm already have a QY of  $46 \pm 11\%$  at the same excitation wavelength. The observed QYs of our Si NPs are relatively low, and may suggest a higher degree of oxidation of the Si NPs,<sup>46</sup> however, IR analysis does not indicate significant oxidation. Furthermore, the measurements that show the lower QYs at higher oxidation grade were performed at an emission wavelength of around 850 nm. Other studies show the wavelength-dependence of the QY, where a longer emission wavelength is correlated to a higher QY.<sup>45</sup> Most likely, the reason for the QY not to exceed 5.5 % appears to be an intrinsic property of the Si NPs, which may be higher for larger Si NPs.

Table 4. Fluorescence quantum yield.

fraction	$\phi \lambda_{exc}$ 350 nm [%]	$\phi \lambda_{exc}$ 366nm [%]	$\phi \lambda_{exc}$ 496 nm [%]
1	$1.77 \pm 0.02$	$2.50 \pm 0.08$	$5.23 \pm 0.29$
2	$1.95 \pm 0.11$	$2.78 \pm 0.12$	$5.06 \pm 0.29$
3	$1.24 \pm 0.03$	$1.79 \pm 0.02$	-
4	$1.80 \pm 0.04$	$2.70 \pm 0.03$	-

The size of the Si NPs was further investigated using Diffusion Ordered Spectroscopy (DOSY) NMR. Table 5 gives a summary of the relative diffusion coefficients of the fractionated samples. A higher relative diffusion coefficient implies that the molecules or particles in the sample move faster. The trend from fraction 1 to 4, from the smallest to the largest Si NPs is confirmed by a lower relative diffusion coefficient for samples with larger Si NPs.

Table 5. Diffusion coefficients in DOSY NMR spectroscopy.

fraction	diffusion coefficient relative to $\text{CDCl}_3$ [-]
1	0.24
2	0.28
3	0.32
4	0.35

The Si NPs were analyzed using X-ray photoelectron spectroscopy (XPS) by dropcasting samples of the different fractions on gold surfaces. The  $\text{C}_{1s}$  narrow scans show a single peak at 285 eV for the carbon bound carbon, with a slight shoulder at the higher binding energy side. This may be due to the presence of bromine-bound carbon in the sample, as a result of the earlier mentioned side reactions with bromo-octanes to the Si NPs. This is also observed by the presence of minor amounts of bromine in each sample. Furthermore, the  $\text{Si}_{2p}$  narrow scans show a single peak at 102.0 eV, indicating a single type of silicon and the absence of silicon oxide, since such a signal would appear at 104.9 eV for Si NPs (Chapter 3). From these measurements, the Si:C ratio in each sample was obtained. Table 6 gives the ratios for the different fractions, which shows that as Si NP size decreases, the relative Si content of the sample also decreases, in line with the size separation.

Table 6. Si:C ratio in the samples as measured with XPS

fraction	Si:C ratio
1	1 : 1.6
2	1 : 7.8
3	1 : 16
4	1 : 36

## 2.3 Conclusions

Butyl-terminated Si NPs were successfully prepared by oxidation of  $\text{Mg}_2\text{Si}$  with  $\text{Br}_2$ . The butyl-terminated Si NPs were characterized by  $^1\text{H}$  NMR,  $^{13}\text{C}$  NMR and IR spectroscopy, which confirmed the structure of the particles, as well as only a minimal degree of oxidation. DOSY NMR spectroscopy revealed that a small fraction of octyl-bromides was attached. The Si NPs with a relatively narrow size distribution of  $2.6 \pm 0.7$  nm, as measured by TEM, were successfully fractionated using SEC. The resulting fractions show a red-shift in UV absorption for the larger particles. Furthermore, a red-shift in fluorescence emission is observed as well from 383 to 455 nm for the smallest and largest Si NPs respectively, which is in line with the size-dependent properties of semiconductor QDs. Furthermore, fluorescence anisotropy, DOSY NMR and XPS experiments confirmed the different sizes of the fractionated Si NPs. This implies that by proper fractionation of Si NPs, the fluorescence wavelength can be tuned, thereby opening up opportunities for applications in bioimaging. For this, the Si NPs are required to be water-soluble, and should possess functional groups for the attachment of specific labels. The (bio)functionalization of Si NPs will be discussed in Chapter 3 and 4.

## 2.4 Experimental

All chemicals were used without further purification unless stated otherwise.  $\text{Mg}_2\text{Si}$  (99+ %), *n*-butyllithium solution (10.0 M in hexanes) and bromine (puriss) were purchased from Sigma-Aldrich. *n*-Octane (97 %, pure, dried over Na wire before use) was purchased from

Acros. THF (GPC Rectapur, distilled directly before use), MeOH (Normapur) and *n*-heptane (Normapur) were purchased from VWR. HCl (for analysis, 37 % in water), dichloromethane (reagent grade), DMF (reagent grade) were purchased from Fisher Scientific. Thioacetic acid (97 %) was purchased from Alfa Aesar. Ethyl acetate (HPLC grade) was purchased from Biosolve. For fractionation of Si NPs an Agilent 5 $\mu$ m, 100Å column with THF as eluens (unstabilized, HPLC grade, Biosolve) was used, unless stated otherwise.

#### *Synthesis and purification of butyl-terminated Si NPs.*

The procedure to synthesize butyl-terminated Si NPs was adapted from a procedure Kauzlarich and co-workers.<sup>2828</sup> The set-up was kept under argon atmosphere until work-up of the mixture, and oven-dried glassware was used. To a suspension of Mg<sub>2</sub>Si (0.50 g, 6.5 mmol) in argon-sparged *n*-octane (500 mL) bromine (2.7 mL, 52 mmol) was added. The suspension was stirred for 2 h at room temperature, during which the red-brown color of the bromine disappeared. The suspension was heated to reflux for 72 h, and during the first 24 h additional bromine (2.7 mL, 52 mmol) was added via an addition funnel in portions of 0.5 mL. The suspension was kept under argon, and solvent and bromooctane, which forms as a by-product, were removed by distillation. To the flask fresh argon-sparged *n*-octane (500 mL) was added, and the suspension was cooled on ice before *n*-BuLi in hexanes (10.0 mL, 10 M, 100 mmol) was added using a gastight syringe. The reaction mixture was stirred overnight at room temperature, after which MeOH (10 mL) was added dropwise to quench the excess of *n*-BuLi, followed by stirring of the mixture for another 1 h. The mixture was filtered and extracted with aqueous HCl (1M, 1×), distilled water (3×), and the organic layer was dried over MgSO<sub>4</sub>. Solvents were removed under reduced pressure and the Si NPs were further purified using automated flash column chromatography (Biotage) using a gradient of ethyl acetate and heptane, yielding 50 mg of Si NPs as a yellow oil.

#### *Size separation of butyl-terminated Si NPs.*

The purified Si NPs were fractionated on size using a Agilent 5 $\mu$ m, 100Å column, using unstabilized THF as eluens. Fractions were collected from 6 – 7, 7 – 8, 8 – 9 and 9 – 10 minutes. Solvent was evaporated before further measurements were carried out. Shown spectra were obtained using an Agilent 5 $\mu$ m, 500Å column with CHCl<sub>3</sub> (HPLC grade, Biosolve) as eluens.

### Optical measurements

UV spectra were recorded on a Varian Cary 50 UV-Vis spectrophotometer using *n*-hexane as solvent. Samples were dissolved in 1,2-dichloroethane for steady-state and time-resolved fluorescence measurements, and the concentration was adjusted to an OD  $\lambda_{\text{exc}} \leq 0.1$ . All fluorescence measurements were performed on an Edinburgh Instruments FLS900 fluorescence spectrometer using F900 software. A 334 nm pulsed LED and a 372 nm pulsed diode laser (PicoQuant, Berlin) were used for the fluorescence lifetime measurements. Fluorescence lifetime emission was measured at the corresponding fluorescence emission maxima, and the resulting data were fit with the Fasta program of Edinburgh Instruments. Fluorescence anisotropy was measured at  $25 \pm 1$  °C using a 372 nm pulsed diode laser (PicoQuant, Berlin) at the corresponding emission wavelength maxima. Data was fitted using the F900 program of Edinburgh Instruments.

Quantum yields were measured by a comparative method, using quinine sulphate in 0.1 M  $\text{H}_2\text{SO}_4$  ( $\lambda_{\text{exc}} = 350$  nm,  $\phi = 0.58$ ), 9,10-diphenylanthracene in cyclohexane ( $\lambda_{\text{exc}} = 366$  nm,  $\phi = 0.95$ ) and fluorescein in 0.1M NaOH ( $\lambda_{\text{exc}} = 496$  nm,  $\phi = 0.95 \pm 0.05$ ) as reference compounds. Si NP samples were dissolved in 1,2-dichloroethane. Data were corrected for optical density of the sample and refractive index of the different solvents used.

Infrared spectra were measured on a Bruker vector 22 FTIR using a solution of the sample in a  $\text{CCl}_4$  film between NaCl crystals.

XPS measurements were performed on a Jeol JPS-9200 system using a standard Al  $\text{K}_{\alpha}$  source with an X-ray power of 300W, an analyzer pass energy of 10 eV, and energy resolution of  $< 0.65$  eV. All  $\text{C}_{1s}$  (C-C) were calibrated to binding energies of 285.0 eV.

$^1\text{H}$  (and  $^{13}\text{C}$ ) NMR spectra were recorded on a Bruker 400 (100) MHz Avance machine with  $\text{CDCl}_3$  or  $\text{D}_2\text{O}$  as solvent. Chemical shifts are reported in parts per million ( $\delta$ ) relative to  $\text{CHCl}_3$  (7.26 ppm for  $^1\text{H}$  and 77.2 ppm for  $^{13}\text{C}$ ) or  $\text{H}_2\text{O}$  (4.79 ppm for  $^1\text{H}$ ) as internal standard.

Transmission electron microscopy (TEM) was performed on a Tecnai G<sup>2</sup> Sphera TEM (FEI) operated at 200 kV. Samples were prepared by dropcasting a diluted solution of the nanoparticles on a carbon coated copper TEM grid (Agar Scientific). Images were analyzed with ImageJ v. 1.42e.

## 2.5 References

- (1) Alivisatos, A. P. *Science* **1996**, 271, 933.
- (2) Brus, L. J. *Phys. Chem.* **1986**, 90, 2555.
- (3) Bruchez, M., Jr.; Moronne, M.; Gin, P.; Weiss, S.; Alivisatos, A. P. *Science* **1998**, 281, 2013.
- (4) Biju, V.; Itoh, T.; Ishikawa, M. *Chem. Soc. Rev.* **2010**, 39, 3031.
- (5) Derfus, A. M.; Chan, W. C. W.; Bhatia, S. N. *Adv. Mater.* **2004**, 16, 961.
- (6) Lidke, D. S.; Nagy, P.; Heintzmann, R.; Arndt-Jovin, D. J.; Post, J. N.; Grecco, H. E.; Jares-Erijman, E. A.; Jovin, T. M. *Nat. Biotechnol.* **2004**, 22, 198.
- (7) Rühle, S.; Shalom, M.; Zaban, A. *ChemPhysChem* **2010**, 11, 2290.
- (8) Zahavy, E.; Heleg-Shabtai, V.; Zafrani, Y.; Marciano, D.; Yitzhaki, S. *J. Fluoresc.* **2010**, 20, 389.
- (9) Han, M.; Gao, X.; Su, J. Z.; Nie, S. *Nat Biotech* **2001**, 19, 631.
- (10) Chan, W. C. W.; Maxwell, D. J.; Gao, X. H.; Bailey, R. E.; Han, M. Y.; Nie, S. M. *Curr. Opin. Biotechnol.* **2002**, 13, 40.
- (11) Calcott, P. D. J.; Nash, K. J.; Canham, L. T.; Kane, M. J.; Brumhead, D. J. *Lumin.* **1993**, 57, 257.
- (12) Dinh, L. N.; Chase, L. L.; Balooch, M.; Siekhaus, W. J.; Wooten, F. *Phys. Rev. B: Condens. Matter* **1996**, 54, 5029.
- (13) Koch, F.; Petrova-Koch, V.; Muschik, T. J. *Lumin.* **1993**, 57, 271.
- (14) Belomoin, G.; Therrien, J.; Smith, A.; Rao, S.; Twesten, R.; Chaieb, S.; Nayfeh, M. H.; Wagner, L.; Mitas, L. *Appl. Phys. Lett.* **2002**, 80, 841.
- (15) Huiskens, F.; Ledoux, G.; Guillois, O.; Reynaud, C. *Adv. Mater.* **2002**, 14, 1861.
- (16) Heinrich, J. L.; Curtis, C. L.; Credo, G. M.; Kavanagh, K. L.; Sailor, M. J. *Science* **1992**, 255, 66.
- (17) Yamani, Z.; Ashhab, S.; Nayfeh, A.; Thompson, W. H.; Nayfeh, M. J. *Appl. Phys.* **1998**, 83, 3929.
- (18) Rogozhina, E. V.; Eckhoff, D. A.; Gratton, E.; Braun, P. V. *J. Mater. Chem.* **2006**, 16, 1421.
- (19) Li, X.; He, Y.; Talukdar, S. S.; Swihart, M. T. *Langmuir* **2003**, 19, 8490.
- (20) Holmes, J. D.; Ziegler, K. J.; Doty, R. C.; Pell, L. E.; Johnston, K. P.; Korgel, B. A. *J. Am. Chem. Soc.* **2001**, 123, 3743.
- (21) English, D. S.; Pell, L. E.; Yu, Z.; Barbara, P. F.; Korgel, B. A. *Nano Lett.* **2002**, 2, 681.
- (22) Rosso-Vasic, M.; Spruijt, E.; van Lagen, B.; De Cola, L.; Zuilhof, H. *Small* **2008**, 4, 1835.
- (23) Warner, J. H.; Hoshino, A.; Yamamoto, K.; Tilley, R. D. *Angew. Chem., Int. Ed.* **2005**, 44, 4550.
- (24) Wilcoxon, J. P.; Samara, G. A. *Appl. Phys. Lett.* **1999**, 74, 3164.
- (25) Wilcoxon, J. P.; Samara, G. A.; Provencio, P. N. *Phys. Rev. B: Condens. Matter* **1999**, 60, 2704.
- (26) Tilley, R. D.; Warner, J. H.; Yamamoto, K.; Matsui, I.; Fujimori, H. *Chem. Commun.* **2005**, 1833.
- (27) Zou, J.; Sanelle, P.; Pettigrew, K. A.; Kauzlarich, S. M. *J. Cluster Sci.* **2006**, 17, 565.
- (28) Pettigrew, K. A.; Liu, Q.; Power, P. P.; Kauzlarich, S. M. *Chem. Mater.* **2003**, 15, 4005.
- (29) Liu, Q.; Kauzlarich, S. M. *Mater. Sci. Eng., B* **2002**, 96, 72.
- (30) Neiner, D.; Chiu, H. W.; Kauzlarich, S. M. *J. Am. Chem. Soc.* **2006**, 128, 11016.
- (31) Ledoux, G.; Guillois, O.; Porterat, D.; Reynaud, C.; Huiskens, F.; Kohn, B.; Paillard, V. *Phys. Rev. B: Condens. Matter* **2000**, 62, 15942.
- (32) Ruizendaal, L.; Bhattacharjee, S.; Pournazari, K.; Rosso-Vasic, M.; De Haan, L. H. J.; Alink, G. M.; Marcelis, A. T. M.; Zuilhof, H. *Nanotoxicology* **2009**, 3, 339.
- (33) Biju, V.; Itoh, T.; Anas, A.; Sujith, A.; Ishikawa, M. *Anal. Bioanal. Chem.* **2008**, 391, 2469.
- (34) Zhang, Y.; Kaji, N.; Tokeshi, M.; Baba, Y. *Expert Review of Proteomics* **2007**, 4, 565.
- (35) Knopp, D.; Tang, D.; Niessner, R. *Anal. Chim. Acta* **2009**, 647, 14.
- (36) Pi, X. D.; Liptak, R. W.; Deneen Nowak, J.; Wells, N. P.; Carter, C. B.; Campbell, S. A.; Kortshagen, U. *Nanotechnology* **2008**, 19.
- (37) Delerue, C.; Allan, G.; Reynaud, C.; Guillois, O.; Ledoux, G.; Huiskens, F. *Phys. Rev. B: Condens. Matter* **2006**, 73, 235318.
- (38) Linnros, J.; Lalic, N.; Galeckas, A.; Grivickas, V. *J. Appl. Phys.* **1999**, 86, 6128.

- (39) Rameshwar, T.; Samal, S.; Lee, S.; Kim, S.; Cho, J.; Kim, I. S. *J. Nanosci. Nanotechnol.* **2006**, 6, 2461.
- (40) Zattoni, A.; Rambaldi, D. C.; Reschiglian, P.; Melucci, M.; Krol, S.; Garcia, A. M. C.; Sanz-Medel, A.; Roessner, D.; Johann, C. *J. Chromatogr., A* **2009**, 1216, 9106.
- (41) Wang, M.; Bardajee, G. R.; Kumar, S.; Nitz, M.; Scholes, G. D.; Winnik, M. A. *J. Chromatogr., A* **2009**, 1216, 5011.
- (42) Lakowicz, J. R. *Principles of Fluorescence Spectroscopy*; third ed.; Springer: Singapore, 2006.
- (43) Zondervan, R.; Kulzer, F.; Berkhout, G. C. G.; Orrit, M. *Proc. Natl. Acad. Sci. U. S. A.* **2007**, 104, 12628.
- (44) Lide, D. *CRC Handbook of Chemistry and Physics, 88th Edition*; CRC, 2007.
- (45) Jurbergs, D.; Rogojina, E.; Mangolini, L.; Kortshagen, U. *Appl. Phys. Lett.* **2006**, 88.
- (46) Anthony, R.; Kortshagen, U. *Phys. Rev. B: Condens. Matter* **2009**, 80.

## 2.6 Appendix

The radius-based polydispersity (PDI), can be calculated as follows:

$$PDI = \frac{R_w}{R_n}$$

$$R_w = \frac{\sum n_i (\frac{4}{3} \pi R_i^3) \rho R_i}{\sum n_i (\frac{4}{3} \pi R_i^3) \rho} = \frac{\sum n_i R_i^4}{\sum n_i R_i^3}$$

$$R_n = \frac{\sum n_i R_i}{\sum n_i}$$

With  $R_w$  the radius weight average,  $R_n$  the radius number average,  $R_i$  the radius of Si NP  $i$ , and  $\rho$  the density of the Si NP. A PDI of 1 indicates a perfect monodisperse collection.





*L. Ruizendaal, S. P. Pujari, V. Gevaerts, J. M. J. Paulusse, H. Zuilhof, Chem Asian J, 2011, published online 24 August, 2011.*

### 3.1 Introduction

Bioimaging is essential in gaining more information about cellular processes and of disease mechanisms. Organic dyes have been successfully employed in the labeling of cells,<sup>1</sup> but are prone to photobleaching, which severely limits the maximum exposure time<sup>2</sup> and makes multi-generation staining of cells nearly impossible. Quantum dots provide for an interesting alternative,<sup>3</sup> since they are highly resistant against photobleaching.<sup>2,4</sup> Furthermore, since the optical properties of QDs are dependent on their size due to the size-dependent band-gap energy, this allows for tuning of their absorption and fluorescence emission wavelengths.<sup>5,6</sup> QDs in biological systems have already found several applications in bioanalysis<sup>4</sup> and bioimaging.<sup>2,4,7-11</sup> These QDs are, however, intolerant to many common solvents due to the non-covalent manner in which the coating is typically attached. Moreover, the inherent toxicity of the core atoms impedes widespread application in biological environments.<sup>12,13</sup> Furthermore, the total size of typical core-shell QDs, including the typically essential stabilizing polymeric coating, is relatively large (20-50 nm), which affects cell penetration.<sup>14</sup> Only particles smaller than 5.5 nm in diameter can be excreted from the body via urine; larger particles accumulate in the body and are exposed of in other ways.<sup>15</sup>

Silicon nanoparticles (Si NPs) with feature sizes smaller than the Bohr exciton radius (~5 nm) have comparable optical properties as conventional QDs, but extensive studies have indicated their non-toxicity,<sup>16,17</sup> which displays their potential for imaging in biological systems. The protective organic coating of the Si NPs may be very thin (~0.5 nm), thereby maintaining the total diameter relatively small. Several methods to obtain Si NPs have been developed thus far, such as electrochemical dispersion of crystalline silicon,<sup>18</sup> ultrasonication of silicon wafers,<sup>19,20</sup> thermal degradation of silanes in supercritical fluids,<sup>21,22</sup> and laser-driven pyrolysis of silanes.<sup>23,24</sup> Furthermore, a number of wet-chemical bottom-up approaches has been developed, such as the synthesis in micelles using organosilanes as silicon source,<sup>25-30</sup> and through the oxidation of Zintl salts.<sup>31-33</sup> These wet-chemical methods typically result in Si NPs that are either hydrogen-terminated or halogen-terminated, and hence highly prone to oxidation. Since oxidation of the Si NPs dramatically affects their optical properties,<sup>34</sup> passivation of the Si NPs using terminal alkenes<sup>25</sup> or alkyl-lithium reagents<sup>31</sup> is essential. The resulting stable Si-C bonds form a stable shell around the Si core and prevent oxidation. However, for application of such Si NPs in selective labeling, functional moieties on the particle are desired. Direct coupling of functional groups is not trivial due to the high reactivity of the passivation agent, as well as the susceptibility of the hydrogen-terminated or halogen-terminated Si NPs towards nucleophilic attack. Several approaches may be

envisioned, for example the use of protective group chemistry,<sup>35</sup> or by employing an innocent reactive group, such as an epoxide,<sup>36</sup> azide<sup>16</sup> or terminal alkene. An excellent option for the functionalization of Si NPs is the use of “click chemistry”. Click reactions are characterized by their mild reaction conditions, the use of benign solvents, high region- and chemoselectivity and high yields.<sup>37</sup> Thiol-ene chemistry, which involves a radical-initiated coupling of a thiol to an alkene, has been known for over a century.<sup>38</sup> Recently, it has attracted great interest as a click reaction, since it does not require a metal catalyst, proceeds under very mild conditions, and is insensitive to water and oxygen.<sup>39,40</sup> The ready availability of thiol-functional biomolecules is an additional advantage. The reaction has for example been successfully applied in the modification of surfaces<sup>41-43</sup> and for the modification of 1,2-polybutadiene,<sup>44</sup> this reaction even works in sunlight without extra irradiation of UV light. Several reviews have been published which exemplify the many applications of the versatile thiol-ene reaction,<sup>40,45-47</sup> such as the synthesis of dendrimeric structures<sup>48,49</sup> and soft polymeric stamps.<sup>50,51</sup> The versatility of the reaction indicated to us that the thiol-ene click reaction may indeed be very suitable for modifying alkene-terminated Si NPs. In this chapter we present the development of alkene-terminated Si NPs, their detailed characterization, and their functionalization with a variety of functional groups using thiol-ene click chemistry (Figure 1).

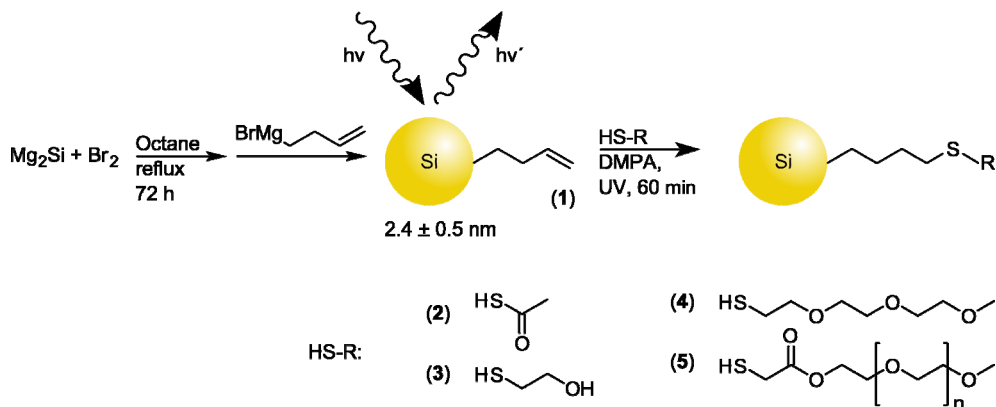


Figure 1. Functionalized fluorescent Si NPs obtained using thiol-ene click chemistry.

## 3.2 Results & Discussion

### 3.2.1 Alkene-Terminated Si NPs

Si NPs were synthesized via the oxidation of  $\text{Mg}_2\text{Si}$  with bromine to yield bromine-terminated Si NPs. Capping these bromine-terminated Si NPs with 3-butenylmagnesium bromide yielded alkene-terminated Si NPs (Si NP-ene, **1**). The resulting Si NPs were purified by size-exclusion chromatography (SEC) with ethyl acetate as eluent yielding per reaction batch Si NPs in 30 mg quantities as an orange waxy material.

The size of the Si NP core was determined by TEM. Figure 2 shows a typical TEM image of **1**; the observed particle diameter is  $2.4 \pm 0.5$  nm, with a radius-based polydispersity (PDI) of 1.12. The alkene-terminated Si NPs have a slightly smaller radius than observed earlier for butyl-terminated Si NPs.<sup>52</sup> This is likely due to the use of size exclusion chromatography (SEC) as part of the purification procedure instead of silica chromatography. SEC is based on hydrodynamic radius and may result in a different range size distribution than that obtained by a predominantly polarity-based separation.

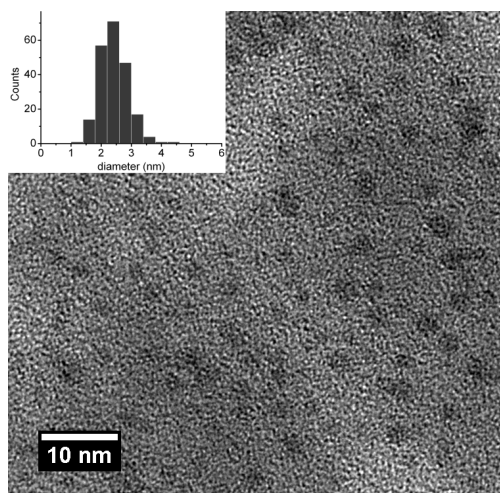


Figure 2. TEM image of alkene-terminated Si NPs (**1**), with corresponding size distribution histogram (inset).

Si NP-ene (**1**) were characterized by NMR spectroscopy. Figure 3 shows a  $^1\text{H}$  NMR spectrum in which the Si- $\text{CH}_2$  protons result in a signal at  $\delta = 0.87$  ppm (a), while the double bond protons are visible at  $\delta = 4.96$  (c) and  $\delta = 5.79$  ppm (d). The observed peak broadening is most likely due to the different chemical environments of the protons,

caused by attachment to different surface sites of the butylene chains. Moreover, due to substantial bromination of the reaction solvent, the attachment of linear and branched octyl chains, and octyl bromides is also observed ( $\delta = 3.5 - 4.5$  ppm). DOSY NMR revealed that the alkene moieties as well as these brominated species are attached to the Si NPs, since they have the same, relatively low diffusion coefficient. The low diffusion coefficient (as compared to the solvent) indicates that the signal is from a relatively large molecule, i.e. a Si NP. By integration of the  $^1\text{H}$  NMR signals, a 1 : 0.36 for the butene : octane content on the surface of the Si NP was calculated (See Appendix). The  $^{13}\text{C}$  NMR spectrum shows signals corresponding to alkene moieties at  $\delta = 112$  ppm (b) and  $\delta = 136$  ppm (c), while the alkyl chain appears as multiple peaks in the  $\delta = 21$ -31 ppm (a) region. The assignment of the signals was confirmed by 2D COSY and 2D HSQC spectra. In the COSY spectrum, it is shown that protons b and c are positioned on neighboring carbon atoms, furthermore, the  $^1\text{H}$ - $^{13}\text{C}$  HSQC confirms the assignment of a, b and c in the  $^{13}\text{C}$  NMR spectrum, due to coupling with the corresponding signals in the  $^1\text{H}$  NMR spectrum. A broad signal at  $\delta = 130$  ppm in the  $^{13}\text{C}$  NMR spectrum (d) indicates the presence of internal alkenes, most likely resulting from elimination reactions taking place on the aforementioned brominated octyl chains, due to the Grignard reagent acting as a base.

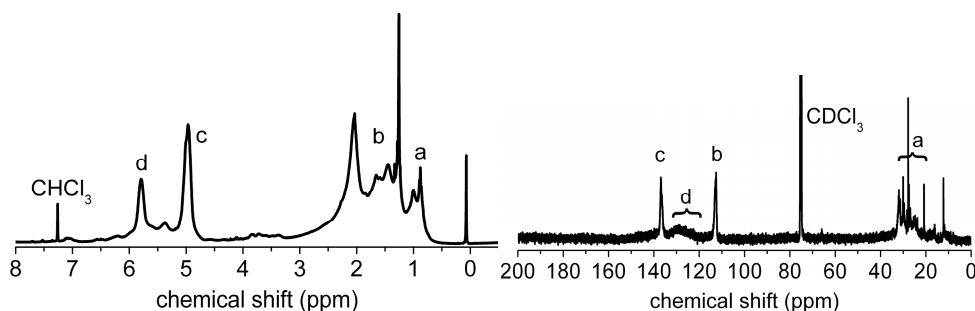


Figure 3. Left:  $^1\text{H}$  NMR spectrum; Right:  $^{13}\text{C}$  NMR spectrum of Si NP-ene (1).

Infrared spectroscopy (IR) (Figure 4) shows characteristic signals corresponding to the  $\text{CH}_2$  groups at  $2871\text{ cm}^{-1}$  and  $2959\text{ cm}^{-1}$ . Furthermore, the antisymmetric C-H stretch of the alkene moiety is visible at  $3077\text{ cm}^{-1}$ . Silicon oxide stretch frequencies are normally observed at approximately  $1000$ - $1100\text{ cm}^{-1}$ , and characterized by strong signals due to the high polarity of the Si-O bond. The silicon oxide stretch signal in the IR spectrum of the Si NP-ene is, however, low which indicates that only relatively little oxidation of the Si NPs took place during the synthesis. Since no increases of the Si-O signals were

observed for aged samples (several months), the Si core of such butylene-coated Si NPs (**1**) is presumably well protected against further oxidation.

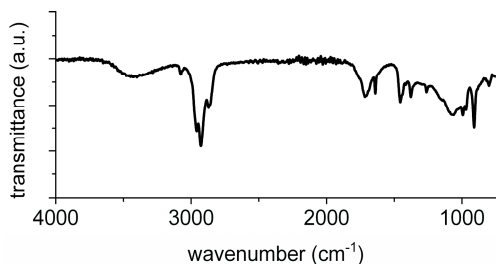


Figure 4. IR spectrum of Si NP-ene (**1**)

The Si NP-ene (**1**) were further characterized by X-ray photoelectron spectroscopy (XPS). The wide-scan XPS spectrum revealed the presence of silicon (21.1%), carbon (61.7 %), bromine (0.4 %) and oxygen (16.9 %). The oxygen in the sample is most likely mostly due to environmental entrapment in the deposited Si NPs within the XPS and not as silicon oxide, since the silicon narrow-scan spectrum displays only a single signal at 101.8 eV, with a FWHM of 1.3 eV (Figure 5, right), which is near-identical to what is observed under similar instrumental conditions for the base peak of Si at 99.4 eV with a FWHM of 0.5 eV in a silicon(111) wafer. The shift in binding energy from 99.4 eV to 101.8 eV is thus at least partially caused by charging effects, which would indeed be expected for a small object that is well-surrounded by an electrically insulating organic shell. Moreover, XPS analysis of samples of oxidized Si NPs resulted in two signals in the silicon region, the first at 101.8 eV corresponding to silicon, and a second signal at 104.9 eV for silicon oxide. The peak shift is in line with the observation that the binding energy shifts to higher levels with decreasing nanoparticle size, as compared to bulk silicon.<sup>53</sup> The narrow scan of the C<sub>1s</sub> region (Figure 5, left) reveals two types of carbon: carbon-bound carbon at 285.0 eV, and a minor fraction (14 %) of carbon atoms bound to electronegative elements such as Br or O (broad shoulder around 287 eV). The precise identity of this peak can, however, not be deduced from the XPS analysis.

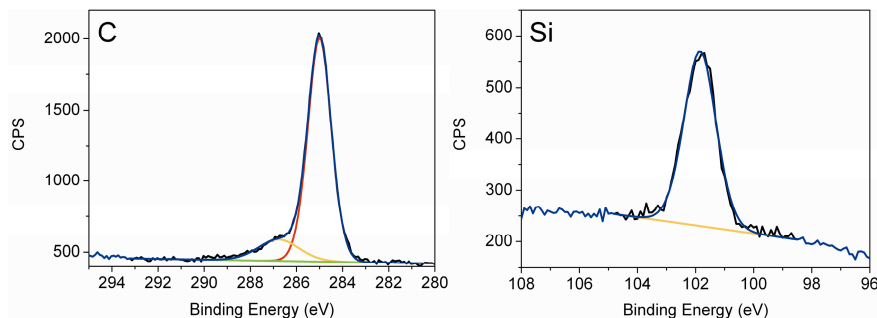


Figure 5. XPS spectra of Si NP-ene (**1**); Left: C<sub>1s</sub> narrow scan; Right: Si<sub>2p</sub> narrow scan.

The UV-Vis absorption spectrum of **1** (Figure 6, left) was recorded, but the spectrum does not display a maximum, it only shows a gradually higher absorption for decreasing wavelengths, as was observed before for this type of Si NPs.<sup>31,52</sup> From these samples, the absorption coefficient was determined to be  $0.14 \text{ (mg mL}^{-1})^{-1} \text{ cm}^{-1}$  at 300 nm and  $0.035 \text{ (mg mL}^{-1})^{-1} \text{ cm}^{-1}$  at 350 nm. The extinction coefficient was determined in  $\text{(mg mL}^{-1})^{-1} \text{ cm}^{-1}$ , since the exact molecular mass of the Si NP is unknown. Based on a molecular weight of 10,000 g/mol – estimated from our TEM-measurements in combination with a dense packing of butylene chains – a molar extinction coefficient of  $3.0 \times 10^2 \text{ M}^{-1} \text{ cm}^{-1}$  at 350 nm and  $1.4 \times 10^3 \text{ M}^{-1} \text{ cm}^{-1}$  at 300 nm was calculated. This value is slightly lower than observed for the 1.5 nm Si NPs prepared by other wet-chemical methods ( $9.4 \times 10^3 \text{ M}^{-1} \text{ cm}^{-1}$ ;  $1.1 \text{ (mg mL}^{-1})^{-1} \text{ cm}^{-1}$ )<sup>25</sup> or for those reported for 1.5 nm QDs of II-VI semiconductors, such as CdSe and CdS ( $7 \times 10^4 \text{ M}^{-1} \text{ cm}^{-1}$ ).<sup>54</sup> However, bulk silicon has an indirect band gap, which makes optical transitions without the assistance of a phonon very inefficient. The optical transition in a Si NP is very efficient in comparison to the transition in bulk silicon. The distinction between indirect and direct bandgaps is blurred in the nanometer size regime.<sup>55</sup>

The fluorescence emission spectrum is strongly dependent on the excitation wavelength. Figure 6 (right) depicts fluorescence emission spectra for several excitation wavelengths ranging from 350 nm to 450 nm. The spectra are corrected for the UV-Vis absorption at each excitation wavelength. The relatively highest fluorescence emission is observed at 535 nm at an excitation wavelength of 430 nm. This is distinctly red-shifted as compared to the Si NPs described previously in Chapter 2, which showed an emission maximum at 390 nm (obtained for irradiation at 340 nm).<sup>31</sup> For Si NPs with a gradual increase in UV-Vis absorption at shorter wavelengths, correction for UV-Vis absorption results in a red-shifted fluorescence emission maximum.

The fluorescence quantum yield (QY) was determined using a comparative method<sup>56,57</sup> at  $\lambda_{\text{exc}} = 350 \text{ nm}$ , 366 nm and 496 nm. The QYs are  $1.5 \pm 0.2 \%$  and  $1.8 \pm 0.3 \%$  for  $\lambda_{\text{exc}} = 350 \text{ nm}$  and 366 nm, respectively. The QY increases further with increasing excitation wavelength; the highest QY is observed at an excitation wavelength of 496 nm, and is  $7.1 \pm 1.2 \%$ . This is about 2 % higher than observed for the highly similar butyl-terminated Si NPs,<sup>52</sup> but still considerably smaller than the highest QY reported for Si NPs (60%).<sup>58</sup> It has been suggested that a high oxidation grade of the Si NPs results in lower quantum yields,<sup>59</sup> however, such high degrees of oxidation are absent in this case as follows from IR and XPS data – the larger size (2.5 nm here) is therefore a more likely cause.

Time-resolved fluorescence spectroscopy was performed, and the amplitude-weighted fluorescence lifetime was determined according to Equation 1, where  $\tau_{\text{av}}$  is the amplitude-weighted average,  $a_i$  the amplitude of decay  $i$ , and  $\tau_i$  the fluorescence lifetime time constant of decay  $i$ . The amplitude-weighted fluorescence lifetime is 3.40 ns, which is similar to the lifetimes observed for butyl-terminated Si NPs.<sup>52</sup> These results indicate that the optical properties of the Si NPs are not significantly influenced by the change in coating from butyl to butylene.

Equation 1.

$$\tau_{\text{av}} = \frac{\sum_{i=1}^n a_i \tau_i^2}{\sum_{i=1}^n a_i \tau_i} \quad (1)$$

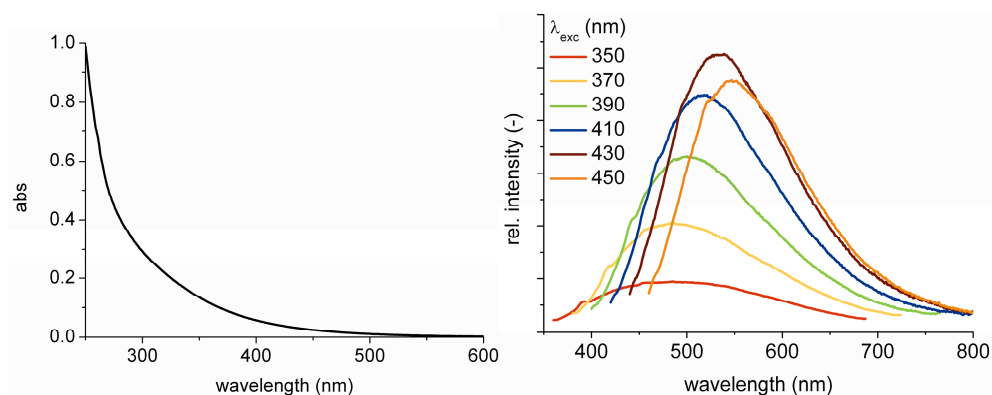


Figure 6. Left: UV-Vis absorption; Right: fluorescence emission map of Si NP-ene (1).



### 3.2.2. Thiol-ene Chemistry on Alkene-Terminated Si NPs

With the alkene moiety present on the surface of the Si NPs, functionalization with thiol-ene chemistry can be applied. Hereby, functional groups can be attached which make the Si NPs suitable for applications that require specific labeling. The Si NPs were mixed with an excess of the respective thiol and 0.2 eq. of 2,2-dimethoxy-2-phenylacetophenone (DMPA), with respect to the thiol, as photoinitiator. The mixture was exposed to UV light (365 nm) while stirring at room temperature, under ambient conditions. After 1 h,  $^1\text{H}$  NMR spectroscopy revealed complete conversion of the alkene moieties, and the functionalized Si NPs were purified via size exclusion chromatography. A broad range of thiols was selected: thiolacetic acid (Si NP-TAA, **2**) and 2-mercaptoethanol (Si NP-OH, **3**) – which provide for a functional group that can be used in further conjugation reactions – as well as thiolated triethylene glycol monomethyl ether (Si NP-EO<sub>3</sub>, **4**) and thiolated poly(ethylene glycol) monomethyl ether with a molecular weight of 5,000 g/mol (Si NP-PEG5000, **5**), both to obtain water-soluble, biocompatible Si NPs (Figure 1).

In the  $^1\text{H}$  NMR spectrum of purified Si NP-TAA (**2**) (Figure 7, left), no terminal alkenes are observed. Furthermore, a new signal at  $\delta = 2.86$  ppm (d) corresponds to the newly formed thioester, signals corresponding to the CH<sub>2</sub> next to the thioester appear at  $\delta = 1.57$  ppm (c), while the signal of the methyl next to the carbonyl appears at  $\delta = 2.32$  ppm (e). The spectra of these and all other modified Si NPs were assigned with the help of 2D-COSY NMR spectroscopy, which confirms quantitative coupling of the thiols to the Si NPs, since no terminal alkenes are observed and the intensity of the new signals fit in ratio.

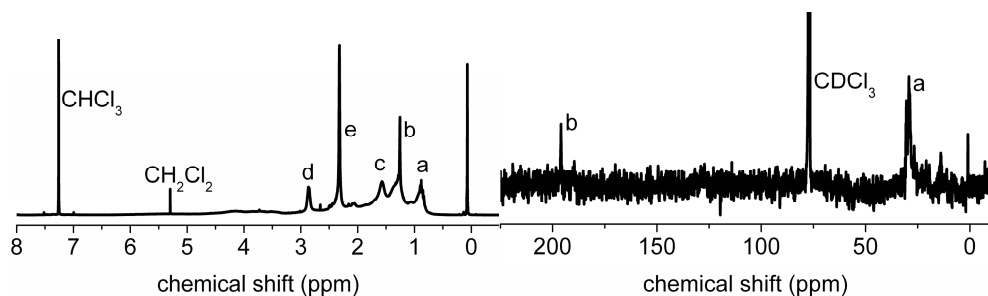


Figure 7. Left:  $^1\text{H}$  NMR spectrum; Right  $^{13}\text{C}$  NMR spectrum of Si NP-TAA (**2**).

Infrared spectroscopy was performed on the Si NPs to confirm the presence of characteristic groups and to determine whether the functionalized Si NPs retained their low oxidation grade (Figure 8). The  $\text{C}=\text{CH}_2$  antisymmetric stretch signal, which appeared at  $3077\text{ cm}^{-1}$  in the case of Si NP-ene, was absent in the spectra of the functionalized Si NPs. All functionalized Si NPs display the typical symmetric and antisymmetric stretch vibrations for  $\text{CH}_2$  bonds. The spectra have in common a weak signal ( $1000\text{--}1100\text{ cm}^{-1}$ ) corresponding to Si-O bonds, which does not increase upon functionalization, indicating that thiol-ene functionalization does not significantly increase the (low) degree of substrate oxidation. Signals for the attached functional groups are readily observed. The Si NP-TAA (2), for example, display a distinct carbonyl stretch signal at  $1690\text{ cm}^{-1}$ , confirming the presence of a thioester moiety. The Si NP-OH (3) display a broad OH stretch at  $3354\text{ cm}^{-1}$ , while the Si NP- $\text{EO}_3$  (4) display characteristic ether-bonds at  $1108\text{ cm}^{-1}$ . For the Si NP-PEG5000 (5)  $\text{CH}_2$  stretch frequencies ( $2879\text{ cm}^{-1}$ ) are broadened, which is due to the large amount of  $\text{CH}_2$  groups that is present as compared to the single terminal methoxy-group. The signals for the ether-bonds are readily observed ( $1104\text{ cm}^{-1}$ ). These typical signals confirm the coupling of the desired thiols to the Si NPs.

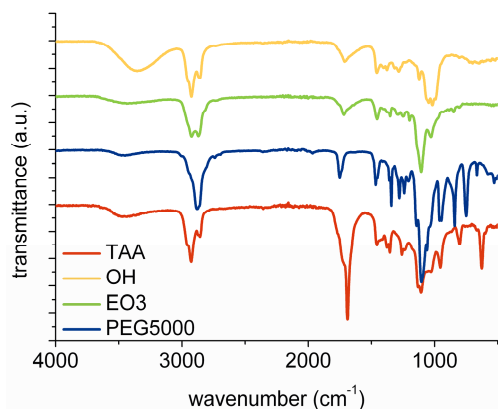


Figure 8. FTIR of Si NP-TAA (2), Si NP-OH (3), Si NP- $\text{EO}_3$  (4) and Si NP-PEG5000 (5)

The apparent size of the Si NPs was investigated using analytical SEC. Functional Si NPs 2, 3 and 4 do not, as expected, display a significantly increased hydrodynamic volume with respect to the original Si NP-ene (1). In contrast, in the case of Si NP-PEG5000 (5) a large increase in hydrodynamic volume is observed. Indications of the size increase can be obtained via comparison with polystyrene standards in SEC. Whereas the apparent

molecular weight of the starting Si NP-ene (**1**) is  $M_n = 1.6 \times 10^3$  g/mol, the attachment of poly(ethylene glycol) chains to the Si core increases this to  $M_n = 1.8 \times 10^4$  g/mol. These values are based on polystyrene reference compounds, and thereby do not give an absolute value for the molecular weight of the Si NPs, but rather a qualitative indication of the increasing hydrodynamic value.

The Si NPs were further characterized using XPS to obtain an elemental composition of the Si NPs, as well as characterizing the different functional groups. A thin film of Si NP-TAA (**2**) was cast onto a gold surface and analyzed. The XPS narrow scan spectrum of the  $C_{1s}$  region of **2** was fit with 4 components, of which the main peak at 285.0 eV corresponds to carbon-bound carbon atoms (Figure 9, left). The intensity of this signal is relatively high (78% of the total carbon content), due to the earlier mentioned side reactions that occur, which lead to significant attachment of alkyl chains (see Supporting Information). The signals for the C=O (288.0 eV) and C-S (286.4 eV) carbon atoms integrate to a 1:1 ratio. The signal at 289.3 eV (2 % of the  $C_{1s}$  total area) may arise from slight oxidation of the C=C bond. The XPS narrow scan of the  $Si_{2p}$  region (Figure 9, center) reveals only a single signal at 101.8 eV, similar as observed for Si NP-ene (**1**). The sulfur region shows a clear signal of a single type of sulfur, which was fit with a single spin-orbital doublet (Figure 9, right), in agreement with the thioether that results from the attachment step.

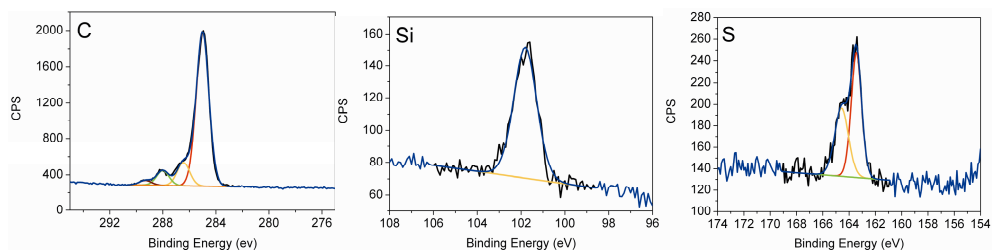


Figure 9. XPS spectra of Si NP-TAA (**2**); Left:  $C_{1s}$  narrow scan; Center:  $Si_{2p}$  narrow scan; Right:  $S_{2p}$  narrow scan.

In order to determine whether the Si NPs retain their optical properties after thiol-ene functionalization, the UV-Vis absorption spectra were recorded (Figure 10, left). As evidenced by the spectra normalized at 320 nm the absorption is not significantly affected by the modification of the Si NPs. This confirms that the Si core remains unaltered. In addition, the fluorescence emission was measured. In Figure 10 (right) the

UV-Vis absorption-corrected fluorescence emission spectra of Si NPs excited at 430 nm are shown, yielding their highest emission. The fluorescence emission maximum does not shift significantly by the modification of the Si NPs with thiol-ene chemistry, and remains at 525 nm. The signal intensity, however, does change to some degree.

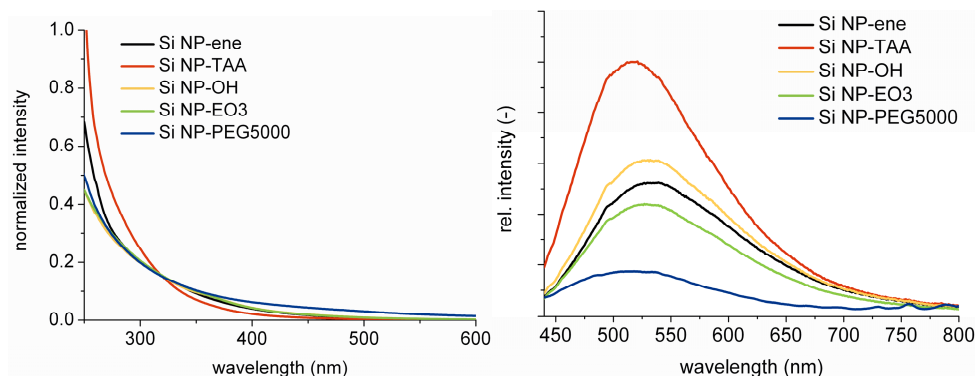


Figure 10. Left: UV-Vis absorption spectra; Right: fluorescence emission of Si NP-ene (1), Si NP-TAA (2), Si NP-OH (3), Si NP-EO<sub>3</sub> (4) and Si NP PEG5000 (5) ( $\lambda_{\text{exc}} = 430\text{nm}$ ).

Besides steady-state fluorescence spectroscopy, time-resolved fluorescence emission was studied. Table 1 summarizes the amplitude-weighted averages of the fluorescence lifetimes of the functional Si NPs excited at 372 nm. The results are all in the same time range ( $\sim 4$  ns), further confirming that thiol-ene modification does not significantly affect the Si NPs.

Table 1. Fluorescence emission lifetimes of Si NPs, before and after thiol-ene functionalization.

Sample	$\tau_{\text{av}}$ (ns)
Si NP-ene (1)	3.40
Si NP-TAA (2)	4.27
Si NP-OH (3)	3.73
Si NP-EO <sub>3</sub> (4)	3.75

### 3.3 Conclusions

The synthesis of Si NPs via the oxidation of  $\text{Mg}_2\text{Si}$  and subsequent capping with 3-butenylmagnesiumbromide resulted in alkene-functionalized Si NPs with a silicon core size of  $2.4 \pm 0.5$  nm. Thiol-ene chemistry performed on these Si NPs proved to be a facile, efficient and versatile approach to obtain a variety of functional Si NPs. The functionalization does not change the optical properties of the functionalized Si NPs significantly, in line with the Si core being the origin of the optical properties of the Si NPs. With this versatile method to couple functional groups to Si NPs, the way is opened to attach biomolecules to the Si NPs to use them as a specific label. The coupling of a carboxylic acid to the Si NPs, followed by the attachment of proteins via the natively present lysines, or  $\text{NH}_2$ -modified DNA strands is highly suitable, and will be discussed in Chapter 4.

### 3.4 Experimental

All chemicals were used without further purification unless stated otherwise.  $\text{Mg}_2\text{Si}$  (99+ %), 4-bromo-1-butene ( $\geq 98$  %), iodine ( $\geq 99.8$  %), bromine (puriss) triethyleneglycol monomethyl ether (purum), *p*-toluenesulfonic acid (reagent grade), polyethyleneglycol 5000 monomethyl ether, thioglycolic acid (99+ %), toluene ( $\geq 99.7$  % (GC)), chlorobenzene (99.9 %), 2,2'-dimethoxy-2-phenylacetophenone (99 %), 2-mercaptoethanol ( $\geq 99$  %) were purchased from Sigma-Aldrich. *n*-Octane (97 %, pure, dried over Na wire before use) and thiourea (99 %) were purchased from Acros. THF (GPC Rectapur, distilled directly before use) was purchased from VWR. HCl (for analysis, 37 % in water), dichloromethane (reagent grade), DMF (reagent grade) were purchased from Fisher Scientific. Thioacetic acid (97 %) was purchased from Alfa Aesar. For purification of the functionalized Si NPs an Agilent 5 $\mu\text{m}$ , 500Å column with chloroform as eluens (HPLC grade, Biosolve) was used, unless stated otherwise.

#### *Synthesis and purification of Si NP-ene.*

The set-up was kept under argon atmosphere until work-up of the mixture; oven-dried glassware was used. To a suspension of  $\text{Mg}_2\text{Si}$  (0.5 g, 6.5 mmol) in Ar-bubbled *n*-octane (500 mL) bromine (2.7 mL, 52 mmol) was added. Additional bromine (2.7 mL, 52 mmol) was added via an addition funnel. The suspension was stirred for 2 h at room temperature, during which the red-brown color of the bromine disappeared completely. The suspension was heated to reflux for 72 h, and during the first 24 h the bromine in

the addition funnel was added in 5 equal portions. The suspension was kept under argon, while the solvent and bromooctane were removed by distillation. To the flask fresh Ar-bubbled *n*-octane (500 mL) was added, and the suspension was cooled on ice. To a suspension of Mg curls (2.7 g, 110 mmol) in freshly distilled THF (200 mL) in an oven-dried setup under argon atmosphere, a solution of 4-bromo-1-butene (10 mL, 100 mmol) in freshly distilled THF (10 mL) was added dropwise over 15 minutes. An iodine crystal was used to initiate the reaction. After addition of the 4-bromo-1-butene, the mixture was stirred for an additional 2 h. The solution of 3-butenylmagnesium bromide was added via a cannula to the bromine-terminated Si NPs, and a white precipitate formed. The reaction mixture was stirred overnight, and MeOH (10 mL) was added dropwise to quench the excess of 3-butenylmagnesium bromide. The mixture was stirred for 1 h. The mixture was filtered, the filtrate was subsequently extracted with aqueous HCl (1M) (1×), distilled water (3×), and the organic layer was dried over  $\text{MgSO}_4$ . Solvent was removed under reduced pressure and the Si NPs were further purified using biobeads S-X1 with EtOAc as eluents, yielding 30 mg Si NPs as an orange wax.

*Synthesis triethyleneoxide-tosylate monomethyl ether (MeO-EO<sub>3</sub>-OTs, 6)*

To a solution of triethyleneglycol monomethyl ether (6.63 g, 40.3 mmol) in THF (10 mL) a solution of NaOH (2.86 g, 71.5 mmol) in water (10 mL) was added. While bubbling with  $\text{N}_2$  gas and cooling with ice, a solution of *p*-toluenesulfonyl chloride (7.85 g, 41.9 mmol) in THF (12 mL) was added dropwise over 30 min. The solution was stirred overnight while warming to room temperature. The reaction mixture was extracted with diethyl ether (3×), and the combined organic layers were extracted with water (3×), until the pH of the extract was neutral. The organic phase was dried over  $\text{MgSO}_4$ , and solvent was evaporated, yielding a white powder (10.47 g, 82%).

$^1\text{H}$  NMR ( $\text{CDCl}_3$ , 400 MHz)  $\delta$  7.8 ppm (d, 2H,  $\text{CH-C-SO}_2$ ), 7.3 ppm (d, 2H,  $\text{CH-C-CH}_3$ ), 4.15 ppm (q, 2H,  $\text{SO}_2\text{-O-CH}_2$ ), 3.67 - 3.52 ppm (m, 10H,  $\text{CH}_2\text{-O}$ ), 3.36 ppm (s, 3H,  $\text{CH}_3\text{-O}$ ), 2.43 ppm (s, 3H,  $\text{CH}_3\text{-C}$ ), in accordance with literature.<sup>60</sup>

*Synthesis 2-(2-(2-methoxyethoxy)ethoxy)ethanethiol (MeO-EO<sub>3</sub>-SH, 7)*

To a solution of MeO-EO<sub>3</sub>-OTs (6) (10.47 g, 32.9 mmol) in ethanol (20 mL) thiourea (2.85 g, 37.5 mmol) and water (14 mL) were added. The solution was refluxed for 3 h under  $\text{N}_2$ . A solution of NaOH (1.61 g, 40.1 mmol) in water (10 mL) was added, and the reaction mixture was refluxed for 2 h. The reaction mixture was cooled to room temperature and the volume was reduced to 20 mL, diluted with 10 mL water and

neutralized with concentrated HCl. The solution was extracted with dichloromethane (3×), the organic phase was dried over  $\text{MgSO}_4$  and the solvent was evaporated. The resulting colorless oil was purified over a silica column using a gradient of diethyl ether in heptane, yielding a colorless oil (5.38 g, 74%).

$^1\text{H}$  NMR ( $\text{CDCl}_3$ , 400 MHz)  $\delta$  1.58 ppm (t, 1H, SH), 2.70 ppm (q, 2H,  $\text{CH}_2\text{-SH}$ ), 3.38 ppm (s, 3H,  $\text{CH}_3\text{-O}$ ), 3.54 - 3.66 ppm (m, 10H,  $\text{CH}_2\text{-O}$ ).

$^{13}\text{C}$  NMR ( $\text{CDCl}_3$ , 100 MHz)  $\delta$  24.26 ppm ( $\text{CH}_2\text{-SH}$ ), 59.04 ppm ( $\text{CH}_3\text{-O}$ ), 70.25 - 71.96 ppm ( $\text{CH}_2\text{-O}$ ), 72.90 ppm ( $\text{HS-CH}_2\text{-CH}_2$ ).

#### *Synthesis of polyethylene glycol 5 000 monomethyl ether thiol (HS-PEG5000-OMe, 8)*

A suspension of polyethylene glycol 5 000 monomethyl ether (20 g, 4.0 mmol), thioglycolic acid (1.12 mL, 16.4 mmol), *p*-toluenesulfonic acid (0.27 g, 0.7 mmol) and  $\text{MgSO}_4$  (5 g) in toluene (150 mL) was refluxed for 8 h and stirred for 3 days at room temperature. Reaction progress was followed by  $^1\text{H}$  NMR spectroscopy. The reaction mixture was extracted with dichloromethane (2×), the organic layer was dried over  $\text{MgSO}_4$  and the solvent was evaporated. The white solid was dissolved in a minimal amount of dichloromethane and precipitated in diethyl ether ( $-78^\circ\text{C}$ ). The precipitate was filtered and dried. (17.4 g, 87 %)

$^1\text{H}$  NMR ( $\text{CDCl}_3$ , 400 MHz)  $\delta$  4.29 ppm (t, 2H,  $\text{CH}_2\text{COOCH}_2$ ), 3.6 ppm (m, 227 H,  $\text{CH}_2\text{-O}$ ,  $\text{CH}_2\text{-SH}$ ,  $\text{CH}_3\text{-O}$ ), 2.0 ppm (t, 1H, SH)

$^{13}\text{C}$  NMR ( $\text{CDCl}_3$ , 100 MHz)  $\delta$  70.56 ppm ( $\text{CH}_2\text{-O}$ )

#### *Thiol-ene click chemistry*

In general, to a solution of 10 mg Si NP-ene (1) (approx. 0.1 mmol alkene groups as determined by  $^1\text{H}$  NMR spectroscopy with an internal standard) in chlorobenzene or DMF, an excess of the thiol and 0.2 eq. of photoinitiator with respect to the thiol were added, the reaction was stirred at room temperature while exposed to UV light (365 nm) under ambient conditions.

#### *Coupling of thioacetic acid to Si NPs (2)*

A solution of thioacetic acid (200  $\mu\text{L}$ , 2.8 mmol), 2,2'-dimethoxy-2-phenylacetophenone (DMPA) in chlorobenzene (100  $\mu\text{L}$  100 mg/mL; 40  $\mu\text{mol}$ ) and Si NP-ene (1) (10 mg) was

stirred for 1 h at room temperature while irradiating with UV light (365 nm). Solvent was evaporated and the Si NPs were purified using SEC using chloroform as eluents, yielding Si NP-TAA (**2**) as an orange wax (9 mg).

#### *Coupling of HS-PEG5000-OMe (**8**) to Si NPs (**5**)*

A solution of HS-PEG5000-OMe (**8**) (1.0 g, 0.2 mmol), DMPA in chlorobenzene (100  $\mu$ L 100 mg/mL; 40  $\mu$ mol) and Si NP-ene (**1**) (10 mg) in chlorobenzene (1.5 mL) was stirred for 1 h at room temperature while irradiating with UV light (365 nm). Solvent was evaporated and the resulting Si NPs were purified using Amicon Ultra-4 centrifugal filter units (NMWL 3 kDa), yielding Si NP-PEG5000 (**5**) as a yellow wax (50 mg).

#### *Coupling of MeO-EO<sub>3</sub>-SH (**7**) to Si NPs (**4**)*

A solution of DMPA in DMF (100  $\mu$ L 100 mg/mL; 40  $\mu$ mol), MeO-EO<sub>3</sub>-SH (**7**) (120  $\mu$ L, 0.8 mmol) and Si NP-ene (**1**) (10 mg) was stirred for 1 h at room temperature while irradiating with UV light (365 nm). Solvent was evaporated and the Si NPs were purified with SEC using chloroform as eluent, yielding Si NP-EO<sub>3</sub> (**4**) as an orange wax (13 mg).

#### *Coupling of 2-mercaptoethanol to Si NPs (**3**)*

A solution of DMPA in DMF (100  $\mu$ L 100 mg/mL; 40  $\mu$ mol), 2-mercaptoethanol (200  $\mu$ L, 2.8 mmol) and Si NP-ene (**1**) (10 mg) was stirred for 1 h at room temperature while irradiating with UV light (365 nm). Solvent was evaporated and the Si NPs were purified with SEC using chloroform as eluent, yielding Si NP-OH (**3**) as an orange wax (10 mg).

#### *Optical measurements*

UV spectra were recorded on a Varian Cary 50 UV-Vis spectrophotometer using 1,2-dichloroethane as solvent. For steady-state and time-resolved fluorescence measurements, the concentrations were adjusted to  $OD_{\lambda_{exc}} \leq 0.1$ . All fluorescence measurements were performed on an Edinburgh Instruments FLS900 fluorescence spectrometer using the F900 software. A 334 nm pulsed LED and 372 nm pulsed diode laser (PicoQuant, Berlin) were used for the fluorescence lifetime measurements. Fluorescence emission lifetimes were measured at the corresponding fluorescence emission maxima and the resulting data was fitted with the Fasta program of Edinburgh Instruments. Fluorescence anisotropy was measured at  $25 \pm 1^\circ\text{C}$  using a 334 nm pulsed LED and 372 nm pulsed diode laser (PicoQuant, Berlin) at the corresponding emission wavelength maxima. Data was fitted using the F900 program of Edinburgh Instruments.



Quantum yields were measured by a comparative method, using quinine sulfate in 0.1 M  $\text{H}_2\text{SO}_4$  ( $\lambda_{\text{exc}} = 350 \text{ nm}$ ,  $\phi = 0.58$ ), 9,10-diphenylanthracene in cyclohexane ( $\lambda_{\text{exc}} = 366 \text{ nm}$ ,  $\phi = 0.95$ ) and fluorescein in 0.1 M NaOH ( $\lambda_{\text{exc}} = 496 \text{ nm}$ ,  $\phi = 0.95 \pm 0.05$ ) as reference compounds. Si NP samples were dissolved in 1,2-dichloroethane. Data were corrected for optical density of the sample and refractive index of the different solvents used.

XPS measurements were performed on a Jeol JPS-9200 system using a standard Al K $_{\alpha}$  source with an X-ray power of 300W, an analyzer pass energy of 10 eV, and energy resolution of < 0.65 eV. All C $_{1s}$  (C-C) were calibrated to binding energies of 285.0 eV.

$^1\text{H}$  (and  $^{13}\text{C}$ ) NMR spectra were recorded on a Bruker 400 (100) MHz Avance machine with  $\text{CDCl}_3$  or  $\text{D}_2\text{O}$  as solvent. Chemical shifts are reported in parts per million ( $\delta$ ) relative to  $\text{CHCl}_3$  (7.26 ppm for  $^1\text{H}$  and 77.2 ppm for  $^{13}\text{C}$ ) or  $\text{H}_2\text{O}$  (4.79 ppm for  $^1\text{H}$ ) as internal standard.

Transmission electron microscopy (TEM) was performed on a Tecnai G $^2$  Sphera TEM (FEI) operated at 200 kV. Samples were prepared by dropcasting a diluted solution of the nanoparticles on a carbon coated copper TEM grid (Agar Scientific). Images were analyzed with ImageJ v. 1.42e.

### 3.5 References

- (1) Pawley, J. B. *Handbook of Biological Confocal Microscopy*; Springer, 2006.
- (2) Wu, X.; Liu, H.; Liu, J.; Haley, K. N.; Treadway, J. A.; Larson, J. P.; Ge, N.; Peale, F.; Bruchez, M. P. *Nat Biotech* **2003**, *21*, 41.
- (3) Biju, V.; Itoh, T.; Ishikawa, M. *Chem. Soc. Rev.* **2010**, *39*, 3031.
- (4) Bruchez, M., Jr.; Moronne, M.; Gin, P.; Weiss, S.; Alivisatos, A. P. *Science* **1998**, *281*, 2013.
- (5) Alivisatos, A. P. *Science* **1996**, *271*, 933.
- (6) Brus, L. *J. Phys. Chem.* **1986**, *90*, 2555.
- (7) Yong, K.-T.; Ding, H.; Roy, I.; Law, W.-C.; Bergey, E. J.; Maitra, A.; Prasad, P. N. *ACS Nano* **2009**, *3*, 502.
- (8) Derfus, A. M.; Chan, W. C. W.; Bhatia, S. N. *Adv. Mater.* **2004**, *16*, 961.
- (9) Lidke, D. S.; Nagy, P.; Heintzmann, R.; Arndt-Jovin, D. J.; Post, J. N.; Grecco, H. E.; Jares-Erijman, E. A.; Jovin, T. M. *Nat. Biotechnol.* **2004**, *22*, 198.
- (10) Mitchell, P. *Nat Biotech* **2001**, *19*, 1013.
- (11) Chan, W. C. W.; Nie, S. M. *Science* **1998**, *281*, 2016.
- (12) Derfus, A. M.; Chan, W. C. W.; Bhatia, S. N. *Nano Lett.* **2004**, *4*, 11.
- (13) Lewinski, N.; Colvin, V.; Drezek, R. *Small* **2008**, *4*, 26.
- (14) Hermanson, G. T. *Bioconjugate Techniques*; 2nd ed.; Academic Press, 2008.
- (15) Soo Choi, H.; Liu, W.; Misra, P.; Tanaka, E.; Zimmer, J. P.; Itty Ipe, B.; Bawendi, M. G.; Frangioni, J. V. *Nat Biotech* **2007**, *25*, 1165.
- (16) Ruizendaal, L.; Bhattacharjee, S.; Pournazari, K.; Rosso-Vasic, M.; De Haan, L. H. J.; Alink, G. M.; Marcelis, A. T. M.; Zuilhof, H. *Nanotoxicology* **2009**, *3*, 339.

- (17) Bhattacharjee, S.; de Haan, L.; Evers, N.; Jiang, X.; Marcelis, A.; Zuilhof, H.; Rietjens, I.; Alink, G. *Part. Fibre Toxicol.* **2010**, *7*, 25.
- (18) Rogozhina, E. V.; Eckhoff, D. A.; Gratton, E.; Braun, P. V. *J. Mater. Chem.* **2006**, *16*, 1421.
- (19) Yamani, Z.; Ashhab, S.; Nayfeh, A.; Thompson, W. H.; Nayfeh, M. *J. Appl. Phys.* **1998**, *83*, 3929.
- (20) Heinrich, J. L.; Curtis, C. L.; Credo, G. M.; Kavanagh, K. L.; Sailor, M. J. *Science* **1992**, *255*, 66.
- (21) Holmes, J. D.; Ziegler, K. J.; Doty, R. C.; Pell, L. E.; Johnston, K. P.; Korgel, B. A. *J. Am. Chem. Soc.* **2001**, *123*, 3743.
- (22) English, D. S.; Pell, L. E.; Yu, Z.; Barbara, P. F.; Korgel, B. A. *Nano Lett.* **2002**, *2*, 681.
- (23) Li, X.; He, Y.; Talukdar, S. S.; Swihart, M. T. *Langmuir* **2003**, *19*, 8490.
- (24) Huisken, F.; Ledoux, G.; Guillois, O.; Reynaud, C. *Adv. Mater.* **2002**, *14*, 1861.
- (25) Rosso-Vasic, M.; Spruijt, E.; van Lagen, B.; De Cola, L.; Zuilhof, H. *Small* **2008**, *4*, 1835.
- (26) Warner, J. H.; Hoshino, A.; Yamamoto, K.; Tilley, R. D. *Angew. Chem., Int. Ed.* **2005**, *44*, 4550.
- (27) Wilcoxon, J. P.; Samara, G. A. *Appl. Phys. Lett.* **1999**, *74*, 3164.
- (28) Wilcoxon, J. P.; Samara, G. A.; Provencio, P. N. *Phys. Rev. B: Condens. Matter* **1999**, *60*, 2704.
- (29) Tilley, R. D.; Warner, J. H.; Yamamoto, K.; Matsui, I.; Fujimori, H. *Chem. Commun.* **2005**, 1833.
- (30) Zou, J.; Sanelle, P.; Pettigrew, K. A.; Kauzlarich, S. M. *J. Cluster Sci.* **2006**, *17*, 565.
- (31) Pettigrew, K. A.; Liu, Q.; Power, P. P.; Kauzlarich, S. M. *Chem. Mater.* **2003**, *15*, 4005.
- (32) Liu, Q.; Kauzlarich, S. M. *Mater. Sci. Eng., B* **2002**, *96*, 72.
- (33) Neiner, D.; Chiu, H. W.; Kauzlarich, S. M. *J. Am. Chem. Soc.* **2006**, *128*, 11016.
- (34) Ledoux, G.; Guillois, O.; Porterat, D.; Reynaud, C.; Huisken, F.; Kohn, B.; Paillard, V. *Phys. Rev. B: Condens. Matter* **2000**, *62*, 15942.
- (35) Tanke, R. S.; Kauzlarich, S. M.; Patten, T. E.; Pettigrew, K. A.; Murphy, D. L.; Thompson, M. E.; Lee, H. W. H. *Chem. Mater.* **2003**, *15*, 1682.
- (36) Shiohara, A.; Hanada, S.; Prabakar, S.; Fujioka, K.; Lim, T. H.; Yamamoto, K.; Northcote, P. T.; Tilley, R. D. *J. Am. Chem. Soc.* **2009**, *132*, 248.
- (37) Kolb, H. C.; Finn, M. G.; Sharpless, K. B. *Angew. Chem., Int. Ed.* **2001**, *40*, 2005.
- (38) Posner, T. *Ber. Dtsch. Chem. Ges.* **1905**, *38*, 646.
- (39) Dondoni, A. *Angew. Chem., Int. Ed.* **2008**, *47*, 8995.
- (40) Hoyle, C. E.; Bowman, C. N. *Angew. Chem., Int. Ed.* **2010**, *49*, 1540.
- (41) Harant, A. W.; Khire, V. S.; Thibodaux, M. S.; Bowman, C. N. *Macromolecules* **2006**, *39*, 1461.
- (42) Caipa Campos, M. A.; Paulusse, J. M. J.; Zuilhof, H. *Chem. Commun.* **2010**, *46*, 5512.
- (43) Jonkheijm, P.; Weinrich, D.; Kohn, M.; Engelkamp, H.; Christianen, P. C. M.; Kuhlmann, J.; Maan, J. C.; Nusse, D.; Schroeder, H.; Wacker, R.; Breinbauer, R.; Niemeyer, C. M.; Waldmann, H. *Angew. Chem., Int. Ed.* **2008**, *47*, 4421.
- (44) ten Brummelhuis, N.; Diehl, C.; Schlaad, H. *Macromolecules* **2008**, *41*, 9946.
- (45) Remzi Becer, C.; Hoogenboom, R.; Schubert, U. S. *Angew. Chem., Int. Ed.* **2009**, *48*, 4900.
- (46) Hoyle, C. E.; Lowe, A. B.; Bowman, C. N. *Chem. Soc. Rev.* **2010**, *39*, 1355.
- (47) Hoyle, C. E.; Lee, T. Y.; Roper, T. *J. Polym. Sci., Part A: Polym. Chem.* **2004**, *42*, 5301.
- (48) Killups, K. L.; Campos, L. M.; Hawker, C. J. *J. Am. Chem. Soc.* **2008**, *130*, 5062.
- (49) Kang, T.; Amir, R. J.; Khan, A.; Ohshimizu, K.; Hunt, J. N.; Sivanandan, K.; Montanez, M. I.; Malkoch, M.; Ueda, M.; Hawker, C. J. *Chem. Commun.* **2010**, *46*, 1556.
- (50) Kade, M. J.; Burke, D. J.; Hawker, C. J. *J. Polym. Sci., Part A: Polym. Chem.* **2010**, *48*, 743.
- (51) Campos, L. M.; Meinel, I.; Guino, R. G.; Schierhorn, M.; Gupta, N.; Stucky, G. D.; Hawker, C. J. *Adv. Mater.* **2008**, *20*, 3728.
- (52) Ruizendaal, L.; Voorhaar, L.; Paulusse, J. M. J.; Sudhölter, E. J. R.; Zuilhof, H. *manuscript in preparation* **2010**.
- (53) Kelly, J. A.; Henderson, E. J.; Clark, R. J.; Hessel, C. M.; Cavell, R. G.; Veinot, J. G. C. *J. Phys. Chem. C* **2010**, 22519.
- (54) Yu, W. W.; Qu, L.; Guo, W.; Peng, X. *Chem. Mater.* **2003**, *15*, 2854.

- (55) de Boer, W. D. A. M.; Timmerman, D.; Dohnalova, K.; Yassievich, I. N.; Zhang, H.; Buma, W. J.; Gregorkiewicz, T. *Nat Nano* **2010**, 5, 878.
- (56) Williams, A. T. R.; Winfield, S. A.; Miller, J. N. *Analyst* **1983**, 108, 1067.
- (57) Lakowicz, J. R. *Principles of Fluorescence Spectroscopy*; third ed.; Springer: Singapore, 2006.
- (58) Jurbergs, D.; Rogojina, E.; Mangolini, L.; Kortshagen, U. *Appl. Phys. Lett.* **2006**, 88.
- (59) Anthony, R.; Kortshagen, U. *Phys. Rev. B: Condens. Matter* **2009**, 80.
- (60) Snow, A. W.; Foos, E. E. *Synthesis* **2003**, 509.

### 3.6 Appendix

Based on  $^1\text{H}$  NMR results, when the integral of the signals for the alkene (4.96 ppm and 5.79 ppm) are set to 3, the total integral of  $\text{CH}_2$ -protons is 10.25 (0.30 ppm to 3.20 ppm). Since the  $\text{CH}_2$ -part of the butene contains 4 protons in this region, an integral of 6.25 is left for the octane chains. These contain 17 protons, which makes a ratio of 1 : 0.36 for the butene : octane content on the surface of the Si NP.

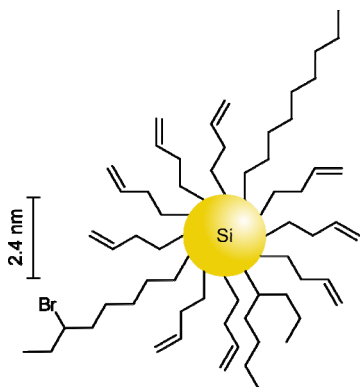


Figure A1: Impression of the Si NP with (brominated) octyl chains in addition to the butane capping.

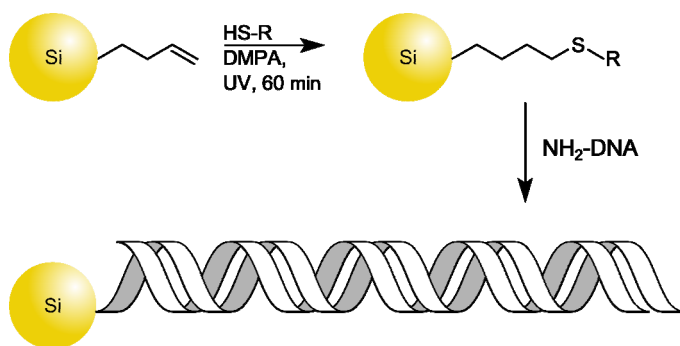


# Chapter 4

## DNA-Functionalized Silicon Nanoparticles

### Abstract

The functionalization of alkene-terminated Si NPs via thiol-ene chemistry is described for a variety of groups. Thioglycolic acid, thiolated tetraethylene glycol-carboxylic acid and thiolated polyethylene glycol 3000-carboxylic acid were coupled to the Si NPs, as confirmed by IR and NMR spectroscopy. The fluorescence emission maxima of all functionalized Si NPs are at 525 nm, and were not influenced by the thiol-ene coupling. Activation of attached carboxylic acid moieties allowed for the first case of conjugation of  $\text{NH}_2$ -terminated oligo-ss-DNA to the Si NPs. Successful coupling was confirmed by UV absorption spectroscopy, which displayed a characteristic new band at 260 nm, and fluorescence spectroscopy, which still showed the distinctive fluorescence of the Si NPs at 525 nm. Gel electrophoresis confirmed coupling of 2 to 3 DNA strands onto the Si NPs, while no uncoupled DNA was observed in the sample.



*This chapter is part of a publication:*

*L. Ruizendaal, S. P. Pujari, V. Gevaerts, J. M. J. Paulusse, H. Zuilhof, Chem Asian J, 2011, published online 24 August, 2011.*

## 4.1 Introduction

The development of new and accurate biodiagnostic tools makes the identification of infectious diseases faster, and thereby prevents unnecessary illness and loss of lives. Current methods to detect pathogenic bacteria and viruses - such as tuberculosis and influenza - are laborious and time-consuming, since typically an amplification step is involved, which may take several days.<sup>1-3</sup> The search for faster tests with even lower detection limits therefore remains important. For DNA and RNA sensing in particular, hybridization of the target sequence with a probe is a commonly used approach, because of its simplicity.<sup>4</sup> Recent developments of nanomaterials for detection of DNA and RNA, which are based on magnetic sensing, electronic detection, surface plasmon resonance or fluorescence spectroscopy, are promising as they suggest to combine fast analysis with high specificity and low detection limits.<sup>5</sup> For these detection systems, the conjugation of biomolecules is often crucial. Fluorescence spectroscopy-based detection methods are more and more employing quantum dots (QDs) as source of fluorescence instead of organic dyes,<sup>6</sup> since they display a strongly diminished photobleaching<sup>7,8</sup> and are characterized by a size-tunable emission wavelength.<sup>9,10</sup> The detection of biomolecules in solution with QDs can be achieved in several ways: making use of Förster resonance energy transfer (FRET),<sup>11</sup> fluorescence quenching and changes in the fluorescence anisotropy. In FRET, the QD acts as a FRET donor onto which a capture molecule is attached; upon binding of the target molecule, i.e. DNA or proteins, a FRET acceptor is brought close enough to the donor to display FRET emission.<sup>12</sup> With this method, detection of DNA target strands was achieved.<sup>13-17</sup> Analogously, binding of target DNA may bring a fluorescence quencher into the close proximity of a QD,<sup>18-20</sup> resulting in the loss of fluorescence. Recently, changes in the fluorescence anisotropy of QDs were used to detect binding of a complementary DNA strand to a single strand DNA-functionalized QD. The rotation correlation time increased drastically upon hybridization of the complementary DNA strand, since a double stranded DNA molecule is very rigid, and thus increases the hydrodynamic radius of the particle accordingly.<sup>21</sup>

The conjugation of biomolecules such as antibodies and proteins with fluorescent labels is of great importance for the targeted labeling of certain parts of cells or cell wall receptors. Jaiswal *et al.* have described a general method to coat QDs with proteins or antibodies for targeting purposes.<sup>22</sup> Hereby, commercially available QDs are coated with avidin, after which the biotinylated molecule of interest can be coupled. Nonetheless it remains a challenge to prepare QDs that can move freely, and are efficiently internalized by cells. Due to the relative large dimensions of QDs (20-50 nm), the normal uptake by cells would be by endocytosis. This leads to encapsulated clusters of QDs, which are

hardly released in the cell.<sup>23</sup> However, QDs functionalized with targeting peptides have been successfully applied in the specific labeling of cell nuclei,<sup>24,25</sup> whereas proteins located in the cytoplasm were specifically labeled making use of His-tag modified QDs.<sup>26</sup> Specific labeling of a certain cell type may also be accomplished by antibody-coated QDs, which may then couple to membrane receptors. In this way, Nie and coworkers achieved the specific targeting of human prostate tumor cells in mice by coupling prostate-specific membrane antigen monoclonal antibodies onto QDs.<sup>27</sup> Other examples are the specific labeling of tumorous cells with peptide-conjugated QDs, as well as the monitoring of diffusion dynamics of single receptors on cell membranes with antibody-coated QDs.<sup>28,29</sup> DNA-conjugated QDs are commonly applied in fluorescence in situ hybridization (FISH)<sup>11</sup> which allows certain parts of chromosomes to be labeled, in order to detect chromosomal defects.<sup>30</sup>

Silicon nanoparticles (Si NPs) may be considered as QDs as well, since they display fluorescent properties of which quantum confinement is the origin,<sup>31-33</sup> as well as minimal photobleaching and a size-dependent fluorescence emission wavelength.<sup>34</sup> In contrast to many conventional QDs, Si NPs are non-toxic,<sup>35,36</sup> which makes them highly suitable for application in biological systems. A versatile and facile conjugation strategy to attach biomolecules onto Si NPs is therefore essential for application of Si NPs as diagnostic labels.

Direct coupling of functional groups or biomolecules onto Si NPs is not trivial due to the high reactivity of the passivation agent (alkyl lithium reagents or Grignard reagents for bromide-terminated Si NPs), as well as the susceptibility of hydrogen-terminated or halogen-terminated Si NPs towards nucleophilic attack.<sup>37</sup> Several approaches have been pursued, for example the use of protective group chemistry,<sup>38</sup> or the use of innocent reactive groups, such as epoxides,<sup>39</sup> azides,<sup>35</sup> amines,<sup>40,41</sup> or terminal alkenes.<sup>39</sup> Wang *et al.* reported on the conjugation of DNA strands onto alkyl-functionalized Si NPs using a photochemical reaction with an aryldiazirine to activate the alkyl moiety via carbene-chemistry.<sup>42</sup> NHS groups attached in this way were subsequently substituted by amine-terminated ss-DNA strands. Gel electrophoresis confirmed attachment of the DNA strands. The thiol-ene click-chemistry approach to prepare functional Si NPs, as described in detail in Chapter 3, will be used to obtain carboxylic acid-terminated Si NPs. Three different spacer lengths will be employed, i.e. no spacer, a tetraethylene glycol (EO<sub>4</sub>) spacer and a polyethylene glycol 3000 (PEG3000) spacer. Amine-functional DNA strands will be coupled to these Si NPs, and the resulting bioconjugates will be characterized in detail.

## 4.2 Results & Discussion

### 4.2.1. Synthesis and Functionalization of Si NPs

Alkene-terminated Si NPs (Si NP-ene, **1**) were synthesized via the oxidation of  $\text{Mg}_2\text{Si}$  with bromine, followed by capping with 3-butenylmagnesium bromide as described in Chapter 3. After purification using SEC, thiol-ene chemistry was employed, to give three different types of Si NPs as shown in Figure 1. The alkene-functional Si NPs **1** were mixed with an excess of the respective thiol (**2**, **4** and **5**, Figure 1) and 0.2 eq. of 2,2'-dimethoxy-2-phenylacetophenone (DMPA) as photoinitiator or 4,4'-azobis(4 cyanovaleric acid) (ACVA) as thermal initiator. The mixture was exposed to UV light (DMPA, 365 nm) or heated to 80 °C (ACVA) while stirring at room temperature under ambient conditions. The reaction progress was checked by  $^1\text{H}$  NMR via the disappearance of the alkene  $\text{CH}_2=\text{C}-\text{H}$  signals ( $\delta = 4.96$  ppm and  $\delta = 5.79$  ppm), and revealed completion after 60 min for both the thermal and UV-initiated samples.

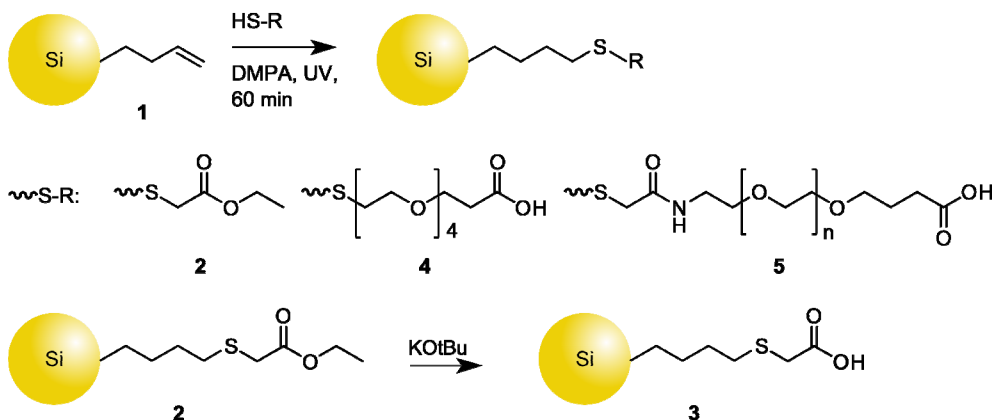


Figure 1. Functionalized Si NPs as obtained by thiol-ene chemistry; deprotection of ester-functionalized Si NPs.

The functionalized thioglycolic acid ethyl ester-modified Si NPs (Si NP-TGAEE, **2**) and tetraethyleneglycol-carboxylic acid-modified Si NPs (Si NP-EO<sub>4</sub>-COOH, **4**) were purified via size exclusion chromatography (SEC), while pegylated Si NPs (**5**) were purified using Amicon Ultra 3k nominal weight cut off (NWCO) centrifugal units. The Si NP-TGAEE (**2**)



were subsequently hydrolyzed with potassium *tert*-butoxide (KOtBu) to obtain thioglycolic acid-modified Si NPs (Si NP-TGA, **3**). The sample was purified by evaporation of the solvents and resulting *tert*-butanol.

NMR spectra were recorded to confirm that coupling of the functional thiols had taken place, as well as to determine the structure of the resulting Si NPs. The  $^1\text{H}$  NMR spectrum of Si NP-TGAEE (**2**) (Figure 2, left) displays characteristic signals of the newly formed thioester at  $\delta = 2.62$  ppm (assignment d) ( $\text{CH}_2\text{-CH}_2\text{-S}$ ) and  $\delta = 3.19$  ppm (e) ( $\text{S-CH}_2\text{-COOEt}$ ). The signals of the ethyl ester moiety were observed at  $\delta = 4.17$  ppm (f) and  $\delta = 1.26$  ppm (g), corresponding to the  $\text{CH}_2$  and  $\text{CH}_3$ , respectively. After hydrolysis with KOtBu, these signals are no longer present. The  $^1\text{H}$  NMR spectrum of Si NP-EO<sub>4</sub>-COOH (**4**) (Figure 2, right) also displays signals at  $\delta = 2.62$  ppm (d) ( $\text{CH}_2\text{-CH}_2\text{-S}$ ) and  $\delta = 2.69$  ppm (e) in agreement with a thioester moiety. The  $\text{CH}_2$ -moieties of the ethylene glycol spacer are observed at  $\delta = 3.64$  ppm (g), while the  $\text{CH}_2\text{-COOH}$  group is observed at  $\delta = 2.89$  ppm (i). The NMR spectra of the modified Si NPs were assigned with the help of 2D COSY NMR spectroscopy, and in all cases confirm quantitative coupling of the indicated thiols to the Si NPs, since no terminal alkenes are observed after modification, while the intensities of the new signals fit accordingly.

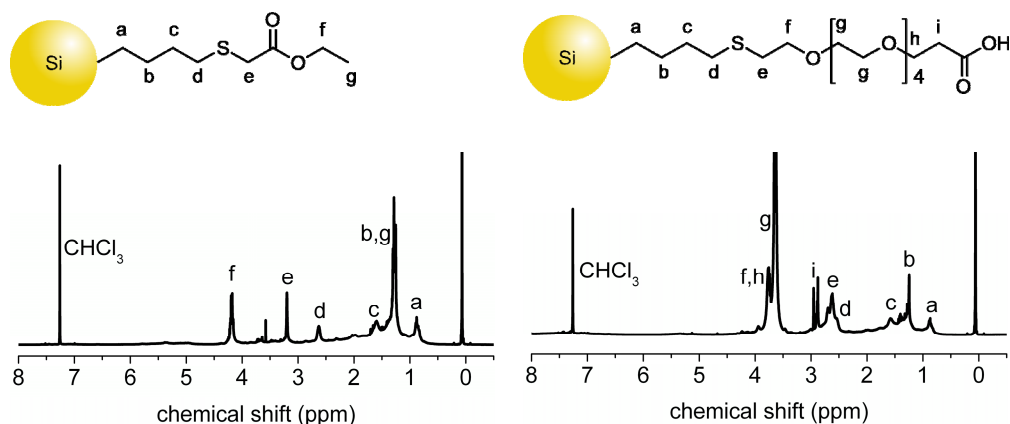


Figure 2. Left:  $^1\text{H}$  NMR spectra of Si NP-TGAEE (**2**); Right: Si NP-EO<sub>4</sub>-COOH (**4**).

To confirm the presence of the corresponding functional groups on the Si NPs, infrared spectroscopy (IR) was performed. Figure 3 gives an overview of the IR spectra of the Si NPs. The spectra of Si NP-TGAEE (**2**), Si NP-TGA (**3**) and Si NP-EO<sub>4</sub>-COOH (**4**) display a clear carbonyl stretch signal at  $1732\text{ cm}^{-1}$ . The signal is, however, hardly observed in Si NP-PEG3000-COOH (**5**), most likely due to the large amount of ether groups (approximately

170 per chain, at  $1103\text{ cm}^{-1}$ ) as compared to other typical groups present in the sample. The presence of ether groups also results in broadening of the signals for the  $\text{CH}_2$  symmetric and antisymmetric stretch (appear as single peak at  $2880\text{ cm}^{-1}$ ). In the IR spectrum of Si NP- $\text{EO}_4\text{-COOH}$  (**4**) the characteristic ether bonds are observed at  $1108\text{ cm}^{-1}$ . Importantly, the signal corresponding to Si-O ( $1000\text{-}1100\text{ cm}^{-1}$ ) is weak in all spectra, despite the high polarity of the Si-O bond, indicating only minimal oxidation of the Si NPs, and no increase in oxidation is observed upon functionalization of the particles.

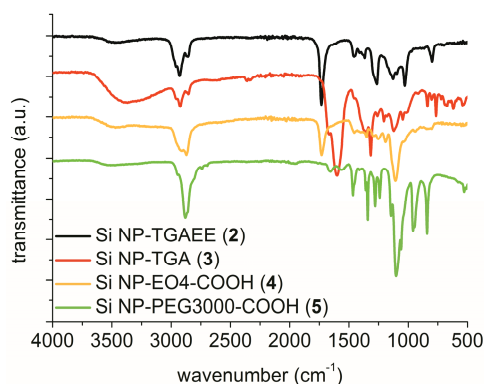


Figure 3. FTIR spectra of Si NP-TGAEE (**2**), Si NP-TGA (**3**), Si NP- $\text{EO}_4\text{-COOH}$  (**4**) and Si NP-PEG3000-COOH (**5**).

To obtain the elemental composition of the Si NPs, as well as detailed binding information, a thin film of Si NP- $\text{EO}_4\text{-COOH}$  (**4**) was cast onto a Au surface and analyzed with X-ray photoelectron spectroscopy (XPS). The XPS narrow scan of the  $\text{C}_{1s}$  region of **4** was fit with 3 components, of which the signal with the lowest binding energy (285.0 eV) is assigned to carbon-bound carbon atoms. The overlapping signals for oxygen-bound and sulfur-bound carbon atoms are observed at 286.5 eV, whereas the signal corresponding to the carbonyl ( $\text{C=O}$ ) carbon atom is found at 289.1 eV. The experimental ratio C-C : C-O/C-S :  $\text{C=O}$  is 7 : 7 : 1, where the theoretical ratio would be 4 : 10 : 1. The intensity of the signal for the carbon-bound carbons is relatively high, which is likely due to side reactions occurring during the Si NP-ene (**1**) synthesis. As a side-reaction, some octyl moieties are attached to the Si NP, as described in detail in Chapter 3. These chains are inert under thiol-ene functionalization conditions. The XPS narrow scan of the  $\text{Si}_{2p}$  region of Si NP-COOH (**4**) is shown in Figure 4, center. A single peak is observed at 102.2 eV (FWHM 1.3 eV), which is slightly shifted as compared to Si NP-ene (**1**) (101.8 eV with a FWHM of 1.3 eV). This value is near-identical to what is

observed under similar instrumental conditions for the base peak of Si at 99.4 eV with a FWHM of 1.0 eV in a silicon(111) wafer. The shift in binding energy from 99.4 eV to 102.2 eV is largely caused by charging effects, which would indeed be expected for a small object that is well-surrounded by an electrically insulating organic shell, while the slightly increased width is too small to indicate the presence of more highly oxidized C atoms and is likely also caused by the combination of charging and intrinsic variation of Si atoms within a NP. Moreover, XPS analysis of samples of partially oxidized Si NPs resulted in two signals in the silicon region, the first at 102.2 eV corresponding to silicon, and a second signal at 104.9 eV for silicon oxide. The peak shift is in line with the observation that the binding energy shifts to higher levels with decreasing nanoparticle size, as compared to bulk silicon.<sup>43</sup> The XPS narrow scan of the  $S_{2p}$  region shows a spin orbital doublet with the main signal at 163.8 eV, which is in agreement with the formation of a thioether.

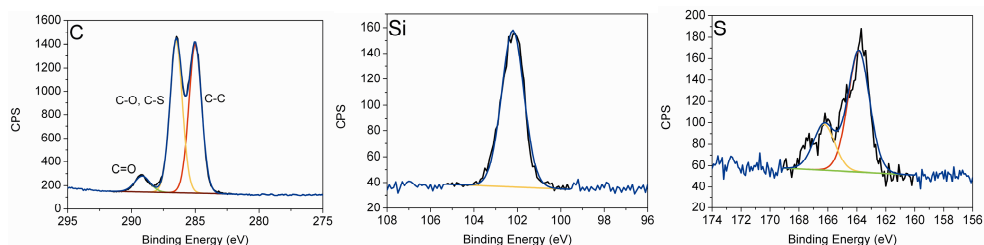


Figure 4. XPS narrow scan spectra of Si NP-EO<sub>4</sub>-COOH (**4**). Left:  $C_{1s}$  region; center:  $Si_{2p}$  region; right:  $S_{2p}$  region.

Figure 5 (left) shows the UV-Vis absorption spectra of the carboxylic acid-functionalized Si NPs in phosphate buffer (pH 6.5). The UV-Vis absorption of the Si NPs does not change significantly upon functionalization. A characteristic gradual increase in absorption towards shorter wavelengths is observed. The fluorescence emission maximum is around 525 nm, as observed before for Si NP-ene (**1**), indicating no significant changes had occurred upon thiol-ene functionalization. A slight shift in maximum is visible when comparing Si NP-PEG3000-COOH (**5**) and the other functionalized Si NPs. This is likely a result of the size-based purification process of **5**, which may cause changes in the size-distribution of the Si NPs. Since the fluorescence emission of Si NPs is size-dependent, changes in the size distribution consequently result in changes in the fluorescence emission maxima.<sup>34</sup> This shift is not expected to be significantly influenced by the thiol-ene conjugation, since fluorescence originates from

the Si core, with only a small electronic coupling to the covering organic layer that is unlikely to extend to the distance at which the conjugation reaction takes place.<sup>44</sup>

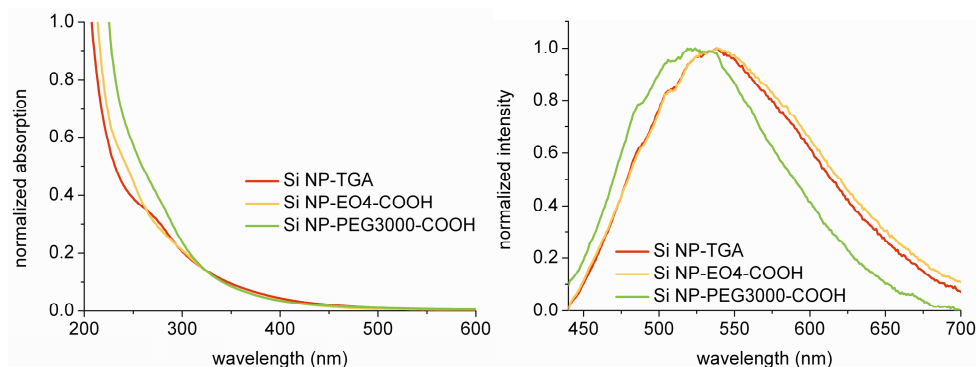


Figure 5. Left: UV-Vis absorption normalized at 320 nm; Right: normalized fluorescence emission at  $\lambda_{\text{exc}} = 430$  nm (right) of Si NP-TGA (3), Si NP-EO<sub>4</sub>-COOH (4) and Si NP-PEG3000-COOH (5) in phosphate buffer pH 6.5.

In addition to steady-state fluorescence spectroscopy, time-resolved fluorescence emission was studied. Table 1 summarizes the amplitude-weighted averages (see appendix for formula) of the fluorescence lifetimes of the functional Si NPs excited at 372 nm. The results are all in the same time range as observed in Chapter 3 ( $\sim 4$  ns), confirming that thiol-ene modification does not significantly affect the Si NPs.

Table 1. Fluorescence emission lifetimes of Si NPs, before and after thiol-ene functionalization.  $\lambda_{\text{exc}} = 372$  nm, in phosphate buffer pH 6.5

Sample	$\tau_{\text{av}}$ (ns)
Si NP-TGA (3)	4.35
Si NP-EO <sub>4</sub> -COOH (5)	3.18
Si NP-PEG3000-COOH (6)	3.77



After coupling of the ssDNA and subsequent purification to obtain ssDNA-functionalized Si NPs, the amount of DNA in the NP sample was determined by UV-Vis absorption measurements to determine its concentration. The complementary 3'-atto 488 dye-modified ssDNA strand was added (1.5 eq) and incubated at 80 °C for 1 min, after which the sample was allowed to cool to room temperature followed by cooling on ice. Excess of complementary ssDNA was removed via filtration over a 50k NWCO Amicon centrifugal filter unit. This resulted in the dsDNA-modified Si NPs Si NP-TGA-dsDNA (6), Si NP-EO<sub>4</sub>-dsDNA (7) and Si NP-PEG-dsDNA (8).

To confirm coupling of the DNA strands to the Si NPs, gel electrophoresis on an agarose gel was performed. Figure 8 shows the agarose gel, after a run-time of 1 hour. Lane 1 contains the reference ladder; the numbers correspond to the number of base-pairs (bp) in the respective band. Lane 2 contains Si NP-TGA-dsDNA (6); lane 3 Si NP-EO<sub>4</sub>-dsDNA (7) and lane 4 contains Si NP-PEG-dsDNA (8). Lane 5 is a reference lane containing uncoupled dsDNA (100 bp), with the same sequence as the strands coupled to the NPs. The band in lane 5 runs slightly lower than the 100 bp ladder reference (arrow I). No DNA of this length is observed in lanes 3 and 4, indicating successful purification of the conjugated Si NPs. The height of the bands in lanes 3 and 4 corresponds to approximately 300 bp (arrow II). The Si NPs to which the DNA is coupled are of a specific size, which may influence the height of the band. As such, the bands are proposed to indicate the presence of two to three DNA strands per NP for Si NP-EO<sub>4</sub>-dsDNA (7) and Si NP-PEG-dsDNA (8). A slightly less clear band at the same height is observed in lane 2, which indicates that in the Si NP-TGA-dsDNA (6) sample, also up to 3 strands are attached to the Si NP. The clearer band in lane 2 just above the 100 bp level (arrow III), most likely corresponds to Si NP-TGA-dsDNA (6) with only a single DNA-strand attached. Tailing of the bands may be due to the range of NP sizes present in the samples (due to a different number of polymeric chains attached), or different numbers or orientations of DNA-strands on the Si NPs, resulting in differently sized DNA-functional particles.

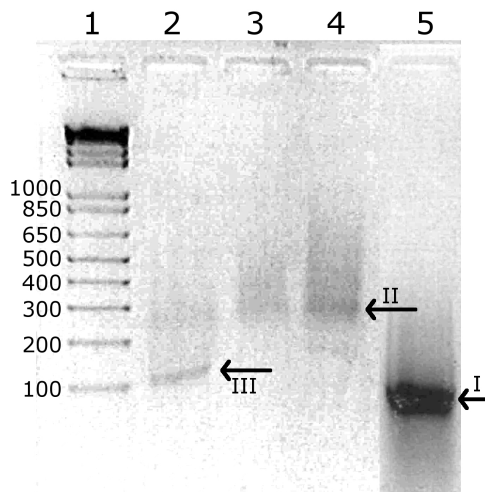


Figure 8. Agarose gel with dsDNA-modified Si NPs. Lane 1: 1kb+ ladder; lane 2: Si NP (6); lane 3: Si NP (7); lane 4: Si NP (8); lane 5: uncoupled 100bp dsDNA.

UV-Vis absorption and fluorescence emission data of the DNA-modified samples with different spacer lengths do not display characteristics that allow for differentiation. The UV-Vis absorption spectrum of the pegylated Si NPs conjugated to ssDNA is shown in Figure 9, left. However, the main absorption observed originates from the DNA. This points to attachment of the DNA strands to the Si NP, since otherwise these would have been removed in the purification process. The absorption of the Si NP core is still observed when ssDNA is conjugated to the particle, albeit only as a minor contribution, since the extinction coefficient of ssDNA ( $9.8 \times 10^5 \text{ M}^{-1} \text{ cm}^{-1}$ , for this particular sequence) is approximately 1000-fold higher than that of the Si NPs at 350 nm ( $3.0 \times 10^2 \text{ M}^{-1} \text{ cm}^{-1}$ , Chapter 3). Furthermore, the fluorescence emission of the Si NPs with ssDNA is still observed, although again as a relatively small signal (Figure 9, center). Fluorescence emission contributions from both the Si NP core, as well as the UV-absorption of the ssDNA-strand, indicate that both the Si NPs and ssDNA are present in the sample.

The UV-absorption spectrum of the Si NP containing dsDNA is shown in Figure 9, left. The spectrum is dominated by the absorption of dsDNA and additionally the Atto 488 dye. This is similar to the ssDNA Si NP samples due to the relative high extinction coefficient for dsDNA ( $1.6 \times 10^6 \text{ M}^{-1} \text{ cm}^{-1}$ , for this particular sequence). The fluorescence emission of the Atto 488 dye fully dominates the fluorescence spectra of the samples containing dsDNA-conjugated Si NPs (Figure 9, center and right).

The fluorescence contribution of the Atto dye indicates that the complementary strand is indeed hybridized to the DNA-strand present on the Si NP. The dominance of the Atto 488 dye in the fluorescence samples with dsDNA is due to the relatively low quantum yield (QY) of the Si NPs (7 %, Chapter 3), whereas the QY of the Atto 488 dye is 80%. Figure 9 (right) shows the UV-Vis absorption and fluorescence emission of Si NP-dsDNA. The spectra are dominated by the absorption and emission of the coupled dsDNA-strands and the Atto 488 dye. This indicates that the fluorescent dye is indeed coupled to the Si NP via the complementary DNA-strand, since all uncoupled DNA-strands are removed by purification as observed by gel electrophoresis.

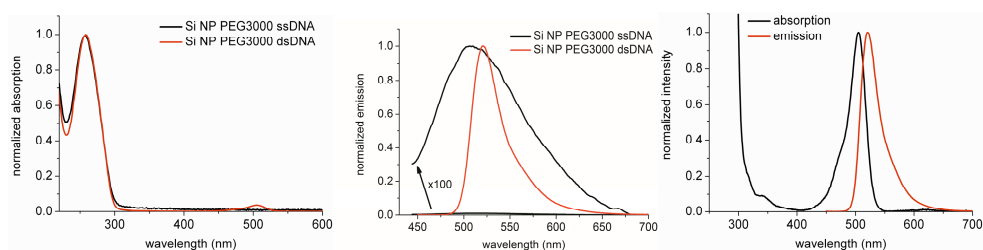


Figure 9. Left: normalized UV-Vis absorption of Si NP-PEG-ssDNA and dsDNA; Center: normalized fluorescence emission of Si NP-PEG-ssDNA ( $\lambda_{\text{exc}} = 430$  nm) and Si NP-PEG-dsDNA ( $\lambda_{\text{exc}} = 501$  nm); Right: normalized UV-Vis absorption and fluorescence emission ( $\lambda_{\text{exc}} = 501$  nm) of Si NP-PEG3000-dsDNA.

### 4.3 Conclusions

Three carboxylic acid-functionalized thiols with different spacer lengths were successfully coupled to alkene-terminated Si NPs via thiol-ene click chemistry. The optical properties of the Si NPs do not change significantly upon functionalization, in line with the Si core being the origin of the optical properties. Coupling of amine-terminated DNA to the carboxylic acid-terminated Si NPs was confirmed by UV-Vis absorption and fluorescence spectroscopy, which indicated both the presence of DNA and Si NPs in the purified samples. Addition of a fluorescently labeled complementary DNA strand yielded Si NPs with two to three covalently coupled dsDNA strands, as confirmed by UV-Vis absorption and fluorescence spectroscopy and by gel electrophoresis. These results demonstrate the successful bioconjugation of DNA onto Si NPs. The employed coupling technique is very mild, and the presented concept is



therefore readily extended to proteins or other biomolecules, bringing the application of biofunctional Si NPs in sensing devices within reach.

#### 4.4 Experimental

All chemicals were used without further purification unless stated otherwise. Thioglycolic acid (99+%), *p*-toluenesulfonic acid (reagent grade), toluene ( $\geq 99.7\%$ , GC), 4,4'-azobis(4-cyanovaleric acid) (purum) and potassium *tert*-butoxide (95%) were purchased from Sigma-Aldrich. Ethanol (Normapur) was purchased from VWR. HCl (for analysis, 37 % in water), dichloromethane (reagent grade) and DMF (reagent grade) were purchased from Fisher Scientific. Sodium phosphate monobasic dihydrate (ultra,  $\geq 99\%$ ), and disodium hydrogen phosphate dihydrate (puris. p.a.  $\geq 99\%$ ) were purchased from Fluka. For purification of the functionalized Si NPs an Agilent 5  $\mu\text{m}$ , 500 Å column was used with chloroform as eluens (HPLC grade, Biosolve). HPLC-purified DNA was purchased from Iba GmbH, Göttingen, Germany.  $\alpha$ -Thio- $\omega$ -carboxy poly(ethylene glycol) PEG-MW 3000 Dalton and 15-mercapto-4,7,10,13-tetraoxa-pentadecanoic acid were purchased from Iris Biotech GmbH, Marktredwitz, Germany and used as received. Agarose (electrophoresis grade), Tris/Borate/EDTA (TBE) buffer and the 1kb+ DNA ladder were purchased from Invitrogen life technologies.

##### *Synthesis and purification of Si NP-ene (1).*

The synthesis of the Si NP-ene (1) is described in Chapter 3.

##### *Synthesis of thioglycolic acid ethyl ester (6)*

A mixture of thioglycolic acid (5.0 mL, 72 mmol), *p*-toluenesulfonic acid (4.8 g, 25 mmol), ethanol (50 mL) and  $\text{MgSO}_4$  (10.0 g) was refluxed for 16 h under  $\text{N}_2$  atmosphere. The mixture was filtered, solvents were removed under reduced pressure, and the resulting solid was purified using automated flash column chromatography (Biotage) using a gradient of ethyl acetate and petroleum ether 40-60, yielding a colorless liquid (3.14 g, 36 %).

$^1\text{H}$  NMR ( $\text{CDCl}_3$ , 400MHz)  $\delta$  1.27 ppm (t, 3H,  $\text{CH}_3$ ), 2.04 ppm (t, 1H, SH), 3.26 ppm (d, 2H,  $\text{HS-CH}_2$ ) 4.19 ppm (q, 2H,  $\text{CH}_3\text{-CH}_2$ ).

$^{13}\text{C}$  NMR ( $\text{CDCl}_3$ , 100MHz)  $\delta$  13.89 ppm ( $\text{CH}_3$ ), 26.29 ppm ( $\text{HS-CH}_2$ ), 61.37 ppm ( $\text{CH}_3\text{-CH}_2$ ), 170.58 ppm ( $\text{C=O}$ ); these NMR results are in accordance with literature.<sup>45</sup>

#### *Thiol-ene coupling to Si NPs*

In general, to a solution of 10 mg Si NP-ene (1) (approx. 0.1 mmol alkene groups as determined by  $^1\text{H}$  NMR spectroscopy with an internal standard) in chlorobenzene or DMF, an excess of the thiol and 0.2 eq of photoinitiator were added, and the reaction mixture was stirred at room temperature while exposed to UV light (365 nm) under ambient conditions.

#### *Synthesis of Si NP-COOH (3)*

A solution of thioglycolic acid ethyl ester (TGAE, **6**) (100  $\mu\text{L}$ , 0.8 mmol), 2,2'-dimethoxy-2-phenylacetophenone (DMPA) in chlorobenzene (100  $\mu\text{L}$  100 mg/mL; 40  $\mu\text{mol}$ ) and Si NP-ene (1) (10 mg) was stirred for 1 h at room temperature, while irradiating with UV light (365 nm). Solvent was evaporated and the Si NPs were purified using SEC with chloroform as eluents, yielding Si NP-TGAE (2) as an orange waxy material (12 mg). To the solvent-free Si NPs, an ice-cooled slurry of KOtBu in dry diethyl ether (100 mg, 0.9 mmol in 3 mL diethyl ether, with 4  $\mu\text{L}$  (0.2 mmol) water) was added and stirred for 72 h at room temperature. Water (2 mL) was added the solution was neutralized, and the solvents were evaporated, yielding Si NP-COOH (3) as a white powder (8 mg). Remaining traces of potassium salts were not observable with NMR.

#### *Synthesis of Si NP-EO<sub>4</sub>-COOH (4)*

A solution of 15-mercapto-4,7,10,13-tetraoxa-pentadecanoic acid ( $\text{HS-EO}_4\text{-COOH}$ ) (200 mg, 0.7 mmol), DMPA in chlorobenzene (100  $\mu\text{L}$  100 mg/mL; 40  $\mu\text{mol}$ ) and Si NP-ene (1) (10 mg) was stirred for 1 h at room temperature while irradiating with UV light (365 nm). The solvent was evaporated under reduced pressure, and the Si NPs were purified using SEC with chloroform as eluents, yielding Si NP-EO<sub>4</sub>-COOH (4) as an orange waxy material (18 mg).

#### *Synthesis of Si NP-PEG3000-COOH (5)*

A solution of  $\alpha$ -thio- $\omega$ -carboxy poly(ethylene glycol) PEG-MW 3000 Dalton ( $\text{HS-PEG3000-COOH}$ ) (450 mg, 0.15 mmol), 4,4'-azobis(4-cyanovaleric acid) in DMF (100  $\mu\text{L}$  110 mg/mL; 40  $\mu\text{mol}$ ,  $\text{N}_2$ -bubbled) and Si NP-ene (1) (10 mg) was stirred for 5 h at 80  $^\circ\text{C}$ . The solvent was evaporated under reduced pressure, and the Si NPs were purified using

Amicon Ultra-4 3000 Da NWCO, yielding Si NP-PEG3000-COOH (**5**) as an orange waxy material (325 mg).

### *DNA coupling to Si NPs*

All tubes, pipette tips, buffers and water were sterilized before use by autoclaving at 120 °C for 20 min. DNA-containing samples were stored in the freezer or on ice before and in between measurements. All handlings involving DNA were carried out wearing gloves.

The DNA sequence coupled to the Si NPs is 5'→3' ACGTTCGGCATTGTGGGCAGAGTGAAGTAT TGGCAAACGTTAAGTGCCGAAC TAGATCTGACCTAACGGTAAGAGAGTTTCATAATACGTCCAGCCGCAT with a 3'-amino modification. The complementary strand has the following sequence: 5'→3' ATGCGGCTGGACGTATTATGAAACTCTCTTACCGTTAGGTCAGATCTAGTTCGGCACTTAACGTTT GCCAATACTTCACTCTGCCCACAATGCCGAACGT with a 3'-atto 488 modification. The sequence was determined by a random DNA generator with 50% GC content (<http://www.faculty.ucr.edu/~mmaduro/random.htm>) and checked with the DNA melt server to check whether the 3' side was not folded, but available for coupling. (<http://mfold.rna.albany.edu/?q=DINAMelt/Two-state-folding>)

In an Eppendorf tube, to a solution of Si NPs (~ 5 nmol) in phosphate buffer, (0.1 M, pH 6.5) N-(3-dimethylaminopropyl)-N'-ethylcarbodiimide hydrochloride (EDC.HCl, 955 µg, 5.0 µmol, from freshly prepared concentrated stock in phosphate buffer, pH 6.5) and N-hydroxysuccinimide (NHS, 575 µg, 5.0 µmol, from freshly prepared concentrated stock in phosphate buffer, pH 6.5) were added. The total volume of the solution was brought to 100 µL, and the solution was shaken for 30 min at room temperature. 3'-Amino-modified DNA (50 nmol) was added and the solution was shaken for 4 h at room temperature. The samples were purified by Amicon Ultra-0.5 50 kDa NWCO centrifugal units, by washing 6 times with phosphate buffer.

By UV-Vis absorption, the amount of DNA in the samples was determined, and 1.5 eq of the 3'-atto 488 modified complementary strand was added, and the solution was heated to 80 °C for 1 min and cooled to room temperature before putting on ice. The samples were purified by Amicon Ultra-0.5 50 kDa NWCO centrifuge tubes, by washing three times with phosphate buffer.

### *Agarose gel electrophoresis*

A standard 2% agarose gel was prepared by dissolving agarose (2 g) in 0.5× Tris/Borate/EDTA (TBE) buffer (100 mL) upon heating in the microwave until nearly cooking. The solution was cooled to 40 °C and ethidium bromide (3 µL, 10 mg / mL) was added and the solution was poured in the rack and left to solidify. Samples were loaded (150 - 200 ng DNA / lane) using loading buffer and a 1kb+ ladder was used as a reference. The gel was run at 100V for 60 min and analyzed with UV light.

### *Optical measurements*

UV-Vis absorption spectra were recorded on a Varian Cary 50 UV-Vis spectrophotometer using phosphate buffer pH 6.5 as solvent. For steady-state and time-resolved fluorescence measurements, concentrations were adjusted to  $OD_{\lambda_{exc}} \leq 0.1$ . All fluorescence measurements were performed on an Edinburgh Instruments FLS900 fluorescence spectrometer using the F900 software. A 372 nm or 444 nm pulsed diode laser (PicoQuant, Berlin) was used for the fluorescence lifetime measurements. Fluorescence emission lifetimes were measured at the corresponding fluorescence emission maxima and the resulting data were fit with the Fasta program of Edinburgh Instruments.

XPS measurements were performed on a Jeol JPS-9200 system using a standard Al  $K_{\alpha}$  source with an X-ray power of 300W, an analyzer pass energy of 10 eV, and an energy resolution of < 0.65 eV.  $C_{1s}$  (C-C) signals were calibrated to a binding energy of 285.0 eV.

$^1H$  (and  $^{13}C$ ) NMR spectra were recorded on a Bruker 400 (100) MHz Avance machine with  $CDCl_3$  or  $D_2O$  as solvent. Chemical shifts are reported in parts per million ( $\delta$ ) relative to  $CHCl_3$  (7.26 ppm for  $^1H$  and 77.2 ppm for  $^{13}C$ ) or  $H_2O$  (4.79 ppm for  $^1H$ ) as internal standard.

## 4.5 References

- (1) Wallis, R. S.; Pai, M.; Menzies, D.; Doherty, T. M.; Walzl, G.; Perkins, M. D.; Zumla, A. *The Lancet* **2010**, 375, 1920.
- (2) Tallury, P.; Malhotra, A.; Byrne, L. M.; Santra, S. *Advanced Drug Delivery Reviews* **2010**, 62, 424.
- (3) Takahashi, H.; Otsuka, Y.; Patterson, B. *Journal of Infection and Chemotherapy* **2010**, 16, 155.
- (4) Merkoçi, A. *Biosensors & Bioelectronics* **2010**, 26, 1164.
- (5) Kumar, C. *Nanomaterials for Biosensors*; Wiley-VCH, 2006.
- (6) Resch-Genger, U.; Grabolle, M.; Cavaliere-Jaricot, S.; Nitschke, R.; Nann, T. *Nature Methods* **2008**, 5, 763.
- (7) Wu, X.; Liu, H.; Liu, J.; Haley, K. N.; Treadway, J. A.; Larson, J. P.; Ge, N.; Peale, F.; Bruchez, M. P. *Nature Biotechnology* **2003**, 21, 41.
- (8) Bruchez, M., Jr.; Moronne, M.; Gin, P.; Weiss, S.; Alivisatos, A. P. *Science* **1998**, 281, 2013.
- (9) Brus, L. *Journal of Physical Chemistry* **1986**, 90, 2555.
- (10) Alivisatos, A. P. *Science* **1996**, 271, 933.
- (11) Lakowicz, J. R. *Principles of Fluorescence Spectroscopy*; third ed.; Springer: Singapore, 2006.
- (12) Smith, A. M.; Duan, H.; Mohs, A. M.; Nie, S. *Advanced Drug Delivery Reviews* **2008**, 60, 1226.
- (13) Gill, R.; Willner, I.; Shweky, I.; Banin, U. *Journal of Physical Chemistry B* **2005**, 109, 23715.
- (14) Zhang, C.-Y.; Yeh, H.-C.; Kuroki, M. T.; Wang, T.-H. *Nature Materials* **2005**, 4, 826.
- (15) Zhang, H.; Stockley, P. G.; Zhou, D. *Faraday Discussions* **2011**, 149, 319.
- (16) Wang, X.; Lou, X.; Wang, Y.; Guo, Q.; Fang, Z.; Zhong, X.; Mao, H.; Jin, Q.; Wu, L.; Zhao, H.; Zhao, J. *Biosensors & Bioelectronics* **2010**, 25, 1934.
- (17) Jiang, G.; Susha, A. S.; Lutich, A. A.; Stefani, F. D.; Feldmann, J.; Rogach, A. L. *ACS Nano* **2009**, 3, 4127.
- (18) Lee, J.; Choi, Y.; Kim, J.; Park, E.; Song, R. *ChemPhysChem* **2009**, 10, 806.
- (19) Li, X.; Qian, J.; Jiang, L.; He, S. *Applied Physics Letters* **2009**, 94.
- (20) Dyadyusha, L.; Yin, H.; Jaiswal, S.; Brown, T.; Baumberg, J. J.; Booy, F. P.; Melvin, T. *Chemical Communications (Cambridge, United Kingdom)* **2005**, 3201.
- (21) Giraud, G.; Schulze, H.; Bachmann, T. T.; Campbell, C. J.; Mount, A. R.; Ghazal, P.; Khondoker, M. R.; Ember, S. W. J.; Ciani, I.; Tlili, C.; Walton, A. J.; Terry, J. G.; Crain, J. *Chemical Physics Letters* **2010**, 484, 309.
- (22) Jaiswal, J. K.; Goldman, E. R.; Mattoussi, H.; Simon, S. M. *Nature Methods* **2004**, 1, 73.
- (23) Delehanty, J. B.; Mattoussi, H.; Medintz, I. L. *Analytical and Bioanalytical Chemistry* **2009**, 393, 1091.
- (24) Chen, F.; Gerion, D. *Nano Letters* **2004**, 4, 1827.
- (25) Derfus, A. M.; Chan, W. C. W.; Bhatia, S. N. *Advanced Materials (Weinheim, Germany)* **2004**, 16, 961.
- (26) Boeneman, K.; Delehanty, J. B.; Susumu, K.; Stewart, M. H.; Medintz, I. L. *Journal of the American Chemical Society* **2010**, 132, 5975.
- (27) Gao, X.; Cui, Y.; Levenson, R. M.; Chung, L. W. K.; Nie, S. *Nature Biotechnology* **2004**, 22, 969.
- (28) Azzazy, H. M. E.; Mansour, M. M. H.; Kazmierczak, S. C. *Clinical Biochemistry* **2007**, 40, 917.
- (29) Smith, A. M.; Gao, X.; Nie, S. *Photochemistry and Photobiology* **2004**, 80, 377.
- (30) Chan, P.; Yuen, T.; Ruf, F.; Gonzalez-Maeso, J.; Sealfon, S. C. *Nucleic Acids Research*, 33, e161.
- (31) Koch, F.; Petrova-Koch, V.; Muschik, T. *Journal of Luminescence* **1993**, 57, 271.
- (32) Dinh, L. N.; Chase, L. L.; Balooch, M.; Siekhaus, W. J.; Wooten, F. *Physical Review B: Condensed Matter* **1996**, 54, 5029.
- (33) Calcott, P. D. J.; Nash, K. J.; Canham, L. T.; Kane, M. J.; Brumhead, D. *Journal of Luminescence* **1993**, 57, 257.
- (34) Huiskens, F.; Ledoux, G.; Guillois, O.; Reynaud, C. *Advanced Materials* **2002**, 14, 1861.

- (35) Ruizendaal, L.; Bhattacharjee, S.; Pournazari, K.; Rosso-Vasic, M.; De Haan, L. H. J.; Alink, G. M.; Marcelis, A. T. M.; Zuilhof, H. *Nanotoxicology* **2009**, *3*, 339.
- (36) Bhattacharjee, S.; de Haan, L. H. J.; Evers, N. M.; Jiang, X.; Marcelis, A. T. M.; Zuilhof, H.; Rietjens, I. M. C. M.; Alink, G. M. *Particle and Fibre Toxicology* **2010**, *7*, 25.
- (37) Chatgililoglu, C.; Griller, D.; Lesage, M. *The Journal of Organic Chemistry* **1989**, *54*, 2492.
- (38) Tanke, R. S.; Kauzlarich, S. M.; Patten, T. E.; Pettigrew, K. A.; Murphy, D. L.; Thompson, M. E.; Lee, H. W. H. *Chemistry of Materials* **2003**, *15*, 1682.
- (39) Shiohara, A.; Hanada, S.; Prabakar, S.; Fujioka, K.; Lim, T. H.; Yamamoto, K.; Northcote, P. T.; Tilley, R. D. *Journal of the American Chemical Society* **2009**, *132*, 248.
- (40) Rosso-Vasic, M.; De Cola, L.; Zuilhof, H. *Journal of Physical Chemistry C* **2009**, *113*, 2235.
- (41) Rosso-Vasic, M.; Spruijt, E.; Popovic, Z.; Overgaag, K.; van Lagen, B.; Grandidier, B.; Vanmaekelbergh, D.; Dominguez-Gutierrez, D.; De Cola, L.; Zuilhof, H. *Journal of Materials Chemistry* **2009**, *19*, 5926.
- (42) Wang, L.; Reipa, V.; Blasic, J. *Bioconjugate Chemistry* **2004**, *15*, 409.
- (43) Kelly, J. A.; Henderson, E. J.; Clark, R. J.; Hessel, C. M.; Cavell, R. G.; Veinot, J. G. C. *Journal of Physical Chemistry C* **2010**, 22519.
- (44) Reboledo, F. A.; Galli, G. J. *Phys. Chem. B* **2005**, *109*, 1072.
- (45) Seliger, H.; Gortz, H.-H. *Synthetic Communications* **1980**, *10*, 175

## 4.6 Appendix

The amplitude-weighted fluorescence lifetime can be calculated according to the following Equation:

Equation 1.

$$\tau_{av} = \frac{\sum_{i=1}^n a_i \tau_i^2}{\sum_{i=1}^n a_i \tau_i}$$

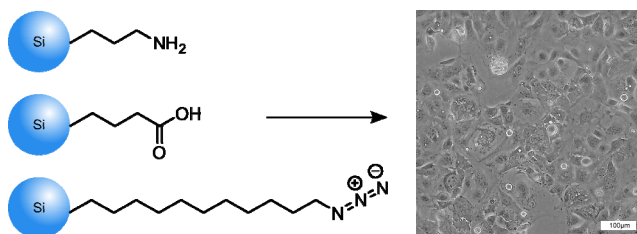
Where  $\tau_{av}$  is the amplitude-weighted average,  $a_i$  the amplitude of decay  $i$ , and  $\tau_i$  the fluorescence lifetime time constant of decay  $i$ .

# Chapter 5

## Synthesis and Cytotoxicity of Silicon Nanoparticles with Covalently Attached Organic Monolayers

### Abstract

A series of highly monodisperse silicon nanoparticles (Si NPs) with either positively (amine), neutral (azide) or negatively (carboxylic acid) charged covalently attached organic monolayers were synthesized and investigated for their cytotoxicity. Infrared data confirmed the presence of these covalently attached surface groups. The Si NPs were characterized by absorption and fluorescence spectroscopy. The cytotoxicity was investigated in Caco-2 cells by determining the cell viability and proliferation. The IC<sub>50</sub> values for the Si NPs ranged from 20 µg/L for the amine-terminated Si NPs, via 550 - 850 µg/L for the azide-terminated Si NPs to non-toxic (no measureable IC<sub>50</sub>) for the carboxylic acid-terminated Si NPs. These results indicate a trend in cytotoxicity, depending on surface charge, i.e. that positively charged Si NPs are more cytotoxic than negatively charged Si NPs. Interestingly, it appeared that the cytotoxicity of the Si NP-NH<sub>2</sub> depends strongly on the presence of fetal calf serum in the medium.



*This work has been published:*

L. Ruizendaal, S. Bhattacharjee, K. Pournazari, M. Rosso-Vasic, L.H.J. de Haan, G. M. Alink, A.T.M. Marcelis, Han Zuilhof, *Nanotoxicology* **2009**, 339-347

## 5.1 Introduction

Compared to the more commonly investigated silica ( $\text{SiO}_2$ ) nanoparticles (NPs), silicon (Si) NPs have the advantage that organic groups can be attached to the surface through a very stable covalent S-C bond<sup>1,2</sup>. Compared to bulk silicon, silicon nanoparticles (Si NPs) have interesting optical fluorescent properties related to their small size. Quantum confinement effects are expected for Si NPs smaller than 5 nm<sup>3</sup>, which makes the study and synthesis of well-defined and monodisperse Si NPs in the 1 – 5 nm range interesting for a variety of optoelectric applications, such as fluorescence bioimaging<sup>4-8</sup>. An attractive way to obtain these functionalized Si NPs is by starting from H-terminated Si NPs, which are then reacted with terminal alkenes to provide stable covalent Si-C bonds, similar to the preparation of functional organic groups on planar H-terminated silicon surfaces<sup>9-12</sup>. The method that probably yields the most well-defined Si NPs is that of Tilley, who reported on the microgram scale synthesis of Si NPs via the use of micelles in apolar solvents. These Si NPs could be made alkyl-terminated<sup>13</sup> and aminoalkyl-terminated<sup>14</sup>. Rosso-Vasic *et al.*<sup>15</sup> have further developed this method to obtain gram-scale yields of well-defined alkyl-capped Si NPs with a Si core size of  $1.6 \pm 0.2$  nm, which now gives the ability to obtain significant amounts Si NPs coated with a wide variety of functional groups, making them also suitable for a wide range of studies and biological applications.

However, little is known about the specific toxicity of NPs in biological systems and human beings. Many NPs proposed for sensing and diagnostics today are semiconductor quantum dots composed of core/shell particles with group II-VI or group III-V elements in the core such as CdSe, CdTe, ZnS, GaAs and InP<sup>16</sup>. Many of these core metals are highly toxic in low concentrations, such as cadmium, selenium, lead and arsenic<sup>17,18</sup>. The degradation of the core is an important factor in the cytotoxicity, mostly prevented by adding a non-toxic shell to the toxic core and thereby slowing down the leakage of the toxic elements. Several studies have shown that these NPs can indeed be toxic<sup>17,19</sup>, although the results of different toxicity studies are difficult to compare in the published literature due to differences resulting from using different methods, materials and cell lines. In contrast, Si NPs have a core of silicon. The absence of toxic elements, together with the fluorescent properties and the fact that the surface can be modified with strong covalent bonds, make these nanoparticle materials potentially very useful as a platform for biomedical applications. Recently, Alsharif *et al.*<sup>20</sup> have found no evidence for *in vitro* cytotoxicity of alkyl-capped Si NPs. Primarily the shell or surface-covering material is therefore expected to be responsible for the potential toxicity of these Si NPs.



To test the cytotoxicity of the Si NPs in a reproducible and quantifiable manner, two different assays were chosen in the present study. First, the colorimetric MTT (3-(4,5-dimethylthiazol-2-yl)-2,5-diphenyl tetrazolium bromide) assay was used, which is a measure for the mitochondrial metabolic activity of living cells. This test is used to monitor cell metabolic function, cell proliferation or cell activation<sup>21,22</sup>. Secondly, the BrdU (5-bromo-2-deoxyuridine) immunoassay was used, which gives an indication of cell proliferation<sup>23,24</sup>.

The human colon adenocarcinoma Caco-2 cell line was chosen to test the toxicity of the Si NPs. Caco-2 cells can differentiate into colonic cells with an unique apico-basal conformation. Hence these cells can be used as a model cell line for testing the toxicity of any orally administered substance. The cells are robust in nature, grow fast under laboratory conditions and are easy to culture. Also the huge amount of data available in literature makes it easier to compare the derived data with published data.

The aim of this study was to asses on the influence of different surface properties, especially surface charge, of the Si NPs on the cytotoxicity in Caco-2 cells. The used Si NPs give the unique opportunity to test the role of surface charge in the cytotoxicity exhibited by nanoparticles. Therefore, similar monodisperse Si NPs with amine, azide and carboxylic acid functionalities were prepared and their toxicity was tested in MTT and BrdU assays over a wide concentration range (0 – 2200 µg/L) in the presence and absence of fetal calf serum (FCS). Under the test-conditions the amine-terminated Si NPs are positively charged, the azide-terminated Si NPs neutral and the carboxylic acid-terminated Si NPs are negatively charged.

## **5.2 Results**

### **5.2.1 Synthesis and characterization of Si NPs.**

Butenoic acid-terminated Si NPs (Si NP-COOH) were synthesized using the method of Zuilhof and co-workers<sup>15</sup> to obtain H-terminated Si NPs, which were converted to carboxylic acid-terminated NPs by the direct attachment of 3-butenic acid. Direct attachment of the carboxylic acid has the advantage over attachment of a methyl ester<sup>25</sup> that subsequent ester hydrolysis is not needed. This circumvents possible incomplete hydrolysis and base-induced or acid-induced damage of the monolayer coverage as was observed during hydrolysis of planar modified Si surfaces.<sup>26-28</sup>

The carboxylic acid-terminated Si NPs were analyzed using infrared spectroscopy (figure 1). The peak at  $1722\text{ cm}^{-1}$  indicates the carbonyl stretch vibration of the acid, while the broad peak around  $3424\text{ cm}^{-1}$  indicates the carboxylic acid OH stretch. Since the peak is not broadened beyond  $3000\text{ cm}^{-1}$ , the COOH moieties do not form hydrogen-bonded dimers, but are largely present as free COOH groups, which is as expected for surface-bound COOH groups. As a result, some of them will be negatively charged (COO<sup>-</sup>) in aqueous media. The antisymmetric and symmetric CH<sub>2</sub> stretching vibrations are clearly visible at  $2858$  and  $2928\text{ cm}^{-1}$ . Furthermore, the CH<sub>3</sub> stretching vibration is visible at  $2956\text{ cm}^{-1}$ . The scissoring vibrations of the Si-C bonds are visible at  $1466\text{ cm}^{-1}$ . There is only a very small Si-O stretch vibration visible at  $1096\text{ cm}^{-1}$ , indicating that there is at most only a small fraction of butenoic molecules that have added to the silicon through the oxygen groups, or that a very small amount of oxidation of the silicon core has occurred.

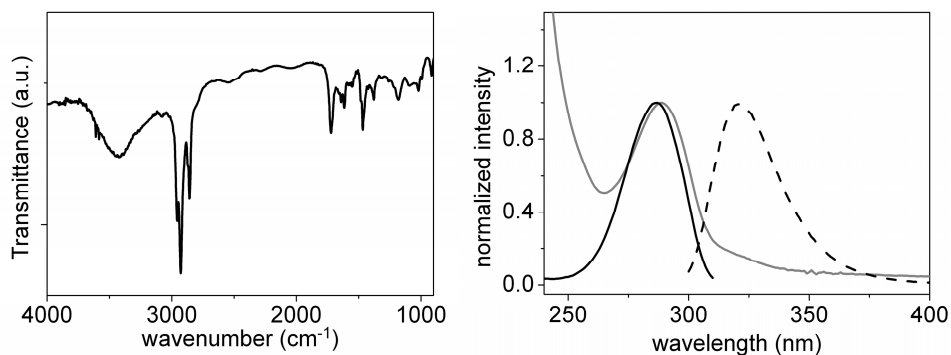


Figure 1. Left: Infrared spectrum of Si NP-COOH; Right: Absorption (grey), excitation (black) and emission (dashed) spectra of Si NP-COOH.

To further characterize the Si NPs, both UV-Vis absorption spectroscopy as well as steady-state and time-resolved fluorescence spectroscopy was performed. The UV-Vis absorption spectrum of the Si NP-COOH showed an absorption maximum at 278 nm. The maximum fluorescence excitation occurs at the same wavelength, whereas the emission has a maximum at 322 nm (figure 1).

Time-resolved measurements showed that the fluorescence anisotropy decay is strictly mono-exponential. This can only be the case when all three perpendicular axes around which the Si NP can rotate are the same, i.e. when the Si NPs are spherical<sup>15,29</sup>. The fluorescence-related data of the Si NPs are summarized in table 1. The fluorescence

lifetimes of the Si NPs are calculated using a stretched exponential fit<sup>30</sup>:  $I(t) = I_0 * \exp [ - (t / \tau)^\beta ]$  where  $I(t)$  = fluorescence intensity at time  $t$ ,  $I_0$  = fluorescence intensity at  $t = 0$ ;  $\tau$  = fluorescence lifetime decay constant, and  $\beta$  = heterogeneity parameter of the sample ( $\beta = 1$  means the fluorescence lifetimes of the molecules in the sample is homogeneous). The fluorescence data showed that the emission characteristics are different (both in energy terms and rates of relaxation to the electronic ground state) for all NPs under study, despite the fact that the Si core is identical in all cases. This points to a clear effect of the terminal substituent on the electronic character of the NPs. The effect of the terminal substituent was therefore also investigated with respect to the cytotoxicity of these NPs.

Table 1. Summarized data of the luminescent properties of the studied Si NPs

Coating	Fluor. maximum		FWHM (nm)	Fluorescence lifetime $\tau$ (ns)
	$\lambda_{exc}$ (nm)	$\lambda_{em}$ (nm)		
- C <sub>3</sub> H <sub>6</sub> NH <sub>2</sub>	390	475	98	4.7 ± 0.16; $\beta$ = 0.75
- C <sub>3</sub> H <sub>6</sub> COOH	278	322	32	1.30 ± 0.09; $\beta$ = 0.98
- C <sub>11</sub> H <sub>22</sub> N <sub>3</sub>	280	315	57	3.13 ± 0.01; $\beta$ = 0.73

Note: FWHM: Full Width Half Maximum; ns: nanoseconds.

### 5.2.2 Effect of Si NP-NH<sub>2</sub> on Caco-2 cells.

In figure 2A, the cell viability in the MTT assay is plotted as a function of the concentration of Si NP-NH<sub>2</sub>. The cells were exposed to the Si NP-NH<sub>2</sub> in a concentration range from 0 – 185 µg/L, both in the presence and absence of fetal calf serum (FCS) in the medium. Without FCS cell viability did not decrease up to a concentration of 185 µg/L after 24 hours of incubation. Therefore, in this concentration range of the Si NP-NH<sub>2</sub> no IC<sub>50</sub> could be determined, and Si NP-NH<sub>2</sub> showed no cytotoxic effects on the cells. When the cells were incubated in the presence of FCS, a sharp drop in cell viability was observed using concentrations of more than 11 µg/L. The IC<sub>50</sub> value for 24 hours incubation in the presence of FCS in the medium was calculated to be 20 µg/L.

Figure 2B shows the effect of Si NP-NH<sub>2</sub> concentration on cell proliferation using the BrdU assay. Without the presence of FCS no effect on the cell proliferation could be measured up to a concentration of 185 µg/L. In the presence of FCS, a gradual decrease in cell

proliferation could be observed, down to 60% of the values compared to the negative control where no Si NP-NH<sub>2</sub> were added.

### 5.2.3 Effect of Si NP-N<sub>3</sub> on Caco-2 cells.

Figure 2C shows the Caco-2 cell viability in the MTT assay plotted as function of Si NP-N<sub>3</sub> concentration, ranging from 0 – 2200 µg/L, both in the presence and absence of FCS. The presence of FCS in the medium almost had no effect on the cytotoxicity of the Si NP-N<sub>3</sub>. An IC50 of 850 µg/L could be determined in the presence of FCS, and an IC50 of 600 µg/L in the absence of FCS. These values are much higher than the IC50 values of the Si NP-NH<sub>2</sub>, indicating that the Si NP-N<sub>3</sub> are less cytotoxic than Si NP-NH<sub>2</sub> in the presence of FCS in the medium.

Figure 2D shows similar effects of the Si NP-N<sub>3</sub> concentration, ranging from 0 - 2200 µg/L, on the Caco-2 cell proliferation in the BrdU test. Similar to the MTT assay, the presence or absence of FCS in the medium has hardly an influence on the cytotoxic effects of the Si NP-N<sub>3</sub>. The calculated IC50 values are 550 µg/L in the presence and 570 µg/L in the absence of FCS.

### 5.2.4 Effect of Si NP-COOH on Caco-2 cells.

In Figure 2E the effect of Si NP-COOH concentration, 0 – 1700 µg/L, on the cell viability as measured in the MTT assay and in Figure 2F, cell proliferation as measured with the BrdU assay are plotted. Remarkably, no effect of increasing concentration on the cell viability is observed even upon incubation with a Si NP-COOH concentration of 1700 µg/L. The results of the MTT assay and the BrdU assay were similar and no effect of the presence of FCS was found. These results show that the Si NP-COOH have less cytotoxic effects on Caco-2 cells than Si NP-N<sub>3</sub>.

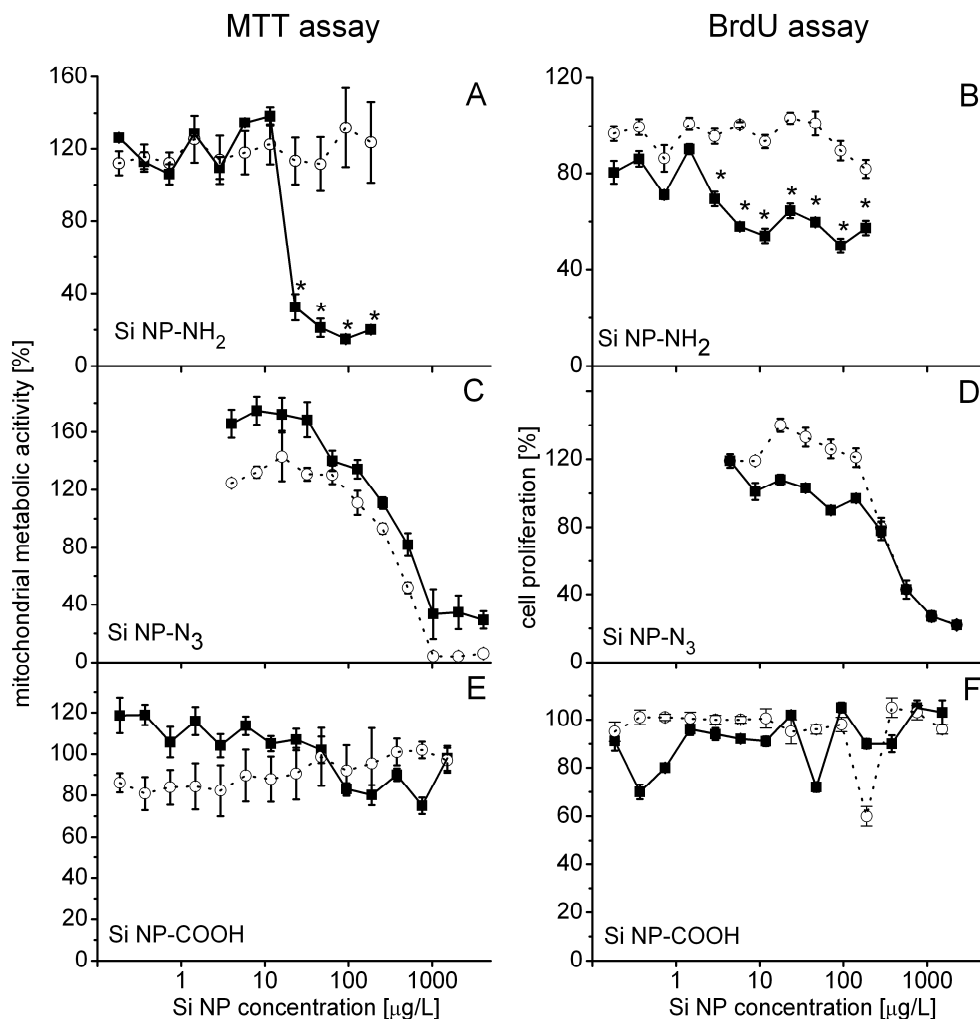


Figure 2. Mitochondrial metabolic activity (MTT assay) and cellular proliferation (BrdU assay) of the Caco-2 cells after 24 hours exposure to Si NP-NH<sub>2</sub> (A and B), Si NP-N<sub>3</sub> (C and D) and Si NP-COOH (E and F). Measurements in the presence (■) and absence (○) of FCS. Number of experiments (n) in the presence and absence of FCS: n = 12 (A and B); n = 9 (C and D); n = 8 (E and F). The asterisk sign (\*) signifies statistically significantly different (p < 0.05) data from respective control values.

### 5.3 Discussion

The synthetic route to make Si NPs by reduction of  $\text{SiCl}_4$  to obtain H-terminated Si NPs, followed by a surface functionalization reaction with alkenes, was successfully further explored by making amine<sup>1</sup>, azide<sup>31</sup> and carboxylic acid surface-modified NPs. The maximum absorption and excitation wavelength of the Si NP-COOH were found at 278 nm and the emission maximum is at 322 nm. This is comparable to the results of Rogozhina *et al.*<sup>25</sup>, who showed that Si NPs terminated with pentenoic acid obtained by the hydrolysis of the corresponding methyl ester had identical absorption and emission wavelengths. Furthermore, these results are also in line with computational studies by Li *et al.*<sup>32</sup>, who calculated the absorption and emission wavelengths for different sizes of Si NPs capped with propionic acid. The Si NPs used in this study and synthesized using the same literature method<sup>25</sup>, show absorption, fluorescence excitation and emission spectra that are characteristic for the type of organic monolayer and the size of the Si NPs (about 1.6 nm). The fluorescence lifetimes are also characteristic for the studied Si NPs and fluorescence anisotropy measurements indicate that the particles are spherical.

An important result of the present study is that the amine-terminated Si NPs showed cytotoxicity after exposure to Caco-2 cells for 24 hours when administered together with FCS. However, they showed no cytotoxicity when administered without FCS up to concentrations of 185  $\mu\text{g/L}$ . These remarkable differences in cytotoxicity caused by the absence or presence of FCS is an interesting feature that is still largely unexplained. Previous studies<sup>33,34</sup> suggested that the proteins in FCS may interact with nanoparticles so that they are better dispersed and thereby facilitate their entry into the cells, thus causing higher cytotoxic effects than in the absence of FCS. Due to the small size of the Si NPs (~1.6 nm), it is thought that they are adsorbed by the proteins in FCS and that by the uptake of the FCS by the cells the Si NPs are also transported into the cells. It is known that positively charged molecules get adsorbed to the negatively charged lipid membrane of cells, e.g. shown by the interaction of the polycationic polymer chitosan with Caco-2 cells<sup>35</sup>. Because of the positive charge on the Si NP-NH<sub>2</sub>, they can interact in a similar manner as chitosan with the lipid membrane of the cells, and when in the cells, have interaction with negatively charged components in the cells such as the cell membrane and DNA backbone. It is also possible that reaction with proteins in FCS makes the cationic NPs more neutral by charge compensation, which might facilitate cellular uptake.

The results described above show that the Si NP-N<sub>3</sub> are much less cytotoxic to the Caco-2 cells than the Si NP-NH<sub>2</sub>. The effect of the presence or absence of FCS in the medium was

less pronounced, but still visible. Furthermore, the transition from cytotoxic to non-cytotoxic concentrations is less sharp as compared to the Si NP-NH<sub>2</sub>. The reason for this could be that the neutral Si NP-N<sub>3</sub> do not have extensive interactions with the lipid membrane, and upon uptake could have less toxic interactions with the contents of the cell. One of the reasons for this limited cytotoxicity could be related to the overall neutral charge of the azide-group. The lack of cytotoxicity of the azide was also observed upon exposing cell cultures to azido-sugars for 1 – 3 days, after which no cytotoxic effects on the cells were observed. Furthermore, upon injection of the azido-sugars in mice, no signs of distress were measured<sup>36</sup>.

The negatively charged Si NP-COOH showed no cytotoxicity to the Caco-2 cells in the current study, both in the presence and absence of FCS. This is in agreement with a study on silica nanotubes that showed that negatively charged nanotubes are less harmful to cells than positively charged NH<sub>2</sub>-coated nanotubes<sup>37</sup>. Although the negatively charged nanotubes still displayed some toxicity, the Si NP-COOH used in the present study displayed no measurable cytotoxicity over a wide concentration range.

There is one report of a toxicity study on alkyl-terminated silicon NPs showing that they are non-toxic. However, these Si NPs were not water-soluble and thus differed from those used in the present study. Furthermore, they were tested at only one concentration<sup>20</sup>, which makes comparison with our study difficult.

The cytotoxicity tests performed in this study indicate that the surface charge of the Si NPs has a great influence on the cytotoxicity towards the colonic Caco-2 cells. The positively charged NH<sub>2</sub>-terminated Si NPs are cytotoxic, whereas the neutral Si NP-N<sub>3</sub> were moderately cytotoxic and the Si NP-COOH showed no cytotoxicity at all. Charge-dependent cellular uptake and associated toxicology has been observed previously in several studies, where positively charged molecules such as polylysine-functionalized silica NPs<sup>38</sup> or cationic PAMAM-dendrimers<sup>39</sup> inherently were taken up faster by cells than neutral molecules. In the study on PAMAM-dendrimers, it was shown that the positively charged dendrimers had a strong interaction with the negatively charged lipid bilayer, while the neutral dendrimers showed little interaction. The lipid bilayer described in that study was used as a model for the phospholipid membrane of cells. The observations were confirmed by calculations, which showed that bigger (G5 or G7; 10 - 13 nm diameter) dendrimers made holes in the lipid bilayer, whereas the smaller (G3; about 3.5 nm diameter) dendrimers did have interactions but did not make permanent holes. A theoretical study confirmed the importance of charge in disrupting membranes by modeling of the specific interaction between these membranes and NPs in general<sup>40</sup>.

Their results indicated that the higher the charge density, the more phospholipid molecules are detached from the membrane and absorbed on the NP surface.

Furthermore, it was shown by atomic force microscopy studies that a wide variety of cationic NPs, including cell-penetrating peptides, polycationic polymers and inorganic NPs (Au-NH<sub>2</sub>, SiO<sub>2</sub>-NH<sub>2</sub>) can induce disruption of supported lipid membranes. These effects were observed as formation of holes, membrane thinning and membrane erosion<sup>41</sup>.

In contrast, a recent study of amine-modified or carboxyl-modified CdSe/ZnS QDs revealed that the intravenous toxicity of the carboxyl-modified QDs is much higher than of the amine-modified QDs<sup>42</sup>. Furthermore, it was shown that QDs with different surface modifications end up in different organs in the mice. This shows that for *in vivo* application of the Si NPs further studies are needed.

Interestingly, a visible increase in both mitochondrial metabolic activity and cellular proliferation was found for low concentrations of Si NP-N<sub>3</sub> nanoparticles. This initial surge in activity is especially clear in the MTT assay, where it also occurs at lower concentrations than in the BrdU assay. It should be noted that mitochondrial metabolic activity and cellular proliferation are two mutually independent parameters and it is quite possible that the cytotoxicity of these silicon nanoparticles affects the mitochondria of the cells before it influences cellular DNA. Similar reports have been published where an initial high mitochondrial activity was observed after exposing cells to nanoparticles or other toxic agents. <sup>43</sup>first found an increased mitochondrial metabolic activity at low carbon nanotube concentrations while testing the effect of bovine serum albumin on the cytotoxicity of carbon nanotubes on A549 cells. Similar results were found by Monteiro-Riviere and co-workers<sup>44</sup> when testing the cytotoxicity of quantum dots on human epidermal keratinocyte (HEK) cells. Although not a nanoparticle toxicity study,<sup>45</sup> found similar results when testing the protective effects of N-methylated derivatives of amyloid- $\beta$ -peptide- $\beta$  (25-35) on a rat pheochromocytoma PC-12 cell line. These findings could be caused by compensatory mechanisms that become activated within the cells to resist the toxicity of these agents at lower initial concentrations which then gets expressed as higher proliferation values in the cytotoxicity assays.

It might be concluded that the cytotoxicity of the Si NPs is highly dependent on the surface charge of the coating group. In addition, the presence of fetal calf serum in the cell medium seems to enhance the cytotoxicity. Given the non-cytotoxicity of negatively charged Si NPs (Si NP-COOH) and because the Si NPs show photoluminescence, they may be highly promising for bioimaging applications. However, more research is required to develop Si NPs which are safe and non-toxic for use in human beings.



## 5.4 Materials & Methods

### 5.4.1 Synthesis and purification of the Si NP-COOH

All chemicals were purchased from Sigma-Aldrich and employed without further purification unless specified differently. Toluene ( $(\text{H}_2\text{O} \leq 0.005 \text{ } \%, \geq 99.7 \text{ } \%$  (GC)) was dried over sodium wire overnight prior to use. Methanol was distilled and stored over anhydrous magnesium sulfate. The 3-butenic acid was distilled and stored over molecular sieves. Dimethyl sulfoxide (DMSO) was purchased from Merck; Dulbecco's modified eagle medium (DMEM), Hank's buffered salt solution (HBSS), phosphate buffer saline (PBS), trypsin, gentamicin and non-essential amino-acids were purchased from Invitrogen.

For the synthesis of the NPs dry and oxygen-free conditions are essential. An argon atmosphere was used during the whole synthetic procedure. Dry toluene (100 mL) was made oxygen-free prior to use by bubbling through argon for 3 hours. Tetraoctylammonium bromide (TOAB,  $\geq 99.0 \text{ } \%$ ; 3.0 g, 5.6 mmol) was dispersed in the toluene by 30 minutes of sonication.  $\text{SiCl}_4$  (200  $\mu\text{L}$ , 1.8 mmol) was added via an air-tight syringe, followed by 30 minutes of sonication. Subsequently, a 1 M  $\text{LiAlH}_4$  (lithium aluminium hydride) solution in tetrahydrofuran (4.6 mL, 4.6 mmol) was injected via an air-tight syringe, followed by a further 30 minutes of sonication in order to form the H-terminated Si NPs. Excess  $\text{LiAlH}_4$  was quenched by adding dry methanol (30 mL, 740 mmol), and the reaction mixture was sonicated for 15 minutes. To obtain the COOH-terminated Si NPs, 3-butenic acid (4.4 mL, 0.052 mol) was added, together with a catalytic amount of chloroplatinic acid (40  $\mu\text{L}$ ; 0.05 M in dry methanol) and the mixture was sonicated for another 30 minutes. The resulting Si NPs were purified by evaporation of all solvents under reduced pressure. Then the material was redispersed in water and solid TOAB was removed by filtration. Further purification was performed by dialysis using a regenerated cellulose membrane with molecular weight cut-off (MWCO) 3500 or MWCO 1000, and subsequent filtration through a hydrophilic 450 nm polyvinylidene fluoride membrane filter (MILLEX-HV, Millipore).

The amine-terminated (Si NP- $\text{NH}_2$ ) and azide-terminated (Si NP- $\text{N}_3$ ) Si NPs were synthesized by reaction of the H-terminated Si NPs with allylamine and 11-azido-undec-1-ene, respectively, as described previously, and yielded Si NPs with a Si core size of  $1.6 \pm 0.2 \text{ nm}$ <sup>1,31</sup>.

### 5.4.2 Optical measurements of Si NPs

All measurements were performed at standard pressure and at room temperature. Electronic absorption spectra were recorded in a quartz cuvette (1 cm, Hellma), using a Cary 1 UV-Vis single beam spectrophotometer and were corrected for the solvent absorption. The scan range was 600-200 nm with a scan rate of 600 nm / minute.

Steady-state and time-resolved fluorescence measurements were performed on a Time-Correlating Single Photon Counting F900 spectrometer (Edinburgh Instruments), with an instrument response function for time-resolved measurements of 87 ps. All steady-state spectra were corrected for the wavelength-dependent sensitivity of the detector and the source by recording reference data simultaneously. Additionally, emission spectra were corrected for Raman scattering using the solvent emission spectrum.

Time-resolved fluorescence measurements were performed with exactly the same solutions used for steady-state spectra (absorption was always adjusted to be  $\leq 0.2$ ). A pulsed light-emitting diode ( $\lambda_{\text{excitation}} = 283 \text{ nm}$ ) was used as a excitation source, and emitted photons were collected (4096 channels) until a maximum of  $10^4$  counts was reached. Origin 8 software was used to fit the data.

For Fourier-transform infrared spectroscopy (Bruker, Vector 22 FTIR spectrometer), thin films of Si NP in carbon tetrachloride solution were placed between sodium chloride crystals. For each measurement 64 scans were collected and corrected for the background signal.

### 5.4.3 Solutions of Si NPs for the toxicology tests

Stock solutions of Si NP-NH<sub>2</sub> and Si NP-COOH were made in water and of Si NP-N<sub>3</sub> in DMSO. In a 24-wells plate, dose-response dilutions of the stock solutions of Si NPs were made using pyrogen-free water. From these solutions, two series of samples were made in the DMEM medium, either with or without 10% heat-inactivated FCS. The concentrations of the series ranged from 0 – 185  $\mu\text{g/L}$  for Si NP-NH<sub>2</sub>, 0 - 1700  $\mu\text{g/L}$  for Si NP-COOH and 0 – 2200  $\mu\text{g/L}$  for Si NP-N<sub>3</sub>. The solutions of the nanoparticles with and without FCS showed no visible signs of aggregation or precipitation. Inspection by dynamic light scattering (DLS) also showed no clear change in particle size upon adding the nanoparticles to the FCS solution.

#### **5.4.4 Cells and treatments**

The Caco-2 cells were maintained in incubators with 5% CO<sub>2</sub> in a humidified atmosphere at 37 °C. The cells were subcultured at a ratio of 1 to 10 in DMEM medium in a 75 cm<sup>2</sup> flask. The Caco-2 cells were grown in DMEM medium, supplemented with 10% heat-inactivated FCS and 0.1 % gentamicin. The cells were used in passage 30 - 40. For the exposure measurements, the cells were plated at a concentration of  $2 \times 10^4$  cells / mL in a 96-wells plate and were incubated for 24 hours. Then the Si NPs were added to the cells in different concentrations in a total volume of 100 µL. After this, the cells were incubated for another 24 hours.

#### **5.4.5. Toxicological assays**

##### *MTT Assay*

The mitochondrial metabolic activity was determined by the colorimetric MTT assay<sup>21</sup>. After 24 hours exposure to the Si NPs, 5 µL MTT solution (3-(4,5-dimethylthiazol-2-yl)-2,5-diphenyl tetrazolium bromide) in PBS (5 mg / mL) was added to each well and incubated for 4 hours. After 4 hours, the medium was removed and 100 µL of DMSO was added to dissolve the formed formazan crystals. The plates were put in the plate shaker for 5 minutes. The absorbance at both 562 nm and 620 nm was measured. The mitochondrial metabolic activity was expressed as the mean percentage of the control values. 0.1% Triton X100 was used as positive control and medium without Si NPs was used as negative control. The mitochondrial metabolic activity was expressed as the mean percentage of the negative control values. Also control tests were done to exclude the possibility of formation of crystals after reaction between the nanoparticles and the MTT solution. For this 100 µL of the tested nanoparticle solutions were mixed with 5 µL of MTT solution in a 96 well plate and subsequently incubated for 4 hours. No crystal formation or change in color of the solution in the wells was observed.

##### *BrdU Assay*

Cell proliferation was quantified using the colorimetric BrdU (5-bromo-2-deoxyuridine) assay (Cat. No. 647229001 Roche Diagnostics, Penzberg, Germany). BrdU acts as a structural analog of thymidine and will be incorporated in newly synthesized DNA during cell replication. This test indicates cell proliferation. After incubation of the Caco-2 cells with the Si NPs and BrdU for 24 hours, the medium containing the Si NPs and BrdU was removed, and the BrdU labeling solution was added to the wells and incubated for 4

hours. Subsequently, the immunoassay was performed according to the protocol of the manufacturer. Cell proliferation was expressed as the mean percentage of the negative control values. 0.1% Triton X100 was used as positive control and medium without Si NPs was used as negative control.

### Statistical Analysis

All data from MTT and BrdU assay was statistically analyzed by Igor Pro 6 software from Wavemetrics inc. Paired student's t-test was performed to determine which data points are statistically significantly different from respective control values and noted with asterisk (\*) only when  $p < 0.05$ .

## 5.5 References

- (1) Rosso-Vasic, M.; De Cola, L.; Zuilhof, H. *J. Phys. Chem. C* **2009**, *113*, 2235-2240.
- (2) Veinot, J. G. C. *Chem. Commun.* **2006**, 4160-4168.
- (3) Krishna, M. V. R.; Friesner, R. A. *J. Chem. Phys.* **1991**, *95*, 8309-8322.
- (4) Chan, W. C. W.; Nie, S. M. *Science* **1998**, *281*, 2016-2018.
- (5) Bruchez, M., Jr.; Moronne, M.; Gin, P.; Weiss, S.; Alivisatos, A. P. *Science* **1998**, *281*, 2013-2016.
- (6) Larson, D. R.; Zipfel, W. R.; Williams, R. M.; Clark, S. W.; Bruchez, M. P.; Wise, F. W.; Webb, W. W. *Science* **2003**, *300*, 1434-1436.
- (7) Michalet, X.; Pinaud, F. F.; Bentolila, L. A.; Tsay, J. M.; Doose, S.; Li, J. J.; Sundaresan, G.; Wu, A. M.; Gambhir, S. S.; Weiss, S. *Science* **2005**, *307*, 538-544.
- (8) Liu, W.; Howarth, M.; Greytak, A. B.; Zheng, Y.; Nocera, D. G.; Ting, A. Y.; Bawendi, M. G. *J. Am. Chem. Soc.* **2008**, *130*, 1274-1284.
- (9) Sieval, A. B.; Linke, R.; Zuilhof, H.; Sudholter, E. J. R. *Adv. Mater.* **2000**, *12*, 1457-1460.
- (10) Buriak, J. M. *Chem. Rev. (Washington, DC, U. S.)* **2002**, *102*, 1271-1308.
- (11) Boukherroub, R. *Curr. Opin. Solid State Mater. Sci.* **2005**, *9*, 66-72.
- (12) Scheres, L.; Arafat, A.; Zuilhof, H. *Langmuir* **2007**, *23*, 8343-8346.
- (13) Tilley, R. D.; Warner, J. H.; Yamamoto, K.; Matsui, I.; Fujimori, H. *Chem. Commun.* **2005**, 1833-1835.
- (14) Warner, J. H.; Hoshino, A.; Yamamoto, K.; Tilley, R. D. *Angew. Chem., Int. Ed.* **2005**, *44*, 4550-4554.
- (15) Rosso-Vasic, M.; Spruijt, E.; van Lagen, B.; De Cola, L.; Zuilhof, H. *Small* **2008**, *4*, 1835-1841.
- (16) Chan, W. C. W.; Maxwell, D. J.; Gao, X. H.; Bailey, R. E.; Han, M. Y.; Nie, S. M. *Curr. Opin. Biotechnol.* **2002**, *13*, 40-46.
- (17) Lewinski, N.; Colvin, V.; Drezek, R. *Small* **2008**, *4*, 26-49.
- (18) Derfus, A. M.; Chan, W. C. W.; Bhatia, S. N. *Nano Lett.* **2004**, *4*, 11-18.
- (19) Hardman, R. *Environ. Health Perspect.* **2006**, *114*, 165-172.
- (20) Alsharif, N. H.; Berger, C. E. M.; Varanasi, S. S.; Chao, Y.; Horrocks, B. R.; Datta, H. K. *Small* **2009**, *5*, 221-228.
- (21) Mosmann, T. *J. Immunol. Methods* **1983**, *65*, 55-63.
- (22) Ciapetti, G.; Cenni, E.; Pratelli, L.; Pizzoferrato, A. *Biomaterials* **1993**, *14*, 359-364.
- (23) Altman, J. *Science* **1962**, *135*, 1127-1128.
- (24) Altman, J.; Das, G. D. *J. Comp. Neurol.* **1965**, *124*, 319-335.

- (25) Rogozhina, E. V.; Eckhoff, D. A.; Gratton, E.; Braun, P. V. *J. Mater. Chem.* **2006**, *16*, 1421-1430.
- (26) Linford, M. R.; Fenter, P.; Eisenberger, P. M.; Chidsey, C. E. D. *J. Am. Chem. Soc.* **1995**, *117*, 3145-3155.
- (27) Sieval, A. B.; Demirel, A. L.; Nissink, J. W. M.; Linford, M. R.; van der Maas, J. H.; de Jeu, W. H.; Zuilhof, H.; Sudholter, E. J. R. *Langmuir* **1998**, *14*, 1759-1768.
- (28) Boukherroub, R.; Morin, S.; Bensebaa, F.; Wayner, D. D. M. *Langmuir* **1999**, *15*, 3831-3835.
- (29) Lakowicz, J. R. *Principles of Fluorescence Spectroscopy*; third ed.; Springer: Singapore, 2006.
- (30) Benny Lee, K. C.; Siegel, J.; Webb, S. E. D.; L  v  que-Fort, S.; Cole, M. J.; Jones, R.; Dowling, K.; Lever, M. J.; French, P. M. W. *Biophys. J.* **2001**, *81*, 1265-1274.
- (31) Rosso-Vasic, M.; Weijers, C. A. G. M.; Spruijt, E.; Ruizendaal, L.; De Cola, L.; Zuilhof, H. **submitted**.
- (32) Li, Q. S.; Zhang, R. Q.; Niehaus, T. A.; Frauenheim, T.; Lee, S. T. *J. Chem. Theory Comput.* **2007**, *3*, 1518-1526.
- (33) Foucaud, L.; Wilson, M. R.; Brown, D. M.; Stone, V. *Toxicol. Lett.* **2007**, *174*, 1-9.
- (34) M  ller, W.; Brown, D. M.; Kreyling, W. G.; Stone, V. *Particle and Fibre Toxicology* **2005**, *2*.
- (35) Schipper, N. G. M.; Olsson, S.; Hoogstraate, J. A.; deBoer, A. G.; Varum, K. M.; Artursson, P. *Pharm. Res.* **1997**, *14*, 923-929.
- (36) Laughlin, S. T.; Agard, N. J.; Baskin, J. M.; Carrico, I. S.; Chang, P. V.; Ganguli, A. S.; Hangauer, M. J.; Lo, A.; Prescher, J. A.; Bertozzi, C. R. In *Methods Enzymol.* 2006; Vol. 415, p 230-250.
- (37) Nan, A.; Bai, X.; Son, S. J.; Lee, S. B.; Ghandehari, H. *Nano Lett.* **2008**, *8*, 2150-2154.
- (38) Li, Z.; Zhu, S. G.; Gan, K.; Zhang, Q. H.; Zeng, Z. Y.; Zhou, Y. H.; Liu, H. Y.; Xiong, W.; Li, X. L.; Li, G. Y. *J. Nanosci. Nanotechnol.* **2005**, *5*, 1199-1203.
- (39) Mecke, A.; Majoros, I. J.; Patri, A. K.; Baker, J. R.; Holl, M. M. B.; Orr, B. G. *Langmuir* **2005**, *21*, 10348-10354.
- (40) Ginzburg, V. V.; Balijepailli, S. *Nano Lett.* **2007**, *7*, 3716-3722.
- (41) Leroueil, P. R.; Berry, S. A.; Duthie, K.; Han, G.; Rotello, V. M.; McNerny, D. Q.; Baker Jr, J. R.; Orr, B. G.; Holl, M. M. B. *Nano Lett.* **2008**, *8*, 420-424.
- (42) Geys, J.; Nemmar, A.; Verbeken, E.; Smolders, E.; Ratoi, M.; Hoylaerts, M. F.; Nemery, B.; Hoet, P. H. *Environ. Health Perspect.* **2008**, *116*, 1607-1613.
- (43) Elgrabli, D.; Abella-Gallart, S.; Aguerre-Chariol, O.; Robidel, F.; Rogerieux, F.; Boczkowski, J.; Lacroix, G. *Nanotoxicology* **2007**, *1*, 266-278.
- (44) Ryman-Rasmussen, J. P.; Riviere, J. E.; Monteiro-Riviere, N. A. *J. Invest. Dermatol.* **2007**, *127*, 143-153.
- (45) Doig, A.; Hughes, E.; Burke, R.; Lu, J.; Su, T. J.; Heenan, R. *Neurobiology of Aging* **2002**, *23*, S107-S108.



## Chapter 6

General discussion

The results described in the previous chapters describe the different aspects of Si NP synthesis, size-separation, functionalization and bioconjugation, and cytotoxicity. With the knowledge gathered here, as well as the devised conjugation methods, applications of Si NPs in biological systems or photovoltaic devices have become much closer. However, two facets should remain at the core of future attention: a robust large-scale synthesis of Si NPs with a well-controlled and tunable size of the Si core, and accurate probing of the possible toxicological effects on biosystems and whole organisms.

In Chapter 2, the successful synthesis of butyl-terminated silicon nanoparticles (Si NPs) is described. The method as described by Kauzlarich and co-workers<sup>1</sup> involved the oxidation of magnesium silicide with bromine. A major side-product formed in this reaction that has so far been overlooked is multiply brominated octane. Moreover, this impurity was, in part, also coupled to the particle surface, besides the desired butyl chains. This was confirmed by DOSY NMR experiments, revealing that these molecules were indeed covalently attached and thus cannot be removed. This makes the precise composition of the Si NPs less defined. Since trace amounts of bromine-containing chains covalently linked to the Si NP may dramatically affect optical properties, the detailed information gained about the surface composition of Si NPs will be of great value in optimizing their structures, as well as application of these Si NPs.

The size and size-distribution of the Si NPs plays an important role, since the fluorescence emission wavelength is dependent on the Si NP size.<sup>2</sup> Due to quantum confinement effects, smaller Si NPs will emit at lower wavelengths, whereas larger Si NPs emit at higher wavelengths. Simultaneously, broadening of the particle size-distribution leads to broadening of the fluorescence emission spectrum. The synthetic procedures for obtaining Si NPs, as presented in this thesis, i.e. oxidation of magnesium silicide and reduction of silicon tetrachloride, yielded Si NPs with a silicon core size of  $2.4 \pm 0.5$  nm and  $1.6 \pm 0.2$  nm, respectively. The Si NPs obtained by the reduction of  $\text{SiCl}_4$  have a narrow size distribution, but still are small and thereby emit at relative short wavelengths. The Si NPs obtained by the oxidation of  $\text{Mg}_2\text{Si}$ , however, are larger and emit at larger wavelength (525 nm) and have a less narrow size distribution that may certainly be improved. The successful size-separation of Si NPs with a silicon core size of  $2.4 \pm 0.5$  nm using size exclusion chromatography (SEC) revealed the size-dependent optical properties, such as a blue-shift of the fluorescence emission wavelength for smaller Si NPs, and a narrower fluorescence emission. Although these properties were indeed confirmed, achieving better size separation on a larger scale is certainly feasible, via preparative SEC and matching exclusion capacity, and desirable. Size-tunability (or size separation) is of particular importance, since many applications require a tunable



fluorescence emission wavelength and preferably a narrow fluorescence emission, to prevent spectral overlap between dyes. Narrow emission bands for example would enable the labeling of different cell parts with different colors (sizes) Si NPs. Other opportunities lie in multiplex analysis of complex mixtures, where the different fluorophores need to remain distinguishable for more accurate detection.

For application in biological systems, such as targeted labeling in whole organisms, the optimal optical window lies between 600 - 2500 nm for minimal loss of signal.<sup>3</sup> The lower limit is marked by the absorption of cellular tissue as well as the autofluorescence of cells. Above 600 nm this contribution is minimal and consequently, a higher cell penetration depth is reached. The synthetic methods for Si NPs reported in this thesis yield different Si NP core sizes, but even the largest Si NPs still emit at relatively short wavelengths (< 530 nm emission maximum). To obtain larger Si NPs with accordingly red-shifted emission wavelength, a different synthetic approach has to be followed. It is generally recognized that in the reduction of  $\text{SiCl}_4$  with  $\text{LiAlH}_4$ , the surfactant employed determines the final Si NP core size. Experiments with different surfactants led already to Si NPs with different sizes, although poorly described and with relative large size distributions.<sup>4</sup> The surfactant forms reversed micelles in which the reaction takes place, thereby limiting the amount of reactant available and hence limiting the final Si NP core size. Therefore, the use of different surfactants, which lead to larger micelles, is an interesting factor to investigate. In the oxidation of  $\text{Mg}_2\text{Si}$  with bromine, no surfactant is employed, and other effects determine particle size. Solutions for altering particle size may be found here. The ratio between  $\text{Mg}_2\text{Si}$  and bromine may be of influence on particle size, since the amount of available bromine is possibly responsible for the amount of surface groups, hence lowering the amount of bromine, may favor the formation of larger Si NPs. The addition of  $\text{SiCl}_4$  after 72 hours of reaction, in analogy to what is described in a Ge NP synthesis,<sup>5</sup> may increase the final Si NP size. Alternatively, an additional amount of  $\text{Mg}_2\text{Si}$  may be added after 72 hours of reaction leading to larger Si NPs. The already existing Si NPs may then act as seeds for the newly added silicon atoms and thereby only a small fraction of new Si NPs are formed, but the available silicon is predominantly used for the further growth of already existing Si NPs. It will be interesting to prepare Si/Ge core/shell nanoparticles in a similar manner, to produce nanoparticles with a shell with a larger band gap, similar to the type I core/shell QDs.<sup>6</sup> This should allow for more accurate tuning and optimizing of optical properties such as the higher quantum yield as observed in the type I core/shell QDs. The exploration of adding germanium to the Si NPs is interesting for another reason; the largest, still fluorescent Si NPs will emit around 900 nm, where Ge NPs will be able to emit up to

1200 nm.<sup>7</sup> This broadens the tuning of the fluorescence in the optimal window for bioimaging.<sup>3</sup>

To be able to employ Si NPs in biological systems or multiplex analysis, functionalization of these Si NPs is required for the attachment of specific target or capture molecules. The ideal functionalization strategy is versatile, yet facile. The prerequisites point to click chemistry, since this type of coupling chemistry is characterized by the use of benign solvents (if any), mild reaction conditions, high regioselectivity and chemoselectivity and high yields. Several reactions qualifying the click-chemistry criteria have been reported in the literature, amongst which thiol-ene click chemistry has gained interest because it proceeds under very mild conditions, does not need a metal catalyst and is insensitive to water and oxygen. The reaction requires an alkene and a free thiol, which are coupled by a radical-initiated mechanism. The ability to attach terminal alkenes onto the Si NPs, by employing an alkene-functional Grignard reagent, was described in Chapter 3. The alkene-functional Si NPs were readily functionalized with a wide range of functional groups, such as alcohols, ethylene glycol and carboxylic acids. The acid-terminated Si NPs are available for further coupling. Thiol-ene coupling did not significantly alter the optical properties, and the oxidation of the Si core remains minimal. These observations confirm that the thiol-ene reaction is very suitable to functionalize the Si NPs. The readily available thiol groups on biomolecules, such as peptides, proteins (cysteine) and commercially available SH-terminated DNA are good candidates to couple to the Si NPs.

With biofunctional Si NPs, applications such as FRET sensors or targeted labeling of cell types or specific parts of a cell become available. The attachment of DNA to the Si NPs allows for the development of diagnostic tools, in which DNA hybridization plays a crucial role.<sup>8</sup> Chapter 4 demonstrates that the activation of carboxylic acid-terminated Si NPs allows for attachment of NH<sub>2</sub>-terminated DNA strands. Although no peptides or proteins were tested, this method is directly applicable also to these materials, since in such materials NH<sub>2</sub> groups are ubiquitously present. The resulting Si NPs can then again be used for diagnostics, or targeted labeling in cells.<sup>9,10</sup>

Another point of attention are the toxicological effects of Si NPs in biological systems. In contrast to conventional II-VI or III-V QDs, Si NPs do not contain intrinsically toxic elements such as Cd and Se. It is therefore likely that possible toxic effects originate from particle's capping groups, charge or particle shape. The influence of the Si NP surface charge has been tested by exposing Caco-2 cells to -NH<sub>2</sub> (positive), -N<sub>3</sub> (neutral) and -COOH (negative) terminated Si NPs (Chapter 5). These tests reveal that positively charged particles induce cytotoxic effects, whereas the negatively charged Si NPs induce

no significant cytotoxic effects and the neutral particles show intermediate cytotoxicity. This confirms the assumption that surface charge is an important factor for the cytotoxic effects of Si NPs. Since this research, tests of the same type of Si NPs on NR8383 cells confirmed the conclusion that surface charge is important in cytotoxic effects on cells.<sup>11</sup> Exposure of amine-terminated Si NPs and Ge NPs to HePG2 cells revealed that in a concentration of 100 µg/mL, 50% cell viability is measured.<sup>12,13</sup> This confirms cytotoxic effects of the NH<sub>2</sub>-termination, however, it is remarkable that the results for both Ge NPs and Si NPs in this study are exactly the same.

With these toxicological tests an important step has been made in the safe application of Si NPs. However, these tests were focused on cell lines and not on whole organisms. As a result effects concerning bioaccumulation and different types of uptake have not been taken in consideration and this topic thus clearly needs further investigation. Although still challenges remain before commercial applications of Si NPs can be realized, the results described in this thesis suggest a bright future for fluorescent Si NPs.

## References

- (1) Pettigrew, K. A.; Liu, Q.; Power, P. P.; Kauzlarich, S. M. *Chem. Mater.* **2003**, *15*, 4005.
- (2) Huisken, F.; Ledoux, G.; Guillois, O.; Reynaud, C. *Adv. Mater.* **2002**, *14*, 1861.
- (3) Smith, A. M.; Mancini, M. C.; Nie, S. *Nat Nano* **2009**, *4*, 710.
- (4) Wilcoxon, J. P.; Samara, G. A.; Provencio, P. N. *Phys. Rev. B: Condens. Matter* **1999**, *60*, 2704.
- (5) Tanke, R. S.; Kauzlarich, S. M.; Patten, T. E.; Pettigrew, K. A.; Murphy, D. L.; Thompson, M. E.; Lee, H. W. H. *Chem. Mater.* **2003**, *15*, 1682.
- (6) Kim, S.; Fisher, B.; Eisler, H.-J.; Bawendi, M. J. *Am. Chem. Soc.* **2003**, *125*, 11466.
- (7) Shirahata, N. *Phys. Chem. Chem. Phys.* **2011**, *in print*.
- (8) Wang, X.; Lou, X.; Wang, Y.; Guo, Q.; Fang, Z.; Zhong, X.; Mao, H.; Jin, Q.; Wu, L.; Zhao, H.; Zhao, J. *Biosens. Bioelectron.* **2010**, *25*, 1934.
- (9) Chen, F.; Gerion, D. *Nano Lett.* **2004**, *4*, 1827.
- (10) Derfus, A. M.; Chan, W. C. W.; Bhatia, S. N. *Adv. Mater.* **2004**, *16*, 961.
- (11) Bhattacharjee, S.; de Haan, L.; Evers, N.; Jiang, X.; Marcelis, A.; Zuilhof, H.; Rietjens, I.; Alink, G. *Part. Fibre Toxicol.* **2010**, *7*, 25.
- (12) Shiohara, A.; Hanada, S.; Prabakar, S.; Fujioka, K.; Lim, T. H.; Yamamoto, K.; Northcote, P. T.; Tilley, R. D. *J. Am. Chem. Soc.* **2009**, *132*, 248.
- (13) Prabakar, S.; Shiohara, A.; Hanada, S.; Fujioka, K.; Yamamoto, K.; Tilley, R. D. *Chem. Mater.* **2010**, *22*, 482.



## Summary

Diagnostics in biological systems are continuously searching for novel materials and systems for more specific detection with lower detection limits. Fluorescent probes are often used in the (selective) labeling of tissues and cellular components, since they give a high signal-to-noise ratio. The disadvantage of commonly used organic dyes is severe photobleaching, which makes prolonged studies impractical. Fluorescent quantum dots (QDs) are not prone to photobleaching, moreover, their fluorescence emission wavelength is size-tunable, making them the ideal candidates for bioimaging purposes. Silicon nanoparticles (Si NPs) in particular have the additional advantage that the core consists of the non-toxic silicon, in contrast to the toxic elements (Cd, Se) typically employed in QDs. The development of a robust synthetic approach towards Si NPs, as well as a versatile functionalization strategy are therefore essential in enabling application in biological systems.

In Chapter 1, a general introduction on quantum dots (QDs) and in particular silicon nanoparticles is given; the origin of fluorescence is explained, and several synthetic methods are discussed. Chapter 2 describes the synthesis of Si NPs via the oxidation of magnesium silicide with bromine, yielding bromine-terminated Si NPs. Subsequent reaction with n-butyl lithium, and purification via column chromatography, resulted in butyl-terminated Si NPs. NMR analysis revealed that the major side-product (multiply brominated octane) was also in part attached to the Si NPs. Detailed characterization by IR and NMR confirmed the attachment of butyl-chains as well as a minor oxidation of the Si core. TEM measurements revealed a Si core size of  $2.6 \pm 0.7$  nm. UV-Vis measurements showed a gradual increase in absorption with decreasing wavelengths, and a fluorescence emission maximum was observed at 390 nm ( $\lambda_{\text{exc}} = 340$  nm). The Si NPs were fractionated using size exclusion chromatography, which yielded four fractions containing Si NPs of different sizes. Fluorescence anisotropy measurements, XPS and DOSY NMR spectroscopy confirmed the size-differences between the fractionated samples. The slope of the UV spectrum increases upon smaller Si NP size, whereas a shift in fluorescence emission maxima was observed from 383 to 445 nm ( $\lambda_{\text{exc}} = 340$  nm), for respectively the smallest and largest Si NPs. Fluorescence quantum yields did not differ significantly between the different fractions, and the highest QY measured at  $\lambda_{\text{exc}} = 496$  nm is 5.2 %. Fluorescence emission lifetimes did not reveal distinct difference in the differently sized Si NPs, most likely due to the relatively small size-differences between the fractions.

In Chapter 3 the synthesis of alkene-terminated Si NPs is described. To this purpose, the bromide-terminated Si NPs were reacted with 3-butenylmagnesium bromide. The resulting Si NPs were purified using SEC, and yielded Si NPs with a core size of  $2.4 \pm 0.5$  nm as measured by TEM. Only minimal oxidation of the silicon core had occurred as observed by IR, while NMR spectroscopy confirmed successful attachment of the terminal alkenes onto the Si NPs. This also allowed for quantification of the amount of bromoalkanes attached to the Si NPs (butene : octane = 1 : 0.36). UV-Vis absorption of the Si NPs did not change significantly as compared to butyl-terminated Si NPs. The extinction coefficient was determined to be  $0.14 \text{ (mg mL}^{-1}\text{)}^{-1}$  at 300 nm and  $0.035 \text{ (mg mL}^{-1}\text{)}^{-1}$  at 350 nm. A fluorescence emission maximum was observed at 525 nm ( $\lambda_{\text{exc}} = 430$  nm), while a QY of  $7.1 \pm 1.2 \%$  was measured ( $\lambda_{\text{exc}} = 496$  nm).

Modification of the alkene-terminated Si NPs using thiol-ene chemistry is described in Chapter 3. This reaction involves the radical-initiated coupling of a thiol to an alkene. The Si NPs were modified with thiolacetic acid, mercaptoethanol, thiolated triethyleneglycol monomethylether, and a thiolated polyethylene glycol 5000 monomethylether. The thiol-ene modification step did not significantly alter the photophysical properties of the Si NPs. Furthermore, IR and XPS showed that the functionalization step did not oxidize the silicon core. NMR and XPS results confirmed successful attachment of the functional thiols. In Chapter 4, carboxylic acid terminated Si NPs were synthesized by thiol-ene chemistry with 3 different spacer lengths; i.e. no spacer, a tetraethyleneglycol spacer and a PEG3000 spacer. The Si NPs were further functionalized by coupling an  $\text{NH}_2$ -terminated single stranded DNA molecule via EDC/NHS chemistry. Coupling and subsequent hybridization with the complementary strand was confirmed by gel electrophoresis, UV-Vis and fluorescence spectroscopy. This revealed that 2 to 3 DNA strands were attached to the Si NPs.

Finally, Chapter 5 describes the initial investigations in the toxicity of Si NPs. To this purpose, Si NPs were synthesized via reduction of silicon tetrachloride, followed by hydrosilylation with functional alkenes. The Si NPs were capped with  $-\text{C}_3\text{H}_6\text{NH}_2$ ,  $-\text{C}_{11}\text{H}_{22}\text{N}_3$  and  $-\text{C}_3\text{H}_6\text{COOH}$  groups, yielding positively and negatively charged, as well as neutral Si NPs. Two types of tests were performed: the MTT test for mitochondrial activity, and the BrdU test for cell proliferation, both in the presence and absence of FCS. Upon exposure of human colonic Caco2 cells, the negatively charged Si NPs showed no observable cytotoxic effects, whereas the  $\text{N}_3$ -terminated Si NPs display a moderate toxicity with an  $\text{IC}_{50}$  of  $500 \text{ }\mu\text{g/L}$  in the presence of FCS in the MTT test, and the  $\text{NH}_2$ -terminated Si NPs display strong cytotoxic effects on the cells with an  $\text{IC}_{50}$  of  $20 \text{ }\mu\text{g/L}$  in the presence of FCS in the MTT assay.

The described synthesis, followed by the versatile functionalization and bioconjugation, in combination with the low inherent cytotoxicity, shows that the Si NPs are readily suitable for applications in biological systems.





## Samenvatting

In de biologische diagnostiek wordt continu gezocht naar nieuwe materialen en systemen om specifiekere tests met lagere detectielimieten te maken. Omdat fluorescente labels goede signaal-tot-ruis verhouding geven, worden ze veel gebruikt in de selectieve labeling van weefsel en componenten in cellen. Het nadeel van de veelgebruikte organische kleurstoffen is, dat ze erg gevoelig zijn voor fotobleaching – het effect dat het materiaal niet meer fluoresceert na langdurig gebruik. Dit maakt langdurige studies onpraktisch. Fluorescente “quantum dots” (QDs) zijn ongevoelig voor fotobleaching, bovendien is de fluorescentie emissie golflengte afhankelijk van de grootte van het deeltje en kan daarmee de emissie van het deeltje sturen. Dit maakt de QDs ideale kandidaten voor biologische toepassingen. Silicium nanodeeltjes (Si NDs) hebben het extra voordeel dat de kern bestaat uit het niet-toxische silicium, terwijl de conventionele QDs een kern hebben van toxische elementen zoals cadmium en selenium. Het ontwikkelen van een robuuste synthese van Si NDs, met daarbij brede mogelijkheden tot functionalisering van deze deeltjes is daarom essentieel om toepassing van Si NDs in biologische systemen te bereiken.

In hoofdstuk 1 wordt er een algemene introductie gegeven op QDs in het algemeen en Si NDs in het bijzonder. De oorsprong van de fluorescente eigenschappen worden uitgelegd, en verschillende synthetische methoden worden besproken. Hoofdstuk 2 beschrijft de synthese van Si NDs door de oxidatie van magnesium silicide met broom, dat resulteert in broom-getermineerde Si NDs. De vervolgreactie met n-butyllithium en opzuivering door kolomchromotografie resulteert in butyl-getermineerde Si NDs. NMR analyse levert op dat het belangrijkste bijproduct van de synthese (meervoudig gebromineerd octaan) ook aan het Si ND koppelt. Gedetailleerde IR en NMR analyse levert het bewijs dat de butyl-ketens gekoppeld zijn aan de Si kern, en dat deze kern minimaal geoxideerd is. TEM metingen leveren een kerngrootte op van  $2.6 \pm 0.7$  nm. UV-Vis metingen geven een regelmatige stijging in absorptie bij lagere golflengtes, en een fluorescentie emissiemaximum wordt gemeten bij 390 nm ( $\lambda_{\text{exc}} = 340$  nm). De Si NDs worden daarna gefractioneerd op grootte, dat 4 fracties deeltjes met verschillende groottes oplevert. Fluorescentie anisotropie metingen, XPS en DOSY NMR bevestigen de aanwezigheid van verschillende groottes deeltjes in de verschillende fracties. De helling van het UV-spectrum stijgt naarmate de Si NDs kleiner zijn, en een verschuiving in het fluorescentie emissiespectrum van 383 naar 445 nm ( $\lambda_{\text{exc}} = 340$  nm) wordt gemeten voor respectievelijk de kleinste en grootste Si NDs. De fluorescentie quantum opbrengst

verschilt niet tussen de verschillende fracties, en de hoogste quantum opbrengst wordt gemeten op  $\lambda_{\text{exc}} = 496 \text{ nm}$  en is 5.2 %. De fluorescentie emissie levensduur geeft geen duidelijk verschil in de verschillende grootte Si NDs, dit wordt waarschijnlijk veroorzaakt door de relatief kleine verschillen tussen de fracties.

In hoofdstuk 3 wordt de synthese van alkeen-getermineerde Si NDs beschreven. Hiervoor worden de broom-getermineerde Si NDs gereageerd met 3-butenyl magnesiumbromide. De resulterende deeltjes worden gezuiverd door middel van chromatografie met scheiding op grootte, en levert Si NDs met een kerngrootte van  $2.4 \pm 0.5 \text{ nm}$ , gemeten in TEM. De kern is minimaal geoxideerd, IR en NMR spectroscopie leveren het bewijs dat de alkeen-groepen gekoppeld zijn aan de Si NDs. Deze NMR studies geven de mogelijkheid tot het kwantificeren van de hoeveelheid bromo-octaan dat gekoppeld is aan de Si kern, welke een verhouding geeft van buteen : octaan = 1 : 0.36. De UV-Vis absorptiespectra veranderen niet significant ten opzichte van butyl-getermineerde Si NDs. De extinctiecoëfficiënt is bepaald op  $0.14 \text{ (mg mL}^{-1}\text{)}^{-1}$  bij 300 nm en  $0.035 \text{ (mg mL}^{-1}\text{)}^{-1}$  bij 350 nm. Een fluorescentie emissiemaximum wordt gemeten bij 525 nm ( $\lambda_{\text{exc}} = 430 \text{ nm}$ ), en een quantum opbrengst van  $7.1 \pm 1.2 \%$  wordt gevonden. ( $\lambda_{\text{exc}} = 496 \text{ nm}$ )

De alkeen-getermineerde Si NDs worden daarna gemodificeerd door gebruik te maken van thiol-ene chemie. Dit is een radicaal-geïnitieerde koppeling van een thiolgroep aan een alkeen. De Si NDs worden gemodificeerd met thioazijnzuur, mercaptoethanol, gethioleerde triethyleenglycol monomethyl ether, en een gethioleerde polyethyleenglycol 5000 monomethyl ether. De thiol-ene modificaties leiden niet tot significante veranderingen in de fotofysische eigenschappen. Bovendien tonen IR en XPS aan dat de functionalisatie de Si kern niet verder oxideert. De succesvolle koppeling van de functionele thiolen wordt aangetoond met NMR en XPS.

In hoofdstuk 4 wordt beschreven hoe carboxylzuur-getermineerde Si NDs gemaakt worden. Door de thiol-ene koppeling van carboxylzuurgroepen met 3 verschillende lengtes - geen extra tussengroepen, een tetraethyleenglycol tussengroep en een PEG3000 tussengroep - worden de Si NDs gefunctionaliseerd. In de vervolgekoppeling wordt enkelstrengs,  $\text{NH}_2$ -getermineerd DNA gekoppeld met behulp van EDC/NHS chemie. De koppeling en vervolgens hybridisatie van het DNA wordt bewezen met gel elektroforese, UV-Vis en fluorescentie spectroscopie. Hieruit blijkt dat 2 tot 3 DNA strengen aan het Si ND worden gekoppeld.

Hoofdstuk 5 beschrijft de start van het onderzoek naar de toxiciteit van Si NDs. Hiervoor worden Si NDs gemaakt door de reductie van silicium tetrachloride, gevolgd door de hydrosilering met functionele alkenen. De Si NDs worden gekoppeld met  $-\text{C}_3\text{H}_6\text{NH}_2$ ,  $-\text{C}_{11}\text{H}_{22}\text{N}_3$  en  $-\text{C}_3\text{H}_6\text{COOH}$  groepen, wat positief, neutraal en negatief geladen deeltjes

oplevert. Twee verschillende tests worden gebruikt: de MTT test voor mitochondriale activiteit, en de BrdU test voor proliferatie, beide in de aanwezigheid en afwezigheid van FCS. De blootgestelde humane Caco2 darmcellen laten geen effecten zien van de negatief geladen Si NDs. De  $N_3$ -getermineerde Si NDs laten een matig toxisch effect zien met een IC50 van 500  $\mu\text{g/L}$  in de aanwezigheid van FCS in de MTT test. De  $NH_2$ -getermineerde Si NDs laten een sterk toxisch effect zien op de cellen met een IC50 van 20  $\mu\text{g/L}$  in de aanwezigheid van FCS in de MTT test.

De beschreven synthese, gevolgd door de veelzijdige functionalisering en bioconjugatie, in combinatie met de lage inherente toxiciteit laten zien dat de Si NDs direct bruikbaar zijn voor toepassingen in biologische systemen.



## Curriculum Vitae

Loes Ruizendaal werd op 13 juni 1983 geboren in Groessen. Na het behalen van het VWO diploma op het Candea College in Duiven, begon ze in 2001 aan de studie scheikunde aan de Radboud universiteit Nijmegen. Ze deed stages bij de afdelingen organische chemie (prof. dr. ir. J.C.M. van Hest) en celbiologie (prof. dr. E.J.J. van Zoelen) aan de Radboud universiteit, en een bedrijfsstage bij Unilever. In november 2006 begon ze aan een promotieonderzoek aan de Wageningen universiteit bij de vakgroep organische chemie, onder leiding van prof. dr. H. Zuilhof, prof. dr. E.J.R. Sudhölter en dr. ir. J.M.J. Paulusse. De belangrijkste resultaten van dit onderzoek staan beschreven in dit proefschrift. Sinds maart 2011 is Loes werkzaam als research chemist op het crosslinkers en specialties laboratorium bij Stahl international in Waalwijk.

Loes Ruizendaal was born on June 13, 1983 in Groessen. After finishing secondary education at the Candea College in Duiven, she studied chemistry at the Radboud University Nijmegen. She did internships the departments of organic chemistry (prof. dr. ir. J.C.M. van Hest), cell biology (prof. dr. E.J.J. van Zoelen) at the Radboud University and an internship at Unilever in Vlaardingen. She started her PhD research at Wageningen University in November 2006 in the laboratory of organic chemistry, under supervision of prof. dr. H. Zuilhof, prof. dr. E.J.R. Sudhölter and dr. ir. J.M.J. Paulusse. The most important results of this research are described in this thesis. From March 2011, Loes is working as a research chemist at the crosslinkers and specialties laboratory at Stahl International in Waalwijk.



## List of publications

### Biofunctional Silicon Nanoparticles by Means of Thiol-Ene Click Chemistry

L. Ruizendaal, S.P. Pujari, V. Gevaerts, J.M.J. Paulusse and H. Zuilhof, published online 24 August, 2011

### Synthesis and Cytotoxicity of Silicon Nanoparticles with Covalently Attached Organic Monolayers

L. Ruizendaal, S. Bhattacharjee, K. Pournazari, M. Rosso-Vasic, L.H.J. de Haan, G.M. Alink, A.T.M. Marcelis, H. Zuilhof, *Nanotoxicology*, **2009**, 3, 339-347

### A Highly Ordered Material from Magnetically Aligned Peptide Amphiphile Nanofiber Assemblies

D.W.P.M. Löwik, I.O. Shklyarevskiy, L. Ruizendaal, P.C.M. Christianen, J.C. Maan, J.C.M. van Hest, *Advanced Materials*, **2007**, 19, 1191-1195

### Switchable peptides

M.B. Hansen, L. Ruizendaal, D.W.P.M. Löwik, J.C.M. van Hest, *Drug Discovery Today: Technologies*, **2009**, 6, e33-e39





# Overview of Completed Training Activities

## ***Discipline specific activities***

### *Courses*

- European short course on Principles and Applications of Time-Resolved Fluorescence Spectroscopy, October 2007, Picoquant, Berlin
- Advanced Macromolecular Systems Across the Length Scales (AMSALS) III, May 2008, Mesa+, Enschede
- HRSMC Summerschool: Photochemistry 2008: Fundamentals and Applications, June 2008, Holland Research School of Molecular Chemistry, Maastricht
- Advanced Organic Chemistry, Laboratory of Organic Chemistry, 2010

### *Meetings*

- Annual NWO Conference, October 2006-2010, Lunteren
- Microned Meetings, 2006-2010
- MicroNed Conference, October 2007
- NanoNed Symposium, December 2007
- Annual MicroNano Conference, 2008-2010
- ACS Spring 2010 National Meeting, San Fransisco, March 2010
- Organic Chemistry Symposium, KNCV, Wageningen, April 2008
- Advanced Electron Microscopy: Novel Perspectives for Soft Matter Sciences, Eindhoven University of Technology, Eindhoven, September 2008
- Creative Coatings Chemistry, KNCV, Waalwijk, 2010

### ***General Courses***

- PhD scientific writing, Centa, Wageningen, 2010
- Vlag PhD week, 2007

### ***Optionals***

- Preparing PhD research proposal
- Colloquia, Laboratory of Organic Chemistry, 2006-2010
- Group meetings, Laboratory of Organic Chemistry, 2006-2010
- PhD studytrip, organized by Laboratory of Organic Chemistry, Sweden, 2007
- PhD studytrip, organized by Laboratory of Organic Chemistry, China, 2009



# Dankwoord

Een promotieonderzoek doe je niet alleen, al lijkt het soms wel zo. De laatste pagina's van dit proefschrift wil ik daarom gebruiken om iedereen te bedanken die op welke manier dan ook geholpen hebben om dit proefschrift tot stand te laten komen.

Als eerst wil ik mijn promotoren en copromotor, Han Zuilhof, Ernst Sudhölter en Jos Paulusse bedanken. Zonder hen was het niet mogelijk geweest om dit promotieonderzoek af te ronden. Ernst, nu meer dan 4 jaar geleden ben ik begonnen in Wageningen aan het onderzoek aan HOSFETs, een systeem dat helaas op de manier zoals wij in gedachten hadden, niet wilde werken. Ook na je verhuizing naar Delft en overstap van mijn onderzoek naar de Si NPs, heb je toch altijd interesse getoond en hebben we goede gesprekken gehad om de resultaten te bespreken en de problemen met de Si NPs op te lossen. Han, jou wil ik bedanken voor je kritische blik op de resultaten, wat er uiteindelijk alleen maar toe leidt dat alles nóg beter bestudeerd werd en beschreven staat. Je enthousiasme voor de Si NPs en je steun tijdens de switch van onderwerp hebben ertoe geleid dat ik nu dit onderzoek kan afronden. En dan Jos, je kwam pas na 2.5 jaar onderzoek van mijn kant in Wageningen werken, maar vanaf dat moment heb ik veel steun aan je begeleiding gehad. Je optimisme, goede suggesties en een andere invalshoek om de Si NPs te benaderen hebben tot goede resultaten geleid, wat terug te vinden is in dit proefschrift en een publicatie.

De leden van de manuscriptcommissie, Tom Gregorkiewicz, Jeroen Cornelissen, Ivonne Rietjens en Maarten Jongsma, wil ik hartelijk bedanken voor het beoordelen van mijn proefschrift. Het laatste lid, Maarten Jongsma, wil ik net als de andere leden van het Microned-workpackage bedanken voor de input tijdens de meetings die we gehad hebben.

Voor het werk in het eerste jaar van mijn promotieonderzoek, alhoewel dit niet in dit proefschrift terug te vinden is, wil ik Erik Faber en zijn lab in Twente bedanken, hij heeft mij de kneepjes van het meten aan (HOS)FETs geleerd. Ook de mensen in het lab bij ORC die mij geleerd hebben om mooie organische monolagen op silicium te maken, met name Ahmed en Luc, ben ik zeer dankbaar. Milena, I would like to thank you for the help you gave me when I started working on the Si NPs. I learned a lot from you! My other Si NP-colleagues, Wouter and Umesh, I would like to thank you for the discussions we had on the Si NPs and the problems we have solved together. Umesh, good luck with your further research on the Si NPs, I hope I've learned you enough to make it a success!

Wouter, bedankt voor je werk als student van mij, hopelijk heb je er veel van geleerd. Ik wil je heel veel succes wensen in je nieuwe baan! Lenny, ook jij bedankt voor je tijd die je als student bij mij hebt doorgebracht. Zonder jouw werk had hoofdstuk 2 van dit proefschrift niet tot stand kunnen komen. Sourav and Kamyar, I would like to thank you for the toxicology tests you have performed with the Si NPs, which led to a publication and chapter 5 in this thesis. Anke, Veronique and Sidhu, I would like to thank you on the help with the gels, TEM and XPS on the Si NPs, which resulted in a nice paper, and the results described in chapter 3 and 4. Mabel, jou wil ik bedanken voor je praktische hulp bij de thiol-ene chemie.

Bart en Kim, we zijn ongeveer tegelijkertijd begonnen met ons promotieonderzoek bij ORC, en ook ongeveer tegelijkertijd hebben we Wageningen verlaten. Hartelijk dank voor de gezelligheid en alle lief en leed dat we gedeeld hebben. Kim, ook hartelijk dank dat je mijn paranimf wil zijn, en heel veel succes na deze "carrièreswitch"! Bart, jouw proefschrift zie ik graag tegemoet, en heel veel succes bij Dow en veel geluk in jullie nieuwe huis!

TuHa, ook jij bedankt dat je mijn paranimf wil zijn! We hebben veel gedeeld tijdens onze dagelijkse carpoolritjes, bedankt daarvoor!

My colleagues at ORC, Ai, Alexandre, Aliaksei, Anke, Bart, Dennis, Feng, Florine, Hamilton, Jaime, Jacinthe, Jerome, Jurjen, Kim, Kishore, Luc, Mabel, Michel, Milena, Nagendra, Nagesh, Paul, Radostina, Rokus, Ruud, Satesh, Sidhu, Sourav, Tin, Tijs, TuHa, Umesh, Willem, Wouter, Yessie, and of course all whose name I forgot in this list, thanks for all the fun we had in the lab and during our PhD trips!

Graag wil ik iedereen bedanken die mij geholpen heeft met alle "randvoorwaarden" van het onderzoek: Barend voor de NMR, fluorescentie en UV, Elbert en Frank voor de hulp bij de chromatografie, Ronald voor de bestellingen, Elly en Aleida voor alle algemene zaken en alle andere medewerkers van ORC voor hun interesse, hulp en input tijdens werkbesprekingen.

Zonder de steun en interesse van mijn vrienden had ik dit promotieonderzoek niet kunnen doen, Inge, Vivike, Arjan, Willem, Stijn, Coen en Nearchos, bedankt voor de gezellige dingen die we afgelopen jaren hebben gedaan, jullie interesse en steun, maar ook Wendy, Luc, Tineke, Hans, Marcel, Alex, Ivo, Ron en Emiel, ook jullie bedankt voor de gezelligheid tijdens het mtb-en, jullie interesse voor mijn werk, al was het misschien niet altijd te begrijpen wat mijn onderzoek nu precies inhield. Hopelijk zien we elkaar nog eens!

Mijn nieuwe collega's bij Stahl wil ik ook bedanken voor de leuke momenten samen, ik hoop dat we het nog lang gezellig samen hebben!

Mijn ouders wil ik graag bedanken voor hun interesse, de leuke dingen die we doen en de onvoorwaardelijke steun die ik krijg. Jos, speciale dank voor je essentiële bijdrage aan dit proefschrift, Mieke en Stefan bedankt voor de interesse en hulp bij alles! Mijn schoonouders, Jannie, Toon en Hermine, wil ik bedanken voor hun interesse en steun, ik hoop dat jullie allemaal met behulp van dit proefschrift iets beter begrijpen waar ik de afgelopen jaren mee bezig ben geweest.

Als laatste, maar zeker niet als minste wil ik Otmar bedanken. Jouw soms ongeken- de vermogen om dingen rustig te bekijken en te relativiseren, heeft mij geleerd me wat minder druk te maken om dingen wanneer dit nodig is. Van jouw liefde hoop ik nog lang te kunnen genieten!

*Loes*

September 2011

The research described in this thesis was financially sponsored by the MicroNed Program, workpackage 2-C-II

Printed by PrintPartners Ipskamp, Enschede